University of Trento

Department of Physics

doctoral thesis

Sound Propagation in Superfluids with Two Broken Continuous Symmetries

Tomasz Zawiślak

Supervisor
Dr. Alessio Recati
Co-supervisor
Prof. Sandro Stringari

Referees
Prof. Dr. Montserrat Guilleumas Morell
Prof. Dr. Lauriane Chomaz

November 2025

Dla Pati, Ani i Jadzi
bez których wsparcia, ta przygoda nie byłaby możliwa

Acknowledgments

There are many people who contributed to making my three-year stay in Trento such a wonderful adventure. First, and foremost, I would like to thank my supervisors, Alessio and Sandro, who made my dreams of becoming a physicist possible. Working with you and learning from you has always been a pleasure and an honor. I truly appreciate every hour we have spent discussing physics. Thank you for always being kind and willing to help whenever I needed it. I thank Marija for our fruitful collaboration and discussions. I am also thankful to Giovanni Modugno for his guidance at the very beginning of my PhD; I really wish we could have collaborated more.

I thank my family, for always supporting me in chasing my goals and dreams, in particular my mom Ania, and my beloved wife Pati. Mamo, dziękuję Ci za wszystko, co dla mnie zrobiłaś bym rozwijał swoje pasje. Wszystko co osiągnąłem, to po części dzięki Tobie. Pati, dziękuję Ci za Twoje poświęcenie by wyjechać wraz ze mną do Włoch. Twoje wsparcie jest dla mnie nieocenione.

I am thankful to all the experimentalists in the BEC Center: Giacomo, Alessandro and Gabriele for fruitful consultations of our ideas of "simple experiments". Big thanks to Comi, for the private lab tour you gave me the other day!

I am grateful for having worked at the Pitaevskii BEC Center, with so many great people, thanks to whom Povo rarely felt like an ordinary workplace. I would like to thank all the people I shared offices with, in particular Stephi, Edoardo, Alberto and Sebastian. I have always been happy to see you at work. Thanks to all the people who regularly gathered for lunch: Andrea, Edoardo, Stephi, Christian, Phillip, Chiara, and others; I love the discussions we had over the lunch. I thank Stephi for our after-lunch routine of sipping and judging different coffees, and also Alberto, Daniela, and others who occasionally joined me for a cup and chat.

I thank everyone who made me feel at home in Trento, in particular Lorenzo, the best flatmate I have ever had. I will miss our pizza afternoons on Wednesdays.

I would like to thank *i miei amici di bici*: Anna Giulia, Stephi, Christian, Julius, and Francesco - who inspired me to take up cycling in Trentino. Thanks guys! Those were unforgettable rides!

I thank everyone from the *Calcetto when?* group, especially those who played with us regularly: Luca, Irene, Ben, Gianmarco, Danial, Andrea, Edoardo, Paolo, Zizou and Mattia. Thank you for all the fun we had together on the pitch, for playing *for real* whenever needed and for all the *golden goals* and *platinum goals* and *diamond goals*.... Last but not least, I would like to thank the entire team *ECT Scars* - the FBK tournament champions. It was an honor to play with you and to win a major trophy in Italy.

Overview

The physics of matter at ultralow temperatures is rich in fascinating phenomena, with superfluidity playing a central role in this work. Initially observed in liquid helium, this unusual effect is characterized by a frictionless flow, even through narrow capillaries or porous media. Furthermore, in closed geometries superfluids can host permanent currents, which flow indefinitely due to the absence of dissipation mechanisms. Shortly after its discovery, superfluidity was linked to Bose-Einstein condensation - a process, in which an ensamble of bosons acts as a coherent matter-wave, as a result of the macroscopic occupation of a single quantum state. The two phenomena are indeed linked but are not equivalent. In particular, there exist systems that form a Bose-Einstein condensate (BEC) but are not entirely superfluid, and conversely, the ultracold ^{4}He itself provides an example of a system that is entirely superfluid while possessing a condensate fraction of at most 10%.

The discovery of Bose-Einstein condensation of ultracold atomic gases has opened a new branch of physics, with tremendous implications for both theoretical physics and development of quantum technologies. BECs of atomic gases have many advantages with respect to liquid helium, their high interaction tunability being the most notable. Thanks to the so-called Feshbach resonances, current experiments can change the strength and the character of the interatomic interactions by means of an externally applied magnetic field. In the last 15 years, part of the efforts, both theoretical and experimental, have shifted towards the physics of ultracold dipolar gases, whose dipole moment is given by the magnetic properties of selected atomic species. Their long-range and anisotropic interactions offer many interesting features, like angular dependence of the dispersion relation or even its rotonization - the appearance of a local minimum in the excitation spectrum, similar to the one in the liquid ^{4}He. The first dipolar BEC was achieved in the gas of ultracold ^{52}Cr, which accurately followed the mean-field theoretical predictions. Interestingly, more recent experiments on dysprosium, whose dipolar interactions are stronger than those of chromium, have contradicted the results previously found in ^{52}Cr. Notably, in the parameter regime, in which the mean-field theory predicts an energetic collapse, the dipolar gas was found to form a stable ensamble of separate droplets. This transition from a uniform dipolar superfluid to a droplet-array resembled the Rosensweig instability, which occurs in ferrofluids exposed on an external magnetic field. Further analysis has shown that the droplet form of the gas is stabilized by quantum fluctuations that are the first-order correction to the mean-field Gross-Pitaevskii theory. The effective microscopic description of dipolar BECs is constructed by incorporating the quantum fluctuation term back into the original theory in a manner similar to the density functional approach. The resulting extended Gross-Pitaevskii equation (eGPE) has become the cornerstone of almost all numerical simulations of dipolar BECs.

The discovery of a droplet array in dipolar BECs has triggered an intense study of this phase. In particular, what was the most sought-after was a state that combines the two

limiting cases: a density-modulated and fully coherent superfluid. Since the independent droplet phase breaks the translational symmetry in a spontaneous manner, to some extent it resembles a solid. According to the Goldstone theorem, every spontaneous breaking of a continuous symmetry is associated with a gapless excitation branch - in this case - the lattice phonon. Therefore, a fully connected density-modulated superfluid would merge the properties of a superfluid and a solid, giving rise to the so-called phenomenon of supersolidity. The first idea of supersolidity emerged in ultracold helium, where superfluid properties would appear in its solid phase. In their seminal papers, Andreev and Lifshitz [1], Chester [2] and Leggett [3], proposed a mechanism, in which the condensation of lattice vacancies would provide the superfluid properties of the solid helium. Unfortunately, solid helium was never shown to exhibit any superfluid properties, and the concept of supersolidity has seen a revival only with the recent observation of the density-modulated phase of superfluid atomic gases. The first experimental evidence of supersolid behavior was found in 2017 in Bose-Einstein condensates with spin-orbit coupling (SOC) [4] and inside optical resonators [5]. Shortly after, in 2019 three independent experiments [6–8] discovered the supersolid phase in magnetic dipolar gases, triggering intense investigation of its properties. In particular, many direct and indirect experiments have shown that dipolar supersolids are superfluid. The most notable one assessed the global coherence of the system [9], which indicates at least partial superfluid behavior. The images of the density suggest that the system has properties of a solid, but a true test requires measuring its rigidity. This feature is reflected in the excitation spectrum, which, apart from the regular superfluid branch, should host additional lattice phonon branches. The first experiments on dipolar supersolids [10–12] have shown a doubling of collective modes in a one-dimensional lattice structure, demonstrating the dual nature of this counterintuitive phase of matter.

There remains one canonical feature of the vacancy-based model of Andreev and Lifshitz, which has not been observed in dipolar supersolids yet - the presence of $d+1$ sound modes in a d-dimensional supersolid. Sound waves are long-wavelength excitations, whose energy linearly depends on their wavevector. They govern the response of the system to low-energy perturbations, and thus are of fundamental interest. In fact, the hydrodynamic theory of supersolids predicts the existence of two separate sound modes of a hybrid superfluid and lattice nature. Before the present work, the sound modes in dipolar supersolids were not well characterized and the validity of supersolid hydrodynamics remained unknown.

This thesis investigates the propagation of sound(s) in superfluids with two broken continuous symmetries, predominantly focusing on newly discovered dipolar supersolids. The first chapter is a review of ultracold physics, covering the Bose-Einstein condensation, superfluidity, physics of dipolar gases and basics of linear response theory in quantum systems. It sets the stage by introducing the fundamental concepts necessary to follow the methods and results discussed in the later parts of this thesis. In Chapter 2, we discuss the numerical methods used to simulate all the systems presented in this thesis. In particular, we provide the algorithms to prepare the initial state and describe the procedure of their time evolution.

In Chapter 3, we design a protocol to excite and measure the two sound modes in the supersolid phase, specifically adapted to current experimental capabilities. We consider the dipolar gas in a toroidal external potential, to mitigate known problems appearing in harmonically trapped systems. In particular, the rotational symmetry of the ring geometry ensures that the density is uniform along the azimuthal angle, and thus the speed of sound is not position dependent. The natural periodic boundary conditions of the ring are even more important in the supersolid phase, where trap inhomogeneities influence the amplitude

of density modulations. To study sound, we require the system to faithfully represent the bulk supersolid, which is a challenging task with a sample of around 10 lattice sites. Our protocol for sound measurement begins with a state preparation in the presence of a small external periodic perturbation in the form of a cosine. By numerically solving the extended Gross-Pitaevskii equation in imaginary time, we find the ground state of the perturbed Hamiltonian. Then, we evolve this state in time, where at $t = 0$ we suddenly remove the perturbation. This abrupt change triggers the density oscillations, from which we extract their frequencies. In the long-wavelength limit the induced excitations are phonons, and thus the measured frequencies correspond to speeds of sound. Using our protocol, we measured the speed of sound across the superfluid-supersolid phase transition in dipolar BECs and we indeed observed the second sound mode appearing in the density-modulated phase. By changing the relative strength ϵ_{dd} of the contact interaction with respect to dipole-dipole repulsion, we characterized the dependence of the two sound modes on the superfluid fraction. Approaching the independent droplet phase, we observed the disappearance of second sound, leaving the lattice phonon as the only gapless mode of such a state.

In addition to the experimental proposal for sound measurement, we quantified the two speeds of sound with the hydrodynamic theory of supersolids. Our work is the first attempt to compare predictions of the macroscopic hydrodynamic theory with the microscopic extended Gross-Pitaevskii equation. We demonstrated that the two approaches yield consistent predictions of the two speeds of sound. Furthermore, our analysis showed that the hydrodynamic approach provides a novel method to measure the superfluid fraction in terms of the two speeds of sound.

Chapter 4 extends the previous study onto supersolids in motion, where only part of the system hosts the supercurrent. The superfluid velocity in closed geometries can take only discretized values, as a consequence of single-valuedness of the order parameter. On the other hand, the normal part of supersolids acts like an ordinary fluid and thus can move at arbitrary velocities. Therefore, in the metastable state, rotating supersolids host two, in general, different velocities. Such a configuration provides an intriguing platform to study the Doppler effect. In ordinary fluids moving at small velocity v, the speed of sound is modified by the current as $c^{\pm} = c \pm v$, depending on whether the sound propagates parallel (+) or antiparallel (-) to the velocity. This effect is purely kinematic, and originates from the Galilean transformation of the speed of sound from the rest frame of the fluid. In the presence of two different velocities, such a rest frame does not exist, and the Doppler effect becomes non-trivial. The first theoretical prediction of such an anomaly was done by Khalatnikov in liquid helium [13] - a system for which he derived the first predictions for the Doppler shift of the second sound. Later studies revealed that the fourth sound will also exhibit an anomalous Doppler effect at finite temperatures [14–16]. Despite some early experimental attempts, none of these theoretical predictions have seen their experimental confirmation.

In this work, we studied the Doppler effect in moving supersolids and superfluids in optical lattices. Even though we studied the zero-temperature limit, both systems feature the normal component as a consequence of the fact that, as predicted by Leggett [3], the presence of density modulation is always associated to a reduction of the superfluid fraction in the system. The periodic structure in BECs in the presence of an optical lattice is not the result of a spontaneous mechanism of breaking of translational invariance and therefore the system cannot host a gapless lattice phonon. On the other hand the presence of the lattice gives rise to a profound modification of the superfluid Bogoliubov sound which takes the name of fourth sound, in analogy with sound propagating in liquid helium in the presence

of porous media. By numerically solving the Gross-Pitaevskii equation, we confirm that the Doppler shift of fourth sound exhibits novel features. The effect is even more intriguing in supersolids, where there are two sound modes of hybrid superfluid and crystal nature. By linearizing their hydrodynamic equations, we derive formulas for Doppler shifts of the two sounds. In order to confirm validity of the hydrodynamic predictions, we perform the eGPE simulations for moving supersolids. We excite and measure the sound modes using the protocol developed in the previous chapter. We found a good agreement between eGPE and hydrodynamic theories, showing that the two sound modes exhibit different Doppler shifts. Notably, for selected superfluid and normal velocities, we demonstrated that the Doppler shift of the second sound can be negative, resulting in the speed of sound of the co-propagating mode being smaller than the counter-propagating one.

In Chapter 5 we investigate the anomalous Doppler effect in superfluid binary Bose mixtures. Two-component BECs also host two sounds, since there are two spontaneously broken gauge symmetries. Their character depends on the magnetization $m_z = (n_1 - n_2)/(n_1 + n_2)$, which defines the population imbalance, and on the inter-species interaction constant g_{12}. If the two components do not interact ($g_{12} = 0$), the two sounds are trivially oscillations of the two single-component densities n_i. On the other hand, for a finite value of g_{12}, the two sounds change the character from single-component oscillations for $n_1 \gg n_2$ (and $n_2 \gg n_1$) to density and spin waves for $n_1 = n_2$. In binary mixtures, both components are superfluids, whose velocities are governed by boundary conditions for the phase of their corresponding order parameters. Analogously to previously studied systems, we can design a metastable state where only one component hosts a permanent supercurrent, while the other one remains at rest. Using a pair of coupled Gross-Pitaevskii equations, we simulate such a system and measure the Doppler shifts with our linear response protocol. The results of the numerical simulations perfectly match the analytic formula for the Doppler shifts derived from the hydrodynamic model of coupled superfluids. Thus, we prove that the anomalous Doppler effect is also present in two-component superfluids.

Bose mixtures are well-studied, long-lived systems with high and precise tunability, and for these reasons, they seem to serve as a perfect platform to explore the anomalous Doppler effect. Consequently, we develop two variants of our linear response protocol to separately measure the Doppler effect of each of the sounds. The general form of our protocol excites both sounds and provides an observable to measure them simultaneously. In Bose mixtures, one can individually address the two components, by using appropriate laser frequencies. Therefore, the first version of the modified protocol adjusts the strengths of external potentials, in such a way to excite just one sound wave and the selected sound mode is then observed in the dynamics of the total density. Since this approach may turn out to be difficult to implement experimentally, we propose another variant of the protocol. There, both sounds are excited by the external potential, which equally affects the two components, and we modify the observable to remove one of the two sound modes from the signal. To demonstrate the utility of either method, we perform a numerical simulation employing GP theory, allowing for the study the Doppler shift of a selected sound looking at the precession of the density profile.

Finally, in this work we extend our analysis to the Andreev-Bashkin effect, according to which superfluid mixtures in motion are predicted to exhibit a mutual drag, which introduces cross-terms in the two single-component currents. In weakly interacting Bose mixtures, this effect is very small and has not been observed so far. We demonstrated that, in Bose mixtures, the inclusion of this effect slightly alters the Doppler shift of each sound. In principle, in systems where the Andreev-Bashkin effect is more pronounced, our protocol

enables the measurement of the dissipation-less drag with the Doppler effect.

Contents

Chapter 1

Introduction

The field of ultracold matter encompasses a wide range of phenomena at the intersection of statistical and quantum physics. Its foundation lies in Bose-Einstein condensation, where a macroscopic number of particles occupies the same quantum state. The physical properties of these systems depend on the form of inter-particle interactions, which unveil a variety of remarkable phenomena. Interacting Bose-Einstein condensates are naturally superfluid, thus can flow without viscosity similarly to the liquid helium. Phase coherence requires the velocity field to be irrotational, which permits the system to host permanent currents and quantized vortices. In this regard, the ultracold atomic BECs are captured by the same hydrodynamic theory of Landau, originally proposed for liquid helium.

In recent years, both experimental and theoretical attention has shifted toward dipolar gases, which are characterized by long-range and anisotropic potentials. With the possibility of changing the character of the interaction from attractive to repulsive, dipolar gases have been shown to host a variety of interesting phases, including the counter-intuitive supersolid phase. This long-sought feature uniting the frictionless flow and crystalline order has been achieved in trapped dipolar BECs only recently. This breakthrough has motivated the development of new microscopic theory and hydrodynamic frameworks, specifically tailored to capture the new state of matter.

In this chapter, we review fundamental theoretical concepts underlying the Bose-Einstein condensation, superfluidity and supersolidity. We begin with the microscopic theory of BECs, introducing the Gross-Pitaevskii equation, its relation to hydrodynamics and the resulting elementary excitation spectrum. In the following section, we focus on the macroscopic theory of superfluids - the Landau two-fluid model, and its connection to Bose-Einstein condensation. Then, we present the rich physics of dipolar gases, with the emphasis on their beyond-mean-field model, which is crucial for an accurate description of the supersolid phase. We conclude the chapter with a short introduction to linear response theory in quantum physics, which will be used throughout the thesis to measure the speed of sound in various systems.

1.1 Bose-Einstein Condensation

The phenomenon of Bose-Einstein condensation refers to the macroscopic occupation of a single quantum state. This basic formulation is the foundation for more advanced concepts underlying the quantitative description of Bose-Einstein condensates. In the context of ultracold gases, a BEC is primarily associated with two phenomena: the so-called off-diagonal

long-range order (ODLRO) and spontaneous breaking of the gauge symmetry. We will explore both in the following sections.

1.1.1 Off-diagonal Long Range Order

As for every many-body quantum system, the BEC is described within the formalism of a quantum field theory, where we introduce creation and annihilation operators acting on a Fock space. In the second quantization framework, Bose-Einstein condensation is characterized by the emergence of coherence across the system, which is manifested in the single-particle density matrix

$$n(\boldsymbol{r}, \boldsymbol{r}') = \langle \hat{\Psi}^\dagger(\boldsymbol{r}) \hat{\Psi}(\boldsymbol{r}') \rangle, \tag{1.1}$$

where the two bosonic field operators $\hat{\Psi}^\dagger(\boldsymbol{r})$ and $\hat{\Psi}(\boldsymbol{r}')$, respectively, create and annihilate one particle in the indicated position. The two fields follow the standard bosonic commutation rules:

$$[\hat{\Psi}(\boldsymbol{r}), \hat{\Psi}^\dagger(\boldsymbol{r}')] = \delta(\boldsymbol{r} - \boldsymbol{r}') \tag{1.2a}$$

$$[\hat{\Psi}(\boldsymbol{r}), \hat{\Psi}(\boldsymbol{r}')] = [\hat{\Psi}^\dagger(\boldsymbol{r}), \hat{\Psi}^\dagger(\boldsymbol{r}')] = 0 \tag{1.2b}$$

The density matrix (1.1) carries important information about the system. In particular, its diagonal elements $n(\boldsymbol{r}, \boldsymbol{r})$ define densities at position $\boldsymbol{r}$, whose integral yields the total number of particles N.

Bose-Einstein condensation refers to a macroscopic occupation of a single quantum state, which in equilibrium usually means the state of vanishing momentum $\boldsymbol{p} = 0$. In general, it can be any state that is indicated by the largest eigenvalue of the density matrix. To see how this phenomenon is reflected in the density matrix, we transform equation (1.1) into momentum space

$$n(\boldsymbol{p}, \boldsymbol{p}') = \langle \hat{\Psi}^\dagger(\boldsymbol{p}) \hat{\Psi}(\boldsymbol{p}') \rangle, \tag{1.3}$$

where $\hat{\Psi}(\mathbf{p}) = (2\pi\hbar)^{-3/2} \int d\mathbf{r}\, e^{-i\mathbf{p}\cdot\mathbf{r}/\hbar}\, \hat{\Psi}(\mathbf{r})$. In line with our observation, the $n(\boldsymbol{p}) \equiv n(\boldsymbol{p}, \boldsymbol{p})$ has a substantial contribution from the $\boldsymbol{p} = 0$ state, which can be singled out with a delta function:

$$n(\boldsymbol{p}) = n_0 \delta(\boldsymbol{p}) + \bar{n}(\boldsymbol{p}), \tag{1.4}$$

where, at a finite temperature, the $\bar{n}$ has a thermal distribution. The distinction above is crucial to understanding the unique indicator of the Bose-Einstein condensation. The δ peak at $\boldsymbol{p}$ will correspond to a constant once transformed back into the position space. In the thermodynamic limit, this means that the elements of the density matrix have a finite value as $|\boldsymbol{r} - \boldsymbol{r}'| \to \infty$. This off-diagonal long-range order is a unique feature of Bose-Einstein condensates and has become the defining criterion of the existence of the BEC in interacting Bose gases. In the limit of large distances, the density matrix elements define the condensate fraction:

$$n_0 = \lim_{|\boldsymbol{r} - \boldsymbol{r}'| \to \infty} n(\boldsymbol{r}, \boldsymbol{r}'), \tag{1.5}$$

which quantifies the number of particles comprising the BEC. Its value decreases with temperature and vanishes above the critical point. At temperatures close to zero, the condensate fraction takes the highest values, which for ultracold atomic gases is very close to unity. On the other hand, in strongly interacting systems like liquid helium, it does not exceed 10% [17].

1.1.2 Mean-field theory

Every quantum system is described by a dedicated theory, in which the equations of motion are derived from the action, built upon symmetry arguments and transformation properties. Bose-Einstein condensates are no exception. In this section, we present a simplified discussion on how to build the theory capturing Bose-Einstein condensation, using the second quantization formalism and applying a semi-classical approximation.

We begin with a general form of a many-body Hamiltonian with two-body interaction potential $U(\boldsymbol{r}, \boldsymbol{r}')$:

$$H = \int d\boldsymbol{r} \hat{\Psi}^\dagger(\boldsymbol{r}) \left[h_0(\boldsymbol{r}) + \frac{1}{2} \int d\boldsymbol{r}' \hat{\Psi}^\dagger(\boldsymbol{r}') U(\boldsymbol{r}, \boldsymbol{r}') \hat{\Psi}(\boldsymbol{r}') \right] \hat{\Psi}(\boldsymbol{r}). \tag{1.6}$$

where $h_0(\boldsymbol{r}) = \frac{\hbar^2}{2m}\nabla^2 + V_{ext}(\boldsymbol{r})$ is the single-particle Hamiltonian that includes the kinetic term and an external potential. The fields $\hat{\Psi}$ entering the Hamiltonian above have to follow the commutation relations (1.2), as they represent bosonic particles. The primary idea to simplify and tailor the equation (1.6) for Bose-Einstein condensates is to single out the condensate wavefunction $\hat{\Psi}_0$ from all other states. This approach is well justified at temperatures well below T_C, where the state corresponding to the operator $\hat{\Psi}_0$ is macroscopically occupied by N_0 particles. Moreover, since $N_0 \gg 1$, the commutation relation $[\hat{\Psi}_0(\boldsymbol{r}), \hat{\Psi}_0^\dagger(\boldsymbol{r})] = \delta(\boldsymbol{r} - \boldsymbol{r}')$ is irrelevant and one might as well assume that the two fields commute[1]. This observation leads to a semi-classical approximation, in which the condensate wavefunction $\hat{\Psi}_0$ is replaced by a c-number ψ. Therefore, we arrive with the ansatz for the fields:

$$\hat{\Psi} = \psi + \delta\hat{\Psi}, \tag{1.7}$$

where the field $\delta\hat{\Psi}$ contains all excited states, including quantum fluctuations characterizing the interaction between the condensate and other states. The relevance of this term, in the context of ground state properties, depends on the system under consideration. For a single Bose-Einstein condensate, it does not bring any significant change to the mean-field picture. However, its inclusion is crucial for the existence of the phase transition to the supersolid phase in dipolar BECs, as we shall see in the following sections. Regardless of the system, the excitation field $\delta\hat{\Psi}$ gives access to the collective properties of every platform. For this reason, we shall analyze them in the latter part of this introduction.

To study the time evolution of the bosonic gas, we need equations of motion, which are provided by the Heisenberg equation $i\hbar\partial_t\hat{\Psi} = \left[\hat{\Psi}, \hat{H}\right]$. Using the commutation relations for the bosonic field $\hat{\Psi}$, for the general many-body Hamiltonian (1.6), the Heisenberg equation reduces to:

$$i\hbar\partial_t\hat{\Psi}(\boldsymbol{r}) = \left(h_0(\boldsymbol{r}) + \int d\boldsymbol{r}' \hat{\Psi}^\dagger(\boldsymbol{r}') U(\boldsymbol{r}, \boldsymbol{r}') \hat{\Psi}(\boldsymbol{r}') \right) \hat{\Psi}(\boldsymbol{r}). \tag{1.8}$$

With the ansatz $\hat{\Psi}(\boldsymbol{r}, t) = \psi(\boldsymbol{r}, t) + \delta\hat{\Psi}(\boldsymbol{r}, t)$, where we now explicitly write the time-dependence of the fields, we obtain the mean-field approximation of the Heisenberg equation for the Bose-Einstein condensate:

$$i\hbar\partial_t\psi(\boldsymbol{r}, t) = \left(h_0(\boldsymbol{r}) + \int d\boldsymbol{r}' U(\boldsymbol{r}, \boldsymbol{r}') |\psi(\boldsymbol{r}', t)|^2 \right) \psi(\boldsymbol{r}, t), \tag{1.9}$$

[1] This approximation introduces a small error of the order $1/N_0$, which is negligible for large number of particles in the condensed state.

where we entirely omit the fluctuations $\delta\hat{\Psi}$. The equation above is a great starting point for building equations of motion for Bose-Einstein condensates of gases interacting with different potentials $U(\boldsymbol{r}, \boldsymbol{r}')$. Thus far we have not made any assumptions on the shape of this potential. Bose-Einstein condensates are primarily realized in ultracold platforms of weakly interacting dilute gases, suggesting that a good estimate for the shape of U can be found with the scattering theory. Indeed, particles that interact at small energy scales are well captured by s-wave scattering, in which only the $l = 0$ angular momentum states contribute to the scattering amplitude [18]. Since this type of interaction is isotropic, it is characterized by a single parameter, the s-wave scattering amplitude a_s. Finally, the interaction potential $U(\boldsymbol{r}, \boldsymbol{r}')$ in the weakly-interacting regime reads

$$U(\boldsymbol{r}, \boldsymbol{r}') = \frac{4\pi\hbar^2 a_s}{m}\delta(\boldsymbol{r} - \boldsymbol{r}'), \tag{1.10}$$

where the constant factor in front of the delta function is called the interaction coupling g. Due to its Dirac delta form, the contact interaction potential introduces another simplification of the equation of motion (1.9). For the weakly interacting Bose gas it reads

$$i\hbar\partial_t\psi(\boldsymbol{r}, t) = \left(\frac{\hbar^2}{2m}\nabla^2 + V_{ext}(\boldsymbol{r}) + g|\psi(\boldsymbol{r}, t)|^2\right)\ \psi(\boldsymbol{r}, t) \tag{1.11}$$

and is called the Gross-Pitaevskii equation. To a great extent, it resembles the Schrödinger equation, often called its nonlinear version. Because of its simplicity, it has become the standard tool for addressing Bose-Einstein condensates.

To conclude this section, let us discuss the normalization condition for the condensate wavefunction ψ. In line with the density matrix (1.1), we require that the square of the modulus of $\psi(\boldsymbol{r}, t)$ equals the density $n_0(\boldsymbol{r}, t)$. In this way, the condensate wavefunction is normalized to the total number of particles in the BEC: $\int d\boldsymbol{r}|\psi(\boldsymbol{r}, t)|^2 = N_0$. Since ψ is a complex function, it can be written as:

$$\psi(\boldsymbol{r}, t) = \sqrt{n_0(\boldsymbol{r}, t)}e^{i\phi(\boldsymbol{r},t)}, \tag{1.12}$$

where in the absence of currents the phase ϕ equals $-\mu t/\hbar$ [19]. After the phase transition to the condensed phase, the density n_0 becomes comparable with the total density of the system. For this reason the condensate wavefunction plays the role of the order parameter of the BEC phase transition.

Hydrodynamic Formulation of the Gross-Pitaevskii Theory

Let us now find the Gross-Pitaevskii Lagrangian and its corresponding action. We will later use them to discuss conservation laws and symmetries of Bose-Einstein condensates. It is straightforward to check that, by varying with respect to ψ^*, the following action produces the Gross-Pitaevskii equation:

$$S[\psi, \psi^*] = \int dt \int d^3\boldsymbol{r}\left(\frac{i\hbar}{2}(\psi^*\partial_t\psi + \psi\partial_t\psi^*) - \frac{\hbar^2}{2m}|\nabla\psi|^2 - V(\boldsymbol{r})|\psi|^2 - \frac{1}{2}g|\psi|^4\right). \tag{1.13}$$

The action above depends on two variables ψ and its complex conjugate ψ^*, which are treated as independent. Since ψ is a complex number, the same equation can be written with its amplitude and phase as the two independent variables. Using equation (1.12) (with

$\rho \equiv n_0$) the GPE action reads:

$$S[\rho,\theta] = \int dt \int d^3\boldsymbol{r} \left(\hbar\rho\partial_t\theta - \frac{\hbar^2}{2m}(\nabla\sqrt{\rho})^2 - \frac{\hbar^2}{2m}\rho(\nabla\theta)^2 - V(\boldsymbol{r})\rho - \frac{1}{2}g\rho^2 \right), \tag{1.14}$$

where ρ and θ depend on the time and space coordinates. Variation of this action with respect to the two variables gives:

$$\frac{\delta S}{\delta\theta} \implies \partial_t\rho + \nabla(\rho\nabla\theta) = 0 \tag{1.15a}$$

$$\frac{\delta S}{\delta\rho} \implies \hbar\partial_t\theta + \frac{\hbar^2}{2m}(\nabla\theta)^2 + V + g\rho - \frac{\hbar^2}{2m}\frac{\nabla^2\sqrt{\rho}}{\sqrt{\rho}} = 0, \tag{1.15b}$$

which are, respectively, the continuity equation and the Euler-like equation. They form the hydrodynamic theory of Bose-Einstein condensates, which is an alternative formulation of the GPE. The equation of continuity is, in fact, the Noether current associated with the conservation of total particle number. The term $\rho\nabla\theta$ corresponds to the mass current; therefore the phase gradient must give the velocity of the condensate $\boldsymbol{v} = \hbar\nabla\theta/m$. Since θ is a scalar function, the velocity of the condensate is irrotational $\nabla \times \boldsymbol{v} = 0$.

With the new interpretation of the phase, the Euler-like equation (1.15b) can be formulated in a more intuitive form. After taking the gradient of both sides, it becomes:

$$\partial_t\boldsymbol{v} + \partial_x\left(\frac{1}{2}v^2 + \frac{gn}{m} + \frac{V}{m} - \frac{\hbar^2}{2m^2}\frac{\nabla^2\sqrt{\rho}}{\sqrt{\rho}} \right) = 0. \tag{1.16}$$

The last term, called the quantum pressure, gives an important contribution only if the density varies rapidly on a short length scale. In the thermodynamic limit, this term is a higher-order correction and can be neglected. Furthermore, in the absence of an external potential, the acceleration of the condensate is driven by the gradient of the chemical potential $\mu = gn$. At zero temperature, the Gibbs-Duhem relation implies that this statement is equivalent to the momentum conservation law, in which the time evolution of the current $j = \rho v$ is given by the gradient of the pressure.

To conclude characterization of the Gross-Pitaevskii theory, let us remark that it is a non-relativistic description of Bose-Einstein condensates. In the absence of external potential, we require the condensate to be invariant with respect to Galilean transformations. Interestingly, this condition is fulfilled only if the wavefunction acquires an additional phase. Considering the following coordinate change $\{\boldsymbol{r}, t\} \to \{\boldsymbol{r} - \boldsymbol{v}t, t\}$, the condensate wavefunction in the moving frame of reference reads:

$$\psi(\boldsymbol{r},t) \;\to\; \psi(\boldsymbol{r}-\boldsymbol{v}t,t)e^{im\left(\boldsymbol{v}\cdot\boldsymbol{r}-\frac{1}{2}v^2t\right)/\hbar} \tag{1.17}$$

and the entire phase of the condensate in this reference frame reads:

$$\theta(\boldsymbol{r}',t) = \left[\left(-\mu - \frac{1}{2}mv^2 \right) t + m\boldsymbol{v}\cdot\boldsymbol{r} \right] /\hbar. \tag{1.18}$$

While the first term is just the chemical potential in the moving reference frame, the second element shows a position-dependent phase contribution, introduced by the finite velocity of the condensate. This observation is consistent with the definition of the velocity as the gradient of the phase θ.

1.1.3 Elementary excitations

The condensate wavefunction ψ gives the appropriate description of the Bose-Einstein condensate in equilibrium, or in a stationary state with a persistent current. Dynamical properties of the BEC, such as collective modes, require knowledge of the elementary excitation spectrum, which is derived using the out-of-condensate field $\delta\hat{\Psi}$. This field operator encapsulates all the excited states, which in the mean-field theory are completely neglected, leading to the Gross-Pitaevskii equation (1.9). Here we sketch the main points in the derivation of the theory underlying the lowest-energy excitations of ultracold gases, the Bogoliubov theory. Its detailed description can be found in various sources [19–22].

We begin with the Heisenberg equation (1.8) and employ the same ansatz for the field $\hat{\Psi} = \psi + \delta\hat{\Psi}$. This time, we keep all terms linear in $\delta\hat{\Psi}$, which leads to:

$$\begin{aligned} i\hbar\partial_t\, \delta\hat{\Psi}(\boldsymbol{r}) &= h(\boldsymbol{r})\delta\hat{\Psi}(\boldsymbol{r}) \\ &+ \int d\boldsymbol{r}' U(\boldsymbol{r},\boldsymbol{r}') \left[|\psi(\boldsymbol{r}')|^2\, \delta\hat{\Psi}(\boldsymbol{r}) + \left(\psi^*(\boldsymbol{r}')\delta\hat{\Psi}(\boldsymbol{r}') + \psi(\boldsymbol{r}')\delta\hat{\Psi}^\dagger(\boldsymbol{r}') \right) \psi(\boldsymbol{r}) \right], \end{aligned} \tag{1.19}$$

where $h = h_0 - \mu$ and the mean-field part (1.9) was already subtracted. The equation above characterizes the time evolution of the elementary excitations. It is usually expressed in another form, using the Bogoliubov transformation:

$$\delta\hat{\Psi}(\boldsymbol{r},t) = \sum_i^\infty \left[u_i(\boldsymbol{r},t)e^{-i\omega_i t}\hat{\alpha}_i + v_i^*(\boldsymbol{r},t)e^{i\omega_i t}\hat{\alpha}_i^\dagger \right], \tag{1.20}$$

where one introduces the quasiparticle annihilation operator $\hat{\alpha}_i$ such that the mean-field ground state is its vacuum. Together with the corresponding creation operator $\hat{\alpha}_i^\dagger$, they satisfy the regular bosonic commutation relations $[\hat{\alpha}_i, \hat{\alpha}_j^\dagger] = \delta_{ij}$ and $[\hat{\alpha}_i, \hat{\alpha}_j] = 0$. These commutation relations impose the orthogonality conditions on the Bogoliubov amplitudes u_i and v_i:

$$\sum_i^\infty \left[u_i(\mathbf{r}',t)u_i^*(\mathbf{r},t) - v_i(\mathbf{r},t)v_i^*(\mathbf{r}',t) \right] = \delta(\mathbf{r}-\mathbf{r}') \tag{1.21a}$$

$$\sum_i^\infty \left[u_i(\mathbf{r}',t)v_i^*(\mathbf{r},t) - u_i(\mathbf{r},t)v_i^*(\mathbf{r}',t) \right] = 0. \tag{1.21b}$$

The general form of equation (1.19) after the Bogoliubov transformation is highly complicated because the amplitudes u_i and v_i are position-dependent. For slowly varying amplitudes, one can use local density approximation that leads to semi-classical results [23], which is valid for most common experimental setups [24–27]. As a didactic example and a proof-of-concept, we will consider a uniform system in which Bogoliubov amplitudes are conveniently labeled with momentum $\boldsymbol{k}$. In such geometries, the equations of motion for the elementary excitations are simplified to the following matrix equation [19, 22]:

$$\begin{pmatrix} \frac{\hbar^2\boldsymbol{k}^2}{2m} + |\psi|^2\tilde{U}(\boldsymbol{k}) & |\psi|^2\tilde{U}(\boldsymbol{k}) \\ -|\psi|^2\tilde{U}(\boldsymbol{k}) & -\frac{\hbar^2\boldsymbol{k}^2}{2m} - |\psi|^2\tilde{U}(\boldsymbol{k}) \end{pmatrix} \begin{pmatrix} u_{\boldsymbol{k}} \\ v_{\boldsymbol{k}} \end{pmatrix} = \epsilon(\boldsymbol{k}) \begin{pmatrix} u_{\boldsymbol{k}} \\ v_{\boldsymbol{k}} \end{pmatrix}, \tag{1.22}$$

where the energy of the quasiparticles depends explicitly on the interaction potential in Fourier space $\tilde{U}(\boldsymbol{k})$ and reads

$$\epsilon(\boldsymbol{k}) = \sqrt{\frac{(\hbar\boldsymbol{k})^2}{2m}\left(\frac{(\hbar\boldsymbol{k})^2}{2m} + 2|\psi|^2\tilde{U}(\boldsymbol{k}) \right)} \tag{1.23}$$

Thus, the shape of the excitation spectrum is characterized by the interaction potential. For most of the systems, the energy exhibits a linear momentum dependence at small momenta, which is referred to as the phonon regime. Analogously to the solid state theory, the slope of the linear part of the excitation spectrum corresponds to the speed of sound. Depending on the type of the system, there can be one or multiple phonon branches of different slopes. In weakly interacting Bose gases, the dispersion law has only one branch of phonon-like dependence at low momenta and particle-like excitations for $\boldsymbol{k} \to \infty$. An example of the elementary excitation spectrum for such a gas is shown in Fig. (1.1).

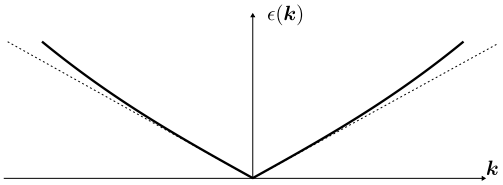

Figure 1.1: Bogoliubov spectrum of elementary excitations for a weakly interacting Bose gas. Dotted line exposes the deviation from linear dependence for large momentum wavevectors.

In weakly interacting Bose gas, particles interact via the contact potential characterized by the delta function, which in momentum space reads $\tilde{U}(\boldsymbol{k}) = g$. This gives the speed of sound

$$c = \lim_{k \to 0} \frac{\epsilon}{\hbar k} = \sqrt{\frac{gn}{m}}, \tag{1.24}$$

which was measured in several experiments [28–31]. Notably, in trapped systems, where the density profile is not uniform, the formula above requires a proper value of the density. Since the entire gas contributes to the propagation of sound, one must average the density in the transverse direction with respect to the sound wavevector. In harmonic traps, this procedure yields $c = \sqrt{gn_0/(2m)}$, where n_0 is the peak density [32].

1.1.4 Spontaneous symmetry breaking

Symmetry plays a central role in modern physics as it is the starting point for building theories accounting for all physical phenomena. Of all the symmetry transformations, the continuous symmetries are of particular interest as their identification leads to the determination of conserved currents and charges owing to the Noether's theorem. In quantum field theory, one is often interested in breaking these symmetries. This can be done in two ways; either by introducing a term in the Hamiltonian that explicitly breaks the symmetry, or by a phase transition, where the symmetry is broken spontaneously. The second way is more intriguing as the Hamiltonian, and thus the equations of motion remain invariant with respect to the symmetry transformation, but it is the state that breaks it. Strictly speaking, it is the vacuum which disobeys the symmetry, which means any state constructed with it, not only the ground state, will exhibit the broken symmetry features.

The Bose-Einstein condensation is an effect associated with a phase transition in which the global gauge symmetry is broken spontaneously. To illustrate this point, let us first observe that the Gross-Pitaevskii equation (1.11) is invariant under the U(1) gauge transformation

$$\psi(\boldsymbol{r}, t) \to \psi(\boldsymbol{r}, t) e^{i\alpha}, \tag{1.25}$$

where $\alpha \in \mathbb{R}$. In the mean-field theory, one neglects all excited states and assumes that every particle is in the state given by the condensate wavefunction. The ψ is a complex function of a certain phase θ, which in principle could be different for all particles occupying this state. However, since the Gross-Pitaevskii equation contains the nonlinear term $|\psi|^2$, any phase difference between two particles introduces interference terms that lead to the energy increase. Thus, it is energetically preferable that all particles in an interacting Bose-Einstein condensate are phase coherent. For this reason, the gauge symmetry is broken in a spontaneous manner.

The spontaneous breaking of the U(1) symmetry characterizes the BEC as a matter-wave, since, due to its coherence, it exhibits properties of a regular wave. Among these properties, the interference of two Bose-Einstein condensates has been studied most commonly [33–35], as it has promising properties for potential quantum technological applications [36, 37].

The phenomenon of spontaneous symmetry breaking has an important consequence in terms of the elementary excitation spectrum of Bose-Einstein condensates. By the Goldstone theorem, for every broken continuous symmetry, there appears one gapless mode - the Nambu-Goldstone boson [38]. In the context of Bose-Einstein condensation, the gauge symmetry is broken spontaneously after the system undergoes the phase transition. Then, the excitation spectrum develops a linear momentum dependence in the long-wavelength limit. Therefore, the phonon, which we have discussed in the previous section, is identified as the Nambu-Goldstone boson.

1.1.5 Binary BEC mixtures

Bose-Einstein condensates are nowadays routinely realized in experimental platforms, predominantly using dilute ultracold atoms. The emergence of this phenomenon, along with its characteristic properties, stems from a fundamental aspect of quantum mechanics: the indistinguishability of individual particles. In order to create a BEC, a macroscopic number of atoms must occupy the same spin state of the the same isotope. Advancements in laser cooling and trapping techniques enabled the exploration of condensates of two or more spin states of the same atomic species or even a mixture of different atomic types. In this section, we briefly characterize the most prominent features of these systems.

The most commonly realized mixtures consist of two hyperfine states of the same atomic species. Once cooled below the critical temperature, each component undergoes the phase transition to the Bose-condensed state. Since the particles, and thus the condensed state, differ in the spin state, the system is composed of two Bose-Einstein condensates. Theoretically, this mixture is understood in terms of two Gross-Pitaevskii equations, coupled by the inter-species potential of the Dirac delta form. This potential is characterized by a coupling constant g_{12}, which is in principle different from the two intra-species ones g_{11} and g_{22}, but it is still given by the corresponding s-wave scattering length. With the use of Feshbach resonances, all three parameters can be tuned to desired values. To avoid collapse, the two constants g_{11} and g_{22} must be positive, while g_{12} can have an arbitrary value.

The collective nature of Bose mixtures, which will be one of the subjects of this thesis, is conveniently classified in terms of density and spin oscillations. Using single-component densities n_i, we define the total density as $n = n_1 + n_2$, the spin density as $s_z = n_1 - n_2$

and the appropriate coupling constants:

$$g = (g_{11} + g_{22})/2 \tag{1.26a}$$
$$g_{ds} = (g_{11} - g_{22})/2 \tag{1.26b}$$
$$g_d = (g + g_{12})/2 \tag{1.26c}$$
$$g_s = (g - g_{12})/2. \tag{1.26d}$$

For a generic homogeneous Bose mixture, the equation of state can be written as [39]

$$\mathcal{E} = \frac{1}{2} g_d n^2 + \frac{1}{2} g_s s_z^2 + \frac{1}{2} g_{ds} n s_z \tag{1.27}$$

The interaction energy above separates the phase diagram of binary BECs into two sectors: the miscible and immiscible ones. The stability of the miscible phase requires the energy to be a convex function of the two densities n and s_z. Using equation (1.27), the stability condition reads:

$$\Delta = 4 g_d g_s - g_{ds}^2 \geq 0, \tag{1.28}$$

which in the single-component notation is $g_1 g_2 - g_{12}^2 \geq 0$.

As we have already observed, the two atomic clouds form different Bose-Einstein condensates after crossing the phase transition. As a result, the system breaks two gauge symmetries, giving rise to two order parameters. According to the Goldstone theorem, there are two gapless modes in binary BEC mixtures. Analogously to the single-component BEC, both modes are phonons, each corresponding to a dedicated linear branch of the elementary excitation spectrum. Therefore, these systems host two sound modes, each characterized by a different speed. Using Bogoliubov theory, one can demonstrate [19, 40], that the two speeds of sound are given by:

$$c_{d/s}^0 = \left[\frac{g n + g_{ds} s_z \pm \sqrt{(g n + g_{ds} s_z)^2 - \Delta (n^2 - s_z^2)}}{2m} \right]^{1/2} \tag{1.29}$$

and have been found in good agreement with experiments [41–43]. The nature of these sounds is very complex, as they are strongly hybridized. In the limit of a non-interacting mixture, when $g_{12} = 0$, the equation (1.29) reduces to $\sqrt{g_{ii} n_i / m}$ and the two modes coincide with single-component density oscillations. On the other hand, when the gas exhibits $\mathbb{Z}_2$ symmetry ($g_{ds} = s_z = 0$), the two sound modes are purely total density and spin density oscillations. For the sake of notation, we will use the d (s) subscript to refer to the sound mode (1.29) with the $+$ ($-$) sign and call it *density-like* (*spin-like*) mode [2].

[2] If g_{12} were negative $\pm$ in the Eq. (1.29) has to be replaced by $\mp$.

1.2 Superfluidity

Every classical fluid has a certain degree of viscosity - the vicious property of dissipating currents due to internal collisions between the particles. However, quantum effects, closely related to the Bose-Einstein condensation lead to entire elimination of viscosity allowing for the existence of permanent currents. In this section, we will review the most fundamental concepts of the hydrodynamic theory of superfluids - the two fluid model.

1.2.1 The Landau criterion

The unusual lack of viscosity exhibited by the superfluid helium while flowing through narrow capillaries has raised the need for a general condition unequivocally providing the answer when such a phenomenon can occur. This condition was found by Landau in 1941 [18], who used a general argument based on the Galilean transformation of the energy of a generic fluid. The derivation of the Landau criterion is important not only to understand when a fluid becomes superfluid, but also to show how the elementary excitation spectrum is affected by the velocity field.

Let us consider a fluid in a reference frame K, of energy E and momentum $\boldsymbol{P}$. The Galilean transformation specifies these two quantities in the frame K' moving with respect to K with velocity V. Straightforward calculations yield the following relation

$$E' = E - \boldsymbol{P}\cdot\boldsymbol{V} + \frac{1}{2}MV^2, \qquad \boldsymbol{P}' = \boldsymbol{P} - M\boldsymbol{V}, \tag{1.30}$$

where M is the mass of the fluid. In a superfluid, the kinetic energy is conserved as the flow is inviscid and the only dissipative processes require creation of elementary excitations. Let the K reference frame be the fluid's rest frame. If an excitation of momentum $\boldsymbol{p}$ and energy $\epsilon(\boldsymbol{p})$ is created, the total energy and momentum of the gas are given by $E = E_0 + \epsilon(\boldsymbol{p})$ and $\boldsymbol{p}$ respectively. In order to see how the energy of the elementary excitation changes with the frame of reference its optimal to choose the laboratory frame as the new K'. Here, the laboratory frame moves with velocity $-\boldsymbol{V}$ relative to K and the formula (1.30) becomes

$$E' = E_0 + \epsilon(\boldsymbol{p}) + \boldsymbol{p}\cdot\boldsymbol{V} + \frac{1}{2}MV^2, \qquad \boldsymbol{p}' = \boldsymbol{p} + M\boldsymbol{V}. \tag{1.31}$$

The equation above reveals that the elementary excitation energy in the reference frame K' is

$$\epsilon'(\boldsymbol{p}) \equiv \epsilon(\boldsymbol{p}) + \boldsymbol{p}\cdot\boldsymbol{V}. \tag{1.32}$$

This relation is key to understand when a superfluid may remain inviscid. Since we are considering dissipative processes induced by elementary excitations, the superfluid flow is permanent if $\epsilon'(\boldsymbol{p})$ is positive. Equivalently, dissipation appears once it becomes energetically favorable to create elementary excitations. This statement leads to the Landau criterion for the superfluid velocity:

$$V_c = \min_{\boldsymbol{p}} \frac{\epsilon(\boldsymbol{p})}{|\boldsymbol{p}|}. \tag{1.33}$$

The critical velocity V_c sets the upper limit for the relative velocity of the superfluid and the container. Its precise value is system-dependent, and requires that the function $\epsilon(\boldsymbol{p})/\boldsymbol{p}$ has a minimum greater than zero for the fluid to become inviscid. In weakly interacting BECs, the V_c equals the speed of sound, as inferred from the Bogoliubov excitation spectrum (1.23). On the other hand, superfluid helium (and also dipolar BECs) exhibit a roton minimum, which effectively lowers the critical velocity.

To conclude this section, let us remark that equation (1.32) provides the formula for the dispersion law in a uniform superfluid system moving with velocity $\boldsymbol{V}$. Therefore, if $\epsilon(\boldsymbol{p})$ involves a linear part at small $|\boldsymbol{p}|$, its slope - corresponding to the speed of sound - will change by $\pm|V|$. This is precisely the Doppler effect caused by permanent currents. One of the key findings of this thesis is that this shift is in general not given by $\pm|V|$, provided that the system consists of two fluids hosting a relative velocity. To identify the systems in which such properties can emerge, let us review the hydrodynamic model of superfluidity.

1.2.2 The two-fluid model

Experimental evidences unequivocally showed that the classical hydrodynamic theory alone cannot account for the peculiar behavior of liquid helium at low temperatures. This fact was immediately understood by Tisza [44] and Landau [45], who developed a new hydrodynamic theory, tailored for the liquid helium - the two-fluid model. The macroscopic theory of Landau is based on the assumption that a superfluid at finite temperature is a mixture of an inviscid superfluid and the normal component, which behaves as a regular fluid and carries all the entropy. Then, the total density ρ and current $\boldsymbol{j}$ consist of two parts:

$$\rho = \rho_s + \rho_n \tag{1.34}$$

$$\boldsymbol{j} = \rho_s \boldsymbol{v}_s + \rho_n \boldsymbol{v}_n, \tag{1.35}$$

where ρ_n and $\boldsymbol{v}_n$ (ρ_s and $\boldsymbol{v}_s$) are the normal (superfluid) density and the normal (superfluid) velocity, respectively. In this model the motion of the two components is independent, which enables counter-flow between the two currents. While in the two-fluid model there are no constraints on the value of the normal velocity, the superfluid velocity is postulated to be irrotational $\nabla \times \boldsymbol{v}_s = 0$.

The complete set of hydrodynamic equations contains the dynamics of the density of the conserved quantities and of the order parameters [46]. In line with classical hydrodynamics, we require the two-fluid model to conserve the mass by imposing the continuity equation:

$$\partial_t \rho + \nabla \cdot \boldsymbol{j} = 0, \tag{1.36}$$

which ensures that the density at a given point in space can be changed only with spatially varying mass current. Furthermore, we require the momentum to be conserved as well with:

$$\partial_t j_i + \partial_{x_j} \Pi_{ij} = 0, \tag{1.37}$$

where the momentum flux density tensor $\Pi_{ij} = \rho_s v_{si} v_{sj} + \rho_n v_{ni} v_{nj} + p\delta_{ij}$ and p is the pressure. Equation (1.37) is the first equation characterizing the motion in the two-fluid model. Since it describes the evolution of the total current, the second equation of motion should concern either the normal or the superfluid part separately. To construct it, one assumes the acceleration of the superfluid (in its rest frame) is given by the gradient of some scalar function

$$(\partial_t + \boldsymbol{v}_s \cdot \nabla)\boldsymbol{v}_s = -\nabla\Phi, \tag{1.38}$$

where this scalar function turns out [20] to be the chemical potential μ_s in the superfluid rest frame. Its relation to the rest frame chemical potential μ is given by $\mu_s - \mu = v_n v_s - \frac{1}{2} v_s^2$ [20, 47]. The last hydrodynamic equation in the two-fluid model at finite temperature is the entropy conservation. Similarly to the mass conservation law (1.36), the entropy changes only with the divergence of its flux. The latter is given by the normal velocity, as the superfluid part does not carry any entropy:

$$\partial_t s + \nabla\,(s\boldsymbol{v}_n) = 0 \tag{1.39}$$

There is actually another conserved quantity - the energy. Its conservation law was initially necessary to evaluate the form of the momentum flux tensor Π_{ij} and to find the scalar function Φ in eq. (1.38). For this reason, its inclusion in the two-fluid model is redundant.

The four equations (1.36)-(1.39) constitute the two-fluid model developed by Landau to account for the dynamics of the superfluid helium. Among the most successful predictions of this theory, the explanation of the second sound deserves a special recognition. Apart from the 'regular', pressure-density first sound, in superfluid helium there exists a second sound mode associated with the entropy wave. The speed of the second sound reads:

$$c_2^2 = \sigma^2 \frac{\rho_s}{\rho_n} \left(\frac{\partial \sigma}{\partial T} \right)^{-1}, \tag{1.40}$$

where $\sigma = s/\rho$. It strongly depends on temperature and vanishes above the Lambda point. Remarkably, this sound mode is undamped, and thus long-wavelength thermal excitations are long-lived. This property is specific to systems exhibiting superfluid behavior.

1.2.3 Bose-Einstein condensation and superfluidity

After its discovery, superfluidity was speculated to be related to Bose-Einstein condensation. Although the two phenomena are indeed deeply connected, they are not synonymous. This can be seen from the hydrodynamic formulation of the Gross-Pitaevskii theory. Provided that the quantum pressure term is negligible, the two equations (1.15) correspond to the two-fluid model of Landau in the absence of the normal part. Indeed, in such a case, the equation (1.36) coincides with (1.15a) and the Josephson equation (1.38) is precisely (1.15b). In this comparison, we identified the velocity of the condensate with the superfluid velocity, as they are both irrotational. This correspondence is well justified if all the variables are slowly varying in space. Therefore, interacting Bose-Einstein condensates are indeed superfluid and, in the long-wavelength limit, can be described by the two-fluid model. With certain modifications, equations (1.36)-(1.39) are also applicable to other systems like superfluid mixtures or supersolids. We will investigate them in the following chapters of this thesis.

The connection between microscopic GPE theory and the macroscopic two-fluid model suggests that there is a correspondence between coherent and superfluid behavior. Although coherent quantum systems are typically superfluid, there are several exceptions, which prevent the two phenomena from being synonymous. The most prominent example of a fully superfluid gas with little coherence is the liquid helium. At temperatures close to zero, the normal part is negligibly small, yet the condensate fraction remains smaller than 10% [17]. Another superfluid system, which is not Bose-condensed is the 2D ultracold gas at finite temperature. Although it may host quantized vortices, the off-diagonal long-range order is precluded by the Hohenberg-Mermin-Wagner theorem [48, 49].

Similarly, there exist systems that are fully coherent but not superfluid. Such gases are characterized by a spatially modulated density profile. In his seminal work [3], Leggett showed that a coherent system of a non-uniform density cannot be entirely superfluid. He introduced the concept of superfluid fraction, which quantifies how much a given system effectively behaves as a superfluid. In a ring geometry, whose width is much smaller than its radius, the upper bound for the superfluid fraction reads:

$$f_s \equiv \frac{\rho_s}{\rho} \leq \left(\frac{1}{2\pi} \int_0^{2\pi} d\varphi \frac{\langle \rho \rangle}{\rho(\varphi)} \right)^{-1} \tag{1.41}$$

where φ is the azimuthal angle. By the Cauchy-Schwarz inequality, the f_s is always smaller or equal than one. The equality condition $f_s = 1$ is satisfied only if the density profile is

uniform. Thus, even though density modulated Bose-Einstein condensates are fully coherent, they are not entirely superfluid. The remaining part effectively acts as a normal fluid. It is worth stating that the discrimination between the superfluid and the normal part of a density-modulated BEC cannot be done on a microscopic level. It is impossible to tell which part of the wavefunction corresponds to the normal part and which is responsible for the superfluid behavior. The concept of the superfluid fraction is inherently macroscopic; therefore it can be related to the microscopic variables only via proper averages (1.41).

1.2.4 Non-Classical Rotational Inertia

Superfluids are characterized by the irrotational velocity field, which in closed geometries, such as rings, precludes the existence of a state with an arbitrary supercurrent. The quantization of the current comes from the definition of the superfluid velocity as a gradient of the phase of the condensate wavefunction. We require that the phase is single-valued, which means that the boundary conditions for the phase allow it to differ only by a integer multiplication of 2π. This leads to the following current quantization:

$$\oint \boldsymbol{v}_s \cdot d\boldsymbol{l} = \frac{\hbar}{m} \oint \nabla\theta \cdot d\boldsymbol{l} = 2\pi \frac{\hbar}{m} n \tag{1.42}$$

where $n \in \mathbb{Z}$ and the integration is done over the circumference of the ring. Therefore, a permanent current originates from the twisted boundary condition for the phase of the order parameter.

How does the phase change in the presence of a small rotation? In a reference frame rotating with a small angular velocity ω, eq. (1.18) suggests that the phase of a superfluid in a ring container develops a linear pattern, whose boundary conditions are not sufficed $\theta(\varphi) \neq \theta(\varphi + 2\pi)$. Such a phase twist violates the condition of single-valuedness of the phase and leads to the energy increase. For this reason, the superfluid does not rotate at small angular velocities. Consequently, superfluidity can be defined as a (lack of) response to a small rotation. In a mixture of a superfluid and a normal gas, which happens at finite temperatures or in spatially modulated superfluids, this property enables the assessment of how much the system behaves like a superfluid. At small angular velocities, only the normal part will rotate, thus, by measuring the angular momentum, one can calculate the superfluid fraction as the non-classical rotational inertia (NCRI):

$$f_s = \lim_{\omega \to 0} 1 - \frac{\langle L_z \rangle}{I_{cl}\ \omega}, \tag{1.43}$$

where for a ring of negligible width, the classical moment of inertia reads NmR^2, with N - the particle number, each of mass m, and R is the radius of the ring. The limit of small ω is important to avoid effects of mass distribution due to the centrifugal force.

In density-modulated superfluids, the relation between the upper bound (1.41) and the superfluid fraction calculated as NCRI depends on the density profile. If the density can be factorized with respect to each coordinate as $\rho(\boldsymbol{r}) = \Pi_i \rho_i(r_i)$, then the two quantities are equal [50] and also coincide with the lower bound of the superfluid fraction [51].

Although we focused on a ring superfluid, all properties presented in this section are also valid in other geometries. The quantized current in a ring is actually equivalent to a quantized vortex in any other simply-connected geometry, like a harmonic trap. For this reason, one may consider the appearance of the quantized current as the emergence of the vortex in the center of the ring.

1.3 Dipolar gases and supersolidity

Following the discovery of the superfluid phase in liquid helium, it was natural to ask whether similar phenomena could occur in solids, yielding a new state of matter called a supersolid. In their seminal work [52], Penrose and Onsager initially dismissed this possibility, arguing that a crystal composed of localized particles could not exhibit off-diagonal long-range order — the hallmark of Bose-Einstein condensation. Shortly after, Andreev and Lifshitz [1], followed by Chester [2], proposed a different theory of supersolidity, based on condensation of lattice defects and vacancies. In this model, the superfluid behavior is not assigned to the particles that form the lattice, but to the vacancies, which also posses Bose-Einstein statistics. Under sufficiently low temperatures, they were predicted to form an interacting BEC, which eventually would provide the superfluid properties for the solid helium.

However, experimental efforts to detect superflow in solid helium under a pressure gradient [53–55] failed to confirm the validity of this theory. Subsequent experiments attempted to confirm the superfluid nature of a rotating solid helium by measuring the reduced rotational inertia [56–59]. The initial claim of observing supersolid helium was retracted a few years later [60] by the same authors, who found a classical explanation for the reduction of the rotational inertia. Therefore, despite decades of extensive investigation, the supersolid phase of helium remains unconfirmed, as is the theory of superfluid crystal defects.

Thanks to a substantial progress in laser cooling techniques over the last few decades, helium is not the only superfluid system in which one can pursue the supersolid phase. Platforms based on ultracold atoms provide many advantages over liquid helium, such as tunable interactions or long-range dipolar interactions given by the magnetic moment of atoms. It is especially the latter that led the ultracold society to pursue the search for the supersolid phase, successfully found by three independent experiments [6–8] in recent years. Theoretical studies of the dispersion law of dipolar gases revealed that under specific conditions the system develops density modulations as a result of energetic instability [61]. This phenomenon is associated with spontaneous breaking of the translational symmetry, thanks to which the system acquires the properties of a solid. Therefore, the supersolid phase of ultracold dipolar gases differs from the one proposed by Andreev and Lifshitz. In contrast to the solid ^{4}He, where each atom constitutes a separate lattice site, in a dipolar supersolid there can be a macroscopic number of atoms occupying one lattice site. In fact, since the whole gas is coherent, every lattice site consists of a macroscopic number of atoms because their wavefunctions are spread over the entire system.

In this section, we review the physics of supersolids, with special emphasis on ultracold dipolar gas platforms. We present the microscopic theory, based on the Gross-Pitaevskii equation, highlight the role of the quantum fluctuations and discuss the dispersion relation. Finally, we will introduce the hydrodynamic theory of supersolids, which will be used to derive the speed of sound.

1.3.1 Dipolar Bose-Einstein condensates

The physics of Bose-Einstein condensates of alkali atoms is inherently interesting because of their coherent nature. However, with the advent of ultracold dipolar atoms brought to degeneracy, the field has expanded and opened up novel exciting possibilities. Following the pioneering realization of the chromium ^{52}Cr condensate [62], the experimental efforts shifted toward ultracold ^{164}Dy [63] and ^{166}Er [64], which have a larger dipolar moment and for that reason became the most commonly studied dipolar gases. Bose-Einstein condensates of these two isotopes were demonstrated to exhibit many interesting features, among which

the supersolid phase is the most notable.

The new attributes arise mainly because of the anisotropy and long-range nature of the dipolar potential. As a result, many properties are sensitive to the relative alignment of the dipoles and thus can be externally tuned to desired values. For two magnetic dipoles $\boldsymbol{d_1}$ and $\boldsymbol{d_2}$, separated by distance $\boldsymbol{r}$, the dipolar potential is given by

$$V_{dd}(\boldsymbol{r}) = \frac{C_{dd}}{4\pi} \frac{(\boldsymbol{d_1} \cdot \boldsymbol{d_2})\boldsymbol{r}^2 - 3(\boldsymbol{d_1} \cdot \boldsymbol{r})(\boldsymbol{d_2} \cdot \boldsymbol{r})}{|\boldsymbol{r}|^5}, \tag{1.44}$$

where the amplitude $C_{dd} = \mu_0 \mu^2$ scales quadratically with the magnetic moment μ and μ_0 denotes the magnetic permeability of the vacuum. The strength of dipolar interactions in a condensate of ultracold atoms is limited by μ, which is determined by the electronic structure of a given isotope, and is given by

$$\mu = g_J \mu_B J, \tag{1.45}$$

where J is the total angular momentum, μ_B is the Bohr magneton and g_J is the Landé g-factor. Among all the elements, the ^{164}Dy has the largest value of the magnetic moment $\mu \approx 10\mu_B$, while for erbium it is slightly lower $\mu \approx 7\mu_B$. Thus, the strength of these interactions in dipolar gases is bounded from above by the availability of stable isotopes with high angular momenta states. Aside from the magnetic moment, the same long-range potentials may be realized with molecules possessing a permanent and tunable electric dipole moment. The first experiments on molecular BECs were reported in 2008 [65], but two- and three-body losses significantly reduced the lifetime of these systems. Recent progress in shielding techniques [66, 67] enabled the first realization of dipolar molecules of NaCs with reported lifetime exceeding 1s [68]. The greatest advantage of molecular dipoles with respect to lanthanides is that their electric moment can be even two orders of magnitude larger. Since the amplitude of the dipolar potential (1.44) scales quadratically with the dipole moment, molecular condensates offer much stronger long-range interactions. Exploration of these strongly interacting part of the phase diagram is predicted to reveal new, interesting phases of matter [69, 70].

The most prominent feature of dipolar interactions is their anisotropy. To demonstrate its utility, let us consider the usual setup, where all dipoles are aligned along a common z-axis. The dipolar potential (1.44) is simplified to the following expression:

$$V_{dd}(\boldsymbol{r}) = \frac{C_{dd}}{4\pi} \frac{1 - 3\cos^2\theta}{r^3}, \tag{1.46}$$

where θ is the angle between the separation vector $\boldsymbol{r}$ and the polarization axis $\hat{z}$. In Fig. (1.2) we schematically show how the dipolar potential changes with the relative angle θ. For $\theta \in (\theta_{cr}, \pi - \theta_{cr})$, where $\theta_{cr} = \arccos(1/\sqrt{3})$, the interaction is repulsive, reaching its maximum value for $\theta = \pi/2$, when the two dipoles are side by side. On the other hand, attractive interaction is achieved by aligning the dipoles at an angle $\theta \in (0, \theta_{cr}) \cup (\pi - \theta_{cr}, \pi)$. The strongest attraction corresponds to the head-to-tail configuration, when $\theta = 0$. The critical angle θ_{cr} separates the two domains, and for this particular value, the dipoles do not interact. The anisotropy leads to the appearance of interesting phenomena like the magnetostriction effect, where the cloud takes an elongated form in the direction of the dipole orientation [71]. It also significantly changes the elementary excitation spectrum, which ultimately leads to the supersolid phase. In order to appreciate all the effects exhibited by dipolar Bose-Einstein condensates, we need to use their microscopic theory.

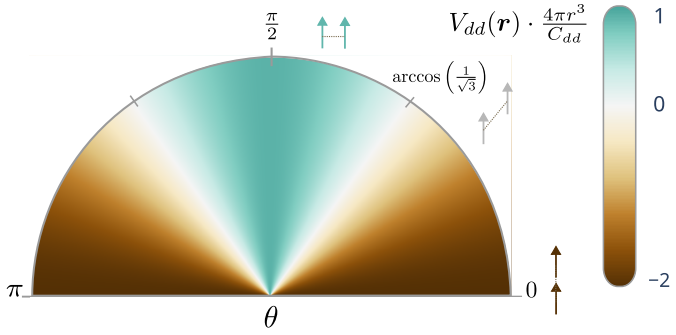

Figure 1.2: Dipole-dipole interaction potential (1.46) dependence on the angle θ between the dipole orientation axis z and their separation vector $\boldsymbol{r}$.

1.3.2 Mean-field and beyond

The microscopic description of dipolar Bose-Einstein condensates is based on the mean-field Gross-Pitaevskii theory (1.9), where along the contact interaction, the dipolar potential (1.46) must also be included. In order to assess the relative strength of the two potentials we first introduce the dipolar length:

$$a_{dd} = \frac{mC_{dd}}{12\pi\hbar^2}, \tag{1.47}$$

which is fixed for a given isotope. For ^{164}Dy, its value is approximately equal $131a_0$, where a_0 is the Bohr radius. The s-wave scattering length can be tuned using Feshbach resonances to reach any values around the a_{dd}. The stability of the system depends on the ratio of these two lengths; therefore, it is useful to introduce it as the relative interaction strength:

$$\varepsilon_{dd} = \frac{a_{dd}}{a_s} \tag{1.48}$$

In the mean-field theory, the system is stable if the two interactions are repulsive, with the short-range potential being dominant. If $\varepsilon_{dd} > 1$, i.e. when the dipolar repulsion becomes stronger than short-range interactions, the mean-field theory predicts an energetic instability [23] and the system collapses [72–75]. Once stability is assured, one can study the effects of anisotropic and long-range interactions in dipolar BECs. The most prominent change with respect to alkali condensates, observed in trapped systems, is the elongation of the cloud in the direction of the dipole orientation. Due to magnetostriction, even if the external potential is isotropic, the aspect ratio of the cloud changes considerably with ε_{dd} [76]. The anisotropy is also manifested in the excitation spectrum [77–79], and thus the speed of sound [80].

The mean-field theory of dipolar BECs has been shown to be in good agreement with experiments provided that ε_{dd} is smaller than 1. However, in the regime, where it predicts the system to collapse, the results differed depending on the atomic species used in experimental setups. Initially, chromium condensates were shown to collapse once the s-wave scattering length was quenched to violate the stability condition [74]. Since the dipolar interaction strength in ^{164}Dy gases is approximately two times larger than in chromium, the same experiment was repeated in dysprosium BEC, yielding a contradictory result [81]. Interestingly, after crossing the $\varepsilon_{dd} = 1$ point, the dipolar BEC, instead of collapsing, formed a

relatively stable ensemble of macroscopic droplets. The resulting state resembled a ferrofluid exhibiting the Rosensweig instability [82]. Its eventual decay was assigned to the atom loss through three-body channels, which are strongly enhanced in the large density regions of the droplets. In fact, the three-body interactions were one of the proposed missing elements to fix the theoretical model of dipolar BECs [83, 84]. Shortly after, a closer investigation of the properties of the system revealed [85] that quantum fluctuations stabilize the droplet form of the gas [23, 86–88].

Quantum fluctuations are the first-order correction to the mean-field theory. They account for all the processes involving the interaction between the condensate and the excited states. In particular, if we denote by $\hat{a}^\dagger_{\boldsymbol{q}}$ the single-particle creation operator corresponding to momentum $\boldsymbol{q}$, quantum fluctuations are described by the following operators:

$$\hat{a}^\dagger_{-\boldsymbol{q}}\hat{a}^\dagger_{\boldsymbol{q}}\hat{a}_0\hat{a}_0 \qquad \hat{a}^\dagger_0\hat{a}^\dagger_0\hat{a}_{-\boldsymbol{q}}\hat{a}_{\boldsymbol{q}} \qquad \hat{a}^\dagger_0\hat{a}^\dagger_{\boldsymbol{q}}\hat{a}_0\hat{a}_{\boldsymbol{q}} \tag{1.49}$$

where the first one is responsible for the depletion of the condensate, the second one brings two particles into the condensed state and the last one leaves the condensate unchanged [19]. By replacing the condensate operators $\hat{a}_0, \hat{a}^\dagger_0$ with the c-number $\sqrt{N_0}$, all the quantum fluctuation terms are quadratic in creation and annihilation operators. Therefore, one may diagonalize the Hamiltonian including the terms (1.49), by means of the Bogoliubov transformation (1.20)[3]. As a result, one obtains the ground state energy of the system:

$$\frac{E}{V} = \frac{1}{2}n^2\tilde{U}(|\mathbf{q}|=0) + \frac{1}{2}\int\frac{d^3q}{(2\pi)^3}\left[\epsilon(\mathbf{q}) - \frac{\hbar^2\mathbf{q}^2}{2m} - n\tilde{U}(\mathbf{q})\right], \tag{1.50}$$

where V is the volume of the gas, $\epsilon(\mathbf{q})$ is the dispersion relation, which we will discuss in the next section, and the potential $\tilde{U}$ includes both contact interactions and dipole-dipole interactions (1.46). The first term on the right side is the mean-field total energy, while the second part provides the contribution of quantum fluctuations. The integral in the equation above is ultraviolet-divergent and needs to be regularized. In order to do that, we consider higher-order corrections of the s-wave scattering length, which are beyond the Born approximation [19, 91]. Since the scattering length defines the strength of the contact interaction $g = 4\pi\hbar^2 a_s/m$, this procedure effectively regularizes the interaction coupling constant:

$$g(|\boldsymbol{q}|=0) \;=\; \tilde{U}(|\boldsymbol{q}|=0) - \frac{m}{\hbar^2}\int\frac{d^3q}{(2\pi)^3}\frac{\tilde{U}(-\boldsymbol{q})\tilde{U}(\boldsymbol{q})}{\boldsymbol{q}^2}. \tag{1.51}$$

The corrected scattering length can now be included in the energy (1.50). Its zero-momentum component gives the mean-field contribution to the total energy:

$$\frac{E_0}{V} = \frac{1}{2}gn^2\left[1 + \varepsilon_{dd}\left(3\cos^2\theta - 1\right)\right], \tag{1.52}$$

where θ is the angle between the momentum $\boldsymbol{q}$ and the dipole's orientation vector. The quantum fluctuation term arises from the integral in equation (1.50) and the second part of (1.51), which together evaluate to

$$\frac{\Delta E}{V} = \frac{64}{15}g\sqrt{\frac{a_s^3 n}{\pi}}\mathcal{Q}_5(\varepsilon_{dd}), \tag{1.53}$$

[3]For a detailed derivation of the quantum fluctuation Hamiltonian in a regular BEC see [19, 89, 90] and in dipolar BEC [23, 87]

where $\mathcal{Q}_\alpha(x) = (1-x)^{\alpha/2}\ {}_2F_1(\frac{-\alpha}{2}, \frac{1}{2}, \frac{3}{2}, \frac{3x}{x-1})$ is defined with hypergeometric function ${}_2F_1$ [92]. For $\alpha = 5$, this function reduces to

$$\mathcal{Q}_5(\varepsilon_{dd}) = \int_0^1 du \left[1 + \varepsilon_{dd}(3u^2 - 1)\right]^{5/2} \tag{1.54}$$

and is real for $\varepsilon_{dd} \in [0, 1)$, whereas in the regime dominated by dipolar interactions, it acquires a small imaginary part. This imaginary part is a consequence of the mean-field energetic instability of the elementary excitations for $\varepsilon_{dd} > 1$. Although not exactly correct, it has become widely accepted to truncate the imaginary part and approximate the function (1.54) with its real part. This approach is well justified for systems studied in this thesis for $\varepsilon_{dd} \lesssim 1.5$, where the imaginary part is two orders of magnitude smaller than the real part [93]. For high values of the relative strength parameter, this practice may not be satisfactorily accurate.

The energy (1.53) is the analog of the Lee-Huang-Yang (LHY) correction calculated for an ordinary BEC [89, 90] hence it became common to adopt this name in the beyond-mean-field description of dipolar gases. Every analytical consideration of the LHY correction in the literature uses the uniform gas as a prototype, which neglects the spatial dependence of the fields. Although this approach is strictly speaking incorrect in terms of trapped systems, it provides a very good first-order estimate of the contribution of quantum fluctuations to the ground-state energy therein.

Finally, to include quantum fluctuations in the microscopic description of dipolar Bose-Einstein condensates, we use the energy term (1.53) to derive an additional potential, which we add to the mean-field Gross-Pitaevskii equation. This procedure is equivalent to the Density Functional Theory (DFT) approach, where unknown potentials are substituted with their best approximations [94–96]. We will describe it in detail in the numerical method section. The final equation is called the extended Gross-Pitaevskii equation (eGPE), where the quantum fluctuations act as a mean-field potential:

$$\begin{aligned} i\hbar\partial_t\psi(\boldsymbol{r},t) = \Bigg(&\frac{\hbar^2}{2m}\nabla^2 + V_{ext}(\boldsymbol{r}) + g|\psi(\boldsymbol{r},t)|^2 + \int d^3\boldsymbol{r}' V_{dd}(\boldsymbol{r}-\boldsymbol{r}')|\psi(\boldsymbol{r}',t)|^2 \\ &+ \gamma(\varepsilon_{dd})|\psi(\boldsymbol{r},t)|^3\Bigg)\,\psi(\boldsymbol{r},t), \end{aligned} \tag{1.55}$$

where $\gamma(\varepsilon_{dd}) = \frac{32}{3\sqrt{\pi}} g a_s^{3/2} \mathrm{Re}\left\{\mathcal{Q}_5(\varepsilon_{dd})\right\}$ and V_{dd} is given by (1.46). The extended Gross-Pitaevskii equation does not predict an immediate collapse in the regime dominated by the dipolar repulsion. Instead, for higher values of the relative interaction strength ε_{dd}, the system forms droplet arrays similar to the ones observed in the dysprosium experiment [81]. In the recent years, the eGPE has been proven to be very accurate and has become the standard tool in the field of dipolar supersolids.

The LHY correction is usually small with respect to the mean-field energy and the necessity of its inclusion is governed by the energy scale. It becomes relevant only when the contribution of quantum fluctuations to the chemical potential is comparable to that of mean-field interactions [85]. Finally, by estimating the contribution of the three-body interactions to the chemical potential, we can explain why the experiments on ultracold chromium failed to observe the supersolid phase [97]. Contrary to erbium and dysprosium, the ^{52}Cr BEC suffers a strong particle loss in the three-body channel before quantum fluctuations take over the mean-field energy. Effectively, this prevents the system from forming any density-modulated state and leads to the collapse.

1.3.3 Dispersion law and supersolidity

The properties of dipolar condensates strongly depend on the external potential, which with modern techniques may take any shape. Particularly interesting physical phenomena occur in oblate traps, where the width of the cloud along the z-axis is much smaller than in the other two directions. In such quasi-2D geometries, the external magnetic field, which sets the alignment of the dipoles, controls the character of the interactions. If it is perpendicular to the z-axis, the dipolar interaction is predominantly attractive, leading to the so-called macrodroplet regime [24, 98–100]. On the other hand, when the dipoles are aligned along the z-axis, the interaction is mainly repulsive, and its strength can be tuned with ϵ_{dd}. This configuration is particularly interesting, as in the strongly interacting regime $\varepsilon_{dd} \gtrsim 1$ the excitation spectrum develops a local minimum [61, 101, 102]. The dispersion relation of dipolar condensates in oblate traps is therefore very similar to the one of liquid helium, and due to this resemblance, the local minimum is referred to as the roton minimum. Unlike in liquid helium, the position and depth of the roton gap can be easily tuned experimentally with the harmonic confinement and the relative interaction strength. The roton minimum appears at a momentum close to $1/l_z$, where $l_z = \sqrt{\hbar/m\omega_z}$ is the harmonic oscillator length in the z-direction [103, 104]. On the other hand, the height of the roton gap can be controlled solely by the ε_{dd} ratio, where stronger dipolar interactions lead to the softening of the minimum (see Fig. (1.3)). Eventually, for a sufficiently high dipolar interactions, the gap closes, enabling the system to create a finite-momentum excitations at no energy cost. These take the form of spatial, periodic modulations of a wavevector given by the roton momentum. Since the Hamiltonian of the system is translationally invariant, the softening of the roton mode breaks this symmetry in a spontaneous manner. The new vacuum state, due to the periodicity of the density oscillations, resembles a solid, where the peaks correspond to the lattice sites. We shall see later in this section that this state has the properties of the supersolid phase. The underlying mechanism of creation of the supersolid phase of the

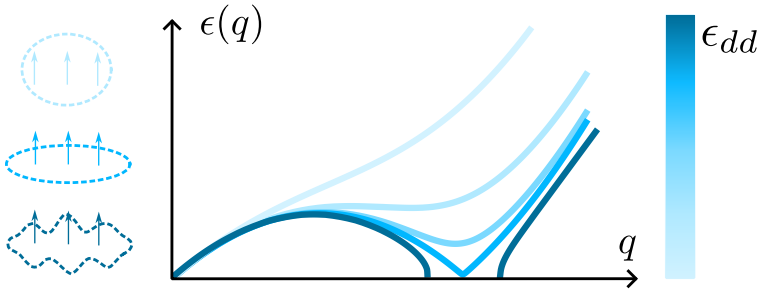

Figure 1.3: Dispersion relation of trapped dipolar gases for different values of relative interaction strength ε_{dd}. Drawings on the left-hand side are schematic representations of the atomic cloud corresponding to specific ε_{dd} indicated by the colorscale. At sufficiently high value, the roton minimum softens, giving rise to the supersolid phase.

dipolar BECs differs from the vacancy-based concept of supersolidity proposed by Andreev and Lifshitz. While they considered a possible way to induce superfluidity in a system already exhibiting the crystalline order, the dipolar supersolids rely on the reverse order of symmetry breaking. In principle, the roton softening can be regarded as the solidification of a superfluid gas.

The proof of superfluid properties of a supersolid has been provided in two ways. Initial experiments focused on assessing the global phase coherence [6–9], which in interacting systems is equivalent to superfluidity. However, the most striking and unequivocal evidence of superfluidity was the observation of quantized vortices [105]. The situation is more subtle with respect to assessing the solid-like properties. Let us investigate similarities and differences between a dipolar supersolid and an ordinary solid. Firstly, we notice that the supersolid phase in dipolar condensates is dependent on the trapping potential. Without confinement in the direction of the magnetic field, the system would form a self-bound macrodroplet. Further confinement in the xy plane is needed to keep the droplets together, as they repel each other. In this regard, the dipolar supersolid differs from an ordinary self-bound solid. However, this property is not the most important as one may argue that the external potential plays the role of pressure that stabilizes many solids also at low temperatures.

Originally, the similarity between the dipolar supersolid and an ordinary solid was associated with the long-range crystalline order, which in ultracold platforms appears due to the spontaneous symmetry breaking. According to the Goldstone theorem, the supersolid phase of dipolar gases is characterized by an additional type of low-energy excitation, which we identify as the lattice phonon. The experimental efforts towards identification of the solid-like properties relied on the appearance of the second mode in collective oscillations. In particular, the breathing mode was demonstrated to be characterized by two frequencies [10]. This experiment confirmed the presence of the lattice-like Goldstone boson, highlighting that the system exhibits a spectrum of collective modes of a hybridized superfluid and lattice-like nature.

Although the periodic modulation of the density resembles a crystalline long-range order of a solid, it is not obvious that the new state exhibits the rigidity and robustness against the shear stress of a true solid. Solids are the only media in which particles can oscillate in the transverse direction in response to the longitudinal perturbation. There have been several theoretical studies (including this thesis) pointing out the finite value of the shear modulus in dipolar supersolids, but up to now there has been no experimental attempt to observe the shear waves in dipolar platforms. Interestingly, in driven BECs, where the s-wave scattering length is periodically modulated, there seems to be no transverse sound [106]. Instead, the authors measured a strong damping of the transverse perturbation. A further study of two-dimensional dipolar condensates is needed to see whether these systems exhibit the same behavior.

In conclusion, there are several properties which we assign to the solid phase of matter. The long-range crystalline order and the existence of the lattice phonon are commonly agreed to be enough to call the modulated phase of dipolar condensates the supersolid. A further argument in favor of the solidity of these systems would be the presence of shear waves.

Thus far we have discussed the faith of a dipolar BEC in an oblate trap for larger values of the relative interaction strength, which lead to the emergence of the roton minimum and its eventual softening. After it becomes energetically allowed to create finite-momenta excitations for free, the system enters the supersolid phase, in which the excitation spectrum exhibits two gapless branches. With the further increase of the relative interaction strength ε_{dd}, the system changes in several aspects. Firstly, the slopes of the two gapless modes change, indicating the change of the two speeds of sound. Part of this thesis is devoted to this phenomenon, and the results can be found in Chapter 3. Secondly, the amplitude of the density modulation increases with ε_{dd} [107, 108]. This effect has a great impact on the thermodynamic properties of the system as it decreases the superfluid fraction, in accor-

dance with the Leggett upper bound (1.41). Thus, the dominance of the dipolar interaction suppresses the superfluid properties, and ultimately leads to a state with the superfluid fraction equal 0. In such a case, the periodic density modulation becomes an ensamble of disconnected droplets. While each droplet is superfluid within its volume, the system as a whole exhibits no global coherence. This phase is called the independent droplet (ID) phase, and is precisely what was observed in the first experiment on dysprosium BEC [81]. Lack of global coherence leads to the restoration of the gauge invariance, which means the independent droplet phase breaks only the translational symmetry. Consequently, during the transition from the superfluid phase to the ID, one of the gapless modes vanishes, leaving only the branch associated with the lattice phonons. The independent droplet phase and its properties have been difficult to study experimentally due to their short life-times. At higher densities, as it happens in the supersolid and the ID phase, the atoms also interact through three-body channels, effectively leading to rapid losses.

To conclude this section, it is worth noting that dipolar BECs are not the only platforms to study supersolidity. States of simultaneously and spontaneously broken gauge and translational symmetries have been reported in spin-orbit coupled Bose mixtures [4, 109, 110], BECs in optical resonator [5], driven BECs [106] and polariton condensates [111, 112]. Recently, an array of self-bound droplets has been observed in a BEC of ultracold NaCs molecules, which poses a strong electric moment. A further study of coherence of this system will likely confirm its supersolid nature.

1.3.4 Hydrodynamic theory of supersolids

The long-wavelength properties of a supersolid are captured by a hydrodynamic theory that accounts for its superfluid and crystalline nature [113–118]. The core of such a theory is based on the Landau two-fluid model [19, 20, 47, 119], as one requires the supersolid HD theory to reduce to the superfluid hydrodynamics when the translational invariance is restored. The novelty with respect to the model of Landau is the inclusion of some elements of the hydrodynamics of solids [120]. In this section, we review the derivation of the supersolid hydrodynamic equations based on conservation laws and symmetry principles. To simplify the theory, we consider a one-dimensional system at zero-temperature. We begin the construction of the hydrodynamic theory of supersolids by reviewing the two-fluid model, which we already introduced in Section (1.2.2), and highlighting important modifications.

The first equation of supersolid HD is the continuity equation, which originates from the conservation of the total number of particles:

$$\partial_t \rho + \partial_x j = 0, \tag{1.56}$$

where $\rho = \rho_n + \rho_s$ is the total density, $j = \rho_n v_n + \rho_s v_s$ is the total current, and ρ_n and v_n (ρ_s and v_s) are, respectively, the normal (superfluid) density and velocity. We anticipate the presence of both parts in the HD theory, as the gas is not translationally invariant [3, 51]. What is here called the *normal* part is not equivalent to the normal part from the Landau two-fluid model. In principle, at finite temperature, the total density consists of three types of inertia [121], among which the superfluid and the normal densities are inherited from the Landau two-fluid model. The novel third part is the crystal density, associated with the lattice structure, which appears in the supersolid phase. The normal and the crystal inertia are in general different, but they coincide in the zero-temperature limit considered in this thesis. For this reason, we will refer to the crystal part as 'normal' throughout the entire thesis.

The second conserved quantity is the momentum. In a one-dimensional system, the corresponding conservation equation reads:

$$\partial_t j + \partial_x \left(p + \rho_n v_n^2 + \rho_s v_s^2 \right) = 0, \tag{1.57}$$

where p is the pressure, whose dependence on other thermodynamic quantities differs from the superfluid formula because it must account for the lattice properties of the supersolid. We refer to this fact at the end of this section and provide the constitutive equation for the pressure.

The first two equations of supersolid hydrodynamics (1.56) and (1.57) originate from conservation laws. In order to complete the theory, we incorporate the two broken symmetries by providing equations governing the dynamics of the order parameters. In the same way that the two-fluid model accounts for the broken gauge symmetry, we incorporate the Josephson equation into the supersolid hydrodynamic theory:

$$\partial_t v_s + \partial_x \left(\mu_s + \frac{1}{2} v_s^2 \right) = 0, \tag{1.58}$$

where μ_s is the chemical potential in the superfluid reference frame. Similarly to momentum p, the chemical potential μ_s also includes additional terms that take into account the crystal properties of the supersolid.

The second symmetry that is broken spontaneously in a supersolid is the translational symmetry. The corresponding order parameter is the lattice displacement u, defined as the difference between the equilibrium position x and the actual position of the lattice sites R. In an ordinary solid, a lattice site consists of a single atom, while in the case of a supersolid, we identify it with the local maximum of the density profile. The dynamics of the lattice is an important element of the collective behavior of the system, and consequently must be included in the supersolid HD equations. This can be done by the so-called Lin's constraint

$$\left(\partial_t + v_n \partial_x \right) R = 0, \tag{1.59}$$

which states that the lattice coordinates do not change along the path of the normal component [114]. Since u is the order parameter of the supersolid phase transition, we rewrite the fourth hydrodynamic equation as

$$\partial_t u + v_n \partial_x u - v_n = 0 \tag{1.60}$$

For small displacements, the middle term may be neglected, revealing that the normal velocity is given by the time derivative of u.

The last important point to discuss is how the presence of stationary currents and of the crystalline order affect the chemical potential and the pressure entering the hydrodynamic equations (1.58) and (1.57). Both quantities are functions of the free energy. By analyzing its change under an infinitesimal Galilean transformation, one can find the explicit dependence of the free energy on v_n and v_s [122]. Consequently, the chemical potential μ in the rest frame has the following dependence on the normal and superfluid velocities:

$$\mu = \mu_0 + \frac{1}{2} \left(\rho_s' w^2 - v_n^2 \right), \tag{1.61}$$

where μ_0 is the chemical potential in the absence of currents, $\rho_s' = \partial_\rho \rho_s$ and $w = v_n - v_s$. In equation (1.58), the chemical potential μ_s is defined in the moving frame of reference,

which is related to μ with $\mu_s - \mu = v_n v_s - \frac{1}{2}v_s^2$ [20, 47]. On the other hand, the pressure p is invariant under the change of the reference frame and depends only on w:

$$p = p_0 + \frac{\rho_n - \rho\rho_n'}{2} w^2, \tag{1.62}$$

where p_0 is the pressure at $v_n = v_s$, while $\rho_n' = \partial_\rho \rho_n$. The two relations (1.61) and (1.62) are true for both superfluid and supersolid hydrodynamics.

With the appearance of solid-like properties, the hydrodynamic functions characterizing the supersolid state depend on new parameters. In particular, the energy is sensitive to lattice deformations, where the rate of this variation is set by the elastic constant λ. For a three-dimensional lattice, this quantity is a tensor, but in our simplified on-dimensional model it reduces to a scalar. The other parameter appearing in the hydrodynamic theory of supersolids is a phenomenological strain-density coupling γ, which in dipolar systems is expected to be less important than the elastic constant [123]. Since the two new parameters change the energy of the system, they also alter the chemical potential μ and pressure p [114]. We can express the complete dependence of μ and p on all relevant variables through infinitesimal variations:

$$\delta\mu = \frac{1}{\rho^2\kappa}\delta\rho + \gamma u_x + \frac{\rho_s'}{2}\delta w^2 - \frac{1}{2}\delta v_n^2 \tag{1.63a}$$

$$\delta p = \left(\frac{1}{\rho\kappa} - \gamma\right)\delta\rho + (\gamma\rho - \lambda)\, u_x + \frac{\rho_n - \rho\rho_n'}{2}\delta w^2, \tag{1.63b}$$

where κ is the compressibility and $u_x \equiv \partial_x u$. The two constitutive equations above are essential for the characterization of the collective behavior of the system.

Ultimately, we can write the hydrodynamic equations of supersolids in their final form:

$$\partial_t \rho + \partial_x j = 0 \tag{1.64a}$$

$$\partial_t j + \partial_x \left(p + \rho_n v_n^2 + \rho_s v_s^2\right) = 0 \tag{1.64b}$$

$$\partial_t v_s + \partial_x (v_n v_s + \mu) = 0 \tag{1.64c}$$

$$\partial_t u_x + \partial_x (v_n u_x - v_n) = 0, \tag{1.64d}$$

where we took the derivative ∂_x of Eq.(1.60) to obtain Eq.(1.64d) and we substituted μ_s in (1.58) with the chemical potential in the rest frame. This particular form of the last two hydrodynamic equations unveils their similarity as they both originate from the occurrence of broken symmetries. The four equations (1.64) characterize the behavior of a supersolid in a macroscopic scale. Together with the constitutive equations (1.63), the theory allows the determination of all the sound modes that propagate in the system. In order to derive the formulae for the speeds of sound one uses the linearization procedure. We consider small deviations from the equilibrium values of the variables entering the hydrodynamic equations (1.64). We identify the set of four independent variables $\xi \in \{\rho, v_s, v_n, u_x\}$ and express them as the sum of their equilibrium values ξ^0 and small variations that change slowly in space and time $\delta\xi(x,t) = \delta\xi \exp(i(qx - \omega t))$. In the $q \to 0$ limit, the dispersion law is linear, and the slope $c = \omega/q$ defines the speed of sound. As a result, the linearized HD equations yield two speeds of sound[4]:

$$c_{1,2}^2 = \frac{1}{2}\left(\beta + c_\kappa^2 - 2\gamma\right) \pm \frac{1}{2}\sqrt{\left(\beta + c_\kappa^2 - 2\gamma\right)^2 - 4\frac{\rho_s}{\rho}\left(\beta c_\kappa^2 - \frac{\rho\gamma^2}{\rho_n}\right)}, \tag{1.65}$$

[4]In the result section, we will provide a detailed derivation of the two speeds of sound

where $c_\kappa^2 = \sqrt{\rho\kappa}^{-1}$ and $\beta = \lambda/\rho_n$. The two sound modes are of a hybrid superfluid and crystal nature and correspond to the two Goldstone modes appearing due to the spontaneous symmetry breaking.

1.4 Linear response theory

A systematic study of quantum systems typically begins with the characterization of their ground state, whose properties determine the most fundamental quantities of the system, such as density and phase, and in the case of a BEC also the superfluid velocity v_s. Once the static properties are well established, it is natural to ask how the system reacts to a small perturbation. This question is addressed by the linear response theory, in which we assume that the expectation value of a certain operator is proportional to the applied perturbation. Within this framework, one obtains powerful tools for determining both static and dynamic quantities. For instance, by analyzing the change in the ground state introduced by an external perturbation, one can measure susceptibilities such as the isothermal compressibility. On the other hand, by driving the system slightly out of equilibrium, one gains access to dynamical properties of the system such as transport coefficients and collective modes, including the speed of sound.

In this section, we revisit the formalism of the linear response theory, which is the cornerstone of the protocol used to excite the sound modes in this thesis. We review the method of sum rules, which provides a simple and model-independent framework to relate physical observables with moments of the dynamic structure factor. A detailed description of the linear response theory in quantum gases can be found in [19].

1.4.1 Response function

Let us consider a general system defined with a Hamiltonian $\hat{H}$, to which we apply a small perturbation $\hat{G}$. Linear response theory provides tools for assessing the change in the expectation value of the operator $\hat{F}$, induced by the perturbation. We consider a generic scenario, in which the system is driven with frequency ω by a small external perturbation represented with the Hamiltonian:

$$\hat{H}_{\mathrm{pert}}(t) = -\lambda e^{-i\omega t} e^{\eta t} \hat{G} - \lambda^* e^{+i\omega t} e^{\eta t} \hat{G}^\dagger, \tag{1.66}$$

where the amplitude λ ensures that the energy scale of $\hat{H}_{\mathrm{pert}}$ is small with respect to that of $\hat{H}$. The factor $e^{\eta t}$ guarantees the adiabaticity of the perturbation and ensures that it vanishes at $t \to -\infty$. In the lowest order, linear response theory assumes that the expectation value of an operator $\hat{F}^\dagger$ is proportional to the perturbation:

$$\delta\langle \hat{F}^\dagger \rangle = \lambda e^{-i\omega t} e^{\eta t} \chi_{\hat{F}^\dagger,\hat{G}}(\omega) + \lambda^* e^{+i\omega t} e^{\eta t} \chi^*_{\hat{F}^\dagger,\hat{G}^\dagger}(-\omega). \tag{1.67}$$

The equation above defines the dynamical polarizability $\chi_{\hat{F}^\dagger,\hat{G}}(\omega)$, also referred to as the response function, which can be calculated using perturbation theory. Provided that initially the system is in equilibrium state of the Hamiltonian $\hat{H}$, at temperature $1/\beta$, the dynamical polarizability reads

$$\chi_{\hat{F}^\dagger,\hat{G}}(\omega) = -\frac{1}{\hbar} Q^{-1} \sum_{m,n} e^{-\beta E_m} \left[\frac{\langle m|\hat{F}^\dagger|n\rangle\langle n|\hat{G}|m\rangle}{\omega - \omega_{nm} + i\eta} - \frac{\langle m|\hat{G}|n\rangle\langle n|\hat{F}^\dagger|m\rangle}{\omega + \omega_{nm} + i\eta} \right], \tag{1.68}$$

where $Q = \sum_n e^{-\beta E_n}$ is the partition function and $\hbar\omega_{mn} = E_m - E_n$ defines the energy difference between states $|m\rangle$ and $|n\rangle$. It is useful to define the dynamic structure factor

$$S_{\hat{F}}(\omega) = Q^{-1} \sum_{m,n} e^{-\beta E_m} \left| \langle n|\hat{F}|m\rangle \right|^2 \delta(\omega - \omega_{nm}), \tag{1.69}$$

which in the case $\hat{F} = \hat{G}$ carries all the Hamiltonian-dependent information regarding the system's response to the external perturbation. Moreover, the difference $S_{\hat{F}}(\omega) - S_{\hat{F}^\dagger}(-\omega)$ quantifies the energy exchange rate between the system and the external perturbation [19]. Thus, knowledge of the structure factor is of fundamental interest in linear response theory. Throughout this thesis, we will only study systems in the zero-temperature limit, which greatly simplifies the dynamical polarizability:

$$\chi_{\hat{F}}(\omega) = -\int_{-\infty}^{+\infty} d\omega' \left[\frac{S_{\hat{F}}(\omega')}{\omega - \omega' + i\eta} - \frac{S_{\hat{F}^\dagger}(\omega')}{\omega + \omega' + i\eta} \right]. \tag{1.70}$$

Note that in the absence of thermal fluctuations, the ground state of the unperturbed Hamiltonian is a single state, denoted by $|0\rangle$. Then the structure factor simplifies to:

$$S_{\hat{F}}(\omega) = \sum_m \left| \langle m|\hat{F}|0\rangle \right|^2 \delta(\omega - \omega_m), \tag{1.71}$$

where $\omega_m \equiv \omega_{0m}$. Since all states $|m \neq 0\rangle$ have higher energy than $|0\rangle$, the dynamic structure factor vanishes for $\omega < 0$.

1.4.2 Density response function and sum rules

Among all the perturbations that can be used to probe the properties of a given system, those coupled to the density are of the highest interest in this thesis. Since sound waves are modes of well-defined small wavevectors $\boldsymbol{q}$, we will consider the density response to such perturbations in the momentum space. The $\boldsymbol{q}$-component of the density operator $\rho_{\boldsymbol{q}}$ in momentum space is given by the Fourier transform of $\rho(\boldsymbol{r}) = \sum_i \delta(\boldsymbol{r} - \boldsymbol{r}_i)$, where the sum includes all particles:

$$\rho_{\boldsymbol{q}} = \int d\boldsymbol{r} e^{-i\boldsymbol{q}\boldsymbol{r}} \rho(\boldsymbol{r}) \tag{1.72}$$

and is equivalent to $\rho^\dagger_{-\boldsymbol{q}}$. The density response function $\chi(\boldsymbol{q}, \omega)$ is defined as the eq. (1.68) for $\hat{F} = \hat{G} = \delta\rho^\dagger_{\boldsymbol{q}} = \rho^\dagger_{\boldsymbol{q}} - \langle\rho^\dagger_{\boldsymbol{q}}\rangle_{eq}$, where the average $\langle\rho^\dagger_{\boldsymbol{q}}\rangle_{eq}$ is calculated in an unperturbed system, at equilibrium. In the limit of vanishing temperature, the density response function reads:

$$\chi(\boldsymbol{q}, \omega) = -\frac{1}{\hbar} \sum_n \left[\frac{|\langle n|\delta\rho_{\boldsymbol{q}}|0\rangle|^2}{\omega - \omega_n + i\eta} - \frac{\left|\langle n|\delta\rho^\dagger_{\boldsymbol{q}}|0\rangle\right|^2}{\omega + \omega_n + i\eta} \right], \tag{1.73}$$

and the dynamic structure factor (1.71) is

$$S(\boldsymbol{q}, \omega) = \sum_m \left| \langle m|\delta\rho^\dagger_{\boldsymbol{q}}|0\rangle \right|^2 \delta(\omega - \omega_m). \tag{1.74}$$

Furthermore, if the ground state $|0\rangle$ is invariant under parity or time-reversal transformation, the structure factor (1.74) is independent of the sign of the wavevector $\boldsymbol{q}$:

$$S(\boldsymbol{q}, \omega) = S(-\boldsymbol{q}, \omega). \tag{1.75}$$

A key strength of linear response theory lies in the use of sum rules, which under specific conditions connect the properties of the system to the moments of the structure factor (1.69):

$$m_r(\boldsymbol{q}) = \hbar^{r+1} \int_{-\infty}^{+\infty} d\omega\, \omega^r S(\boldsymbol{q}, \omega). \tag{1.76}$$

Using the definition of the dynamic structure factor and the completeness relation $\mathbb{I} = \sum_n |n\rangle \langle n|$, one can derive many useful sum rules, among which the energy-weighted one plays a crucial role:

$$m_1(\hat{F}) + m_1(\hat{F}^\dagger) = \left\langle \left[\hat{F}^\dagger, [\hat{H}, \hat{F}]\right] \right\rangle. \tag{1.77}$$

For the operator $\hat{F} = \delta\rho_{\boldsymbol{q}}$, the commutator $\left[\rho_{-\boldsymbol{q}}, [\hat{H}, \rho_{\boldsymbol{q}}]\right]$ yields $N\hbar^2\boldsymbol{q}^2/(2m)$. This comes from the only part of the Hamiltonian $\hat{H}$ that does not commute with the $\boldsymbol{q}$-component of the density – the kinetic term. Using the symmetry (1.75), the energy-weighted sum rule reads:

$$m_1(\boldsymbol{q}) = \hbar^2 \int_{-\infty}^{+\infty} d\omega\, \omega S(\boldsymbol{q}, \omega) = N\frac{\hbar^2\boldsymbol{q}^2}{2m}. \tag{1.78}$$

Also known as the f-sum rule, equation (1.78) provides a simple and model-independent tool to identify the missing modes in measured spectra. Another important sum rule is given by the inverse-energy weighted moment:

$$m_{-1}(\boldsymbol{q}) = \int_{-\infty}^{+\infty} d\omega\, \frac{S(\boldsymbol{q}, \omega)}{\omega} \xrightarrow{\omega \to 0} \frac{N}{2}\chi(\boldsymbol{q}, 0), \tag{1.79}$$

where $\chi(\boldsymbol{q}, 0)$ is the static polarizability. In the context of ultracold gases, in the limit of small perturbation wavevectors $\boldsymbol{q} \to 0$, this quantity gives the isothermal compressibility of the gas $\rho\kappa = (\rho\partial\mu/\partial\rho)^{-1}$. For this reason, the limit (1.79) is also known as the compressibility sum rule. It is very important in the context of this thesis, as in hydrodynamics the compressibility κ defines the speed of sound.

Chapter 2

Numerical Methods

In the quantum theory, every ultracold atomic gas is associated with a many-body wavefunction, which determines all properties of the system. Numerical simulations of many-body problems are in general time- and resource-consuming for a large number of particles, as each single-particle wavefunction requires spatial discretization. Consequently, numerical calculation of any two-body potential is not feasible for even a small number of particles. Fortunately, thanks to their coherence, Bose-Einstein condensates are predominantly characterized by one macroscopically occupied state. In the limit of zero temperature, this state is the only wavefunction one needs to find to gain access to all physical properties of the system and to observe its evolution in time. In simple cases, Bose-Einstein condensates can be studied analytically, using, for instance, the Thomas-Fermi approximation of the Gross-Pitaevskii equation [19]. However, the presence of external potentials that introduce density modulations limits the information that can be gained through analytical analysis. For this reason, we need a way to simulate the condensates subject to arbitrary external conditions.

Numerical simulations of BECs are based on the Gross-Pitaevskii equation, which is a first-order differential equation in time. Therefore, to solve it one needs an initial state and an algorithm to integrate it in time. In this thesis, we study three types of systems which require a customized treatment. In order to put them all into a common framework, we employ Density Functional Theory (DFT). The DFT originates from the condensed matter physics, where an unknown form of the exchange interaction energy of an electronic cloud has to be approximated with the best guess [96]. While this approach is redundant for ordinary BECs and binary Bose mixtures, it is essential for the treatment of dipolar gases. The extended Gross-Pitaevskii equation, which we derived in Chapter 1, involves the quantum-fluctuation term, which for a trapped condensate does not have an analytical form. We will address this issue with the DFT.

2.1 Ground state

The simplest method to explore the ground state solutions of the GPE is the imaginary time evolution. It makes use of the fact that once the time is purely imaginary, any state undergoes an exponential decay. Since the ground state has the lowest energy, its decay is the slowest and therefore becomes the only one surviving a long imaginary time evolution. In general, this method is suitable for problems of well-defined Hamiltonians such as single and multicomponent BECs. For dipolar supersolids, as elaborated in the introduction, one needs to account for beyond mean-field corrections, for which the GPE has to be modified.

For such problems, where one needs to add phenomenologically determined energy term, we use a similar, yet more general approach, based on the Density Functional Theory.

The DFT was originally proposed to solve condensed matter problems, where the system consists of electrons. Owing to the Hohenberg-Kohn theorem [94], the electron many-body wavefunction can be replaced with their density $n(\boldsymbol{r})$. Consequently, all observables can be calculated with the knowledge of a single function, dependent on three spatial dimensions and time. The second pillar of DFT is the Kohn-Sham theorem [95], which proves that one can replace a set of interacting Schrödinger equations with non-interacting ones, experiencing an effective potential specific to a given problem. Thus, in the DFT approach one has to define an appropriate energy density functional $\mathcal{E}[\rho]$, and minimize it by finding the ground state density $\rho(\boldsymbol{r}) = |\psi(\boldsymbol{r})|^2$. To demonstrate the core principle of this method, let us consider a simple BEC, described by the Gross-Pitaevskii equation. The corresponding energy density functional is given by

$$\mathcal{E}[\psi^*, \psi] = \int d^3\boldsymbol{r}\ \psi^*(\boldsymbol{r}, t) \left(-\frac{\hbar^2}{2m}\nabla^2 + V_{ext}(\boldsymbol{r}) + \frac{g}{2}|\psi(\boldsymbol{r}, t)|^2 \right) \psi(\boldsymbol{r}, t) \tag{2.1}$$

and is related to the GPE with the functional derivative:

$$\frac{\delta\mathcal{E}[\psi^*, \psi]}{\delta\psi^*} = \left(-\frac{\hbar^2}{2m}\nabla^2 + V_{ext}(\boldsymbol{r}) + g|\psi(\boldsymbol{r}, t)|^2 \right) \psi(\boldsymbol{r}, t) = i\hbar\partial_t\psi(\boldsymbol{r}, t). \tag{2.2}$$

When the system is in equilibrium, the amplitude of the ground state condensate wavefunction does not change during the time evolution, while the phase is modified by $-\mu t/\hbar$ and the right-hand side of (2.2) becomes simply μ. It is a common practice to move the chemical potential to the Gross-Pitaevskii Hamiltonian, so that the ground state solution does not imply any time evolution. This procedure is equivalent to fixing the number of particles by adding the chemical potential to the equation of motion as the Lagrange multiplier. Once done, the functional derivative on the left-hand side of (2.2) is equal zero, indicating that the condensate wavefunction ψ that minimizes the energy density functional is also the solution of the GPE.

In order to find the ground state wavefunction we use the gradient descend method [124]. It is an iterative approach, based on a self-consistent search, which begins from an initial guess - a wavefunction ψ_0, which one believes to be of a form similar to the ground state solution. Algorithmically, the method can be simply put as:

$$\psi_{n+1} - \psi_n = -d\tau\frac{\delta\mathcal{E}[\psi_n]}{\delta\psi_n^*} + \beta(\psi_n - \psi_{n-1}), \tag{2.3}$$

where lower indices indicate the iteration number, $d\tau$ is the equivalent of the imaginary time step and β is the linear mixing parameter, used to enhance convergence. It is not necessary, but for $\beta \approx 0.9$ it was found to significantly improve the efficiency of the algorithm. One can see, that with $\beta = 0$ equation (2.3) highly resembles imaginary time evolution, provided that $\frac{\delta\mathcal{E}[\psi_n]}{\delta\psi_n^*} = \frac{1}{\hbar}\hat{H}\psi_n$. Therefore, for simplicity, hereafter we will refer to it as imaginary time evolution.

Every self-consistent calculation must begin with an initial wavefunction ψ_0, which should be of a form similar to the ground state. For a harmonically trapped system, one may begin with a ψ_0 given by the Thomas-Fermi profile. The energy landscape may be formed by many local minima, so it is in general desirable not to begin the algorithm with a function favoring any state. It is a good practice to include a small-amplitude, complex white noise to the initial wavefunction to decrease the odds of finding a local minimum. On the other

hand, there are situations in which we ask the algorithm to converge to a given state, even though it is only a local minimum. For example, in the case of dipolar gases, we will require the supersolid to have specific number of droplets, by beginning the algorithm from highly biased state of N periods. Another example, where the biased state may turn out useful is the ground state search close to a phase transition. The exact position of the critical point is then determined by comparison of the final states obtained from initial conditions representing both sides of the transition. The ultimate judge is the energy - the lowest value determines which state is the ground state.

The last element of the imaginary time evolution is renormalization. With each step, the new wavefunction ψ_{n+1} must be normalized to the desired number of particles $\int d^3\boldsymbol{r}|\psi_{n+1}(\boldsymbol{r})|^2 = N$. In this way, each iteration provides a better estimate of the ground state.

The imaginary time evolution does not specify when the algorithm should be terminated. One may implement a clever condition for the assessment of the convergence, based on the relative energy change. If the algorithm is convergent, the subsequent energy change $\mathcal{E}[\psi_{n+1}]-\mathcal{E}[\psi_n]$ should decrease monotonically to zero with each imaginary time step. Based on this assumption, we define the algorithm termination condition as:

$$\frac{|\mathcal{E}[\psi_{n+1}] - \mathcal{E}[\psi_n]|}{\mathcal{E}[\psi_n]} \leq \epsilon, \tag{2.4}$$

where $\epsilon \leq 10^{-6}$. Such a small value of this parameter guarantees that the state is well converged. Such a state carries all the static properties of a BEC. In order to calculate the expectation value of a generic observable $\hat{O}$ one needs to evaluate the following expression:

$$\langle\hat{O}\rangle = \frac{\int d^3\boldsymbol{r}\psi^\dagger\hat{O}\psi}{\int d^3\boldsymbol{r}\psi^\dagger\psi}, \tag{2.5}$$

where the normalization factor $\int d^3\boldsymbol{r}\psi^\dagger\psi$ gives the number of particles N. In practice, the wavefunction ψ and the $\hat{O}\psi$ are stored in two arrays of complex variables. To calculate the expectation value (2.5) one needs to sum products of corresponding elements of these arrays. There are two kinds of observables we will be interested in: ones that depend only on the position and ones that involve gradients. The first ones are easy to calculate in the real space, in which also the wavefunction is represented. On the other hand, observables such as momentum or kinetic energy are more conveniently calculated in the Fourier space where the gradient ∇ is simply $i\boldsymbol{k}$. Therefore, in order to calculate the kinetic energy, one needs to evaluate:

$$\nabla^2\psi(\boldsymbol{r}) = \mathcal{F}^{-1}\left\{-k^2\mathcal{F}\{\psi(\boldsymbol{r})\}\right\}, \tag{2.6}$$

where $\mathcal{F}$ is the Fourier transform. Depending on the implementation of the Fourier transform, the expression on the right-hand side may require a proper normalization. Commonly used libraries, such as cuFFT [125] or FFTW3 [126] enforce periodic boundary conditions on the numerical domain, which has important consequences for long-range potentials. We will elaborate on them in the following section devoted to numerical simulations of dipolar BECs.

The last general element of numerical simulations related to the ground state is the use of Lagrange multipliers. We have already discussed how one can fix the number of particles using the chemical potential as the Lagrange multiplier. This method is particularly useful in the context of systems in motion. In an ordinary BEC, the superfluid velocity is given by the gradient of the phase, which is linear if the system is uniform. In this case, it is

straightforward to introduce a finite velocity field. In contrast, supersolids in motion will exhibit a more complicated phase pattern, in which both the superfluid and normal velocity are encoded. It is difficult to know the position-dependence of the phase a priori. To solve this problem, one can use the method of Lagrange multipliers to find the ground state in the moving frame of reference. Then, the algorithm finds the phase pattern corresponding to the minimal energy solution. The same pattern can be later used in the real-time evolution in the laboratory frame. Depending on the configuration, one may change the reference frame to a linearly moving one with $\hat{H} \to \hat{H} - v_x \hat{P}_x$, where the system moves with velocity v_x along the x-axis. In configurations with rotational symmetry along the z-axis the change of the reference frame rotating with angular velocity ω is achieved by adding the $-\omega \hat{L}_z$ term to the Hamiltonian. The $\hat{P}_i$ and $\hat{L}_i$ are the i-th component of the momentum and angular momentum operator, respectively.

2.1.1 BEC mixtures

Simulation of multi-component gases requires one Gross-Pitaevskii equation for each spin-component. Here we are only interested in binary mixtures, represented by two hyperfine states of the same atom of mass m. The Hamiltonian of such a system consists of two single-component Hamiltonians, supplemented with a term that accounts for inter-species interactions, and whose strength is set by a coupling constant g_{12}. It is convenient to introduce a matrix notation and represent the state of the entire system with a vector $(\psi_1 \ \psi_2)^T$. The Hamiltonian is diagonal in this basis, with the two matrix elements equal:

$$H_{ii} = -\frac{\hbar^2}{2m}\nabla^2 + V_{ext}(\boldsymbol{r}) + g_i|\psi_i|^2 + g_{12}|\psi_{3-i}|^2 \tag{2.7}$$

From the algorithmic point of view, this problem does not differ much from solving the single Gross-Pitaevskii equation twice. The only difference with respect to the single-component gas lies in the interaction, which requires the imaginary time evolution to be carried out simultaneously for both spin species. Therefore, one can use algorithm (2.3) with the following substitution $\psi \mapsto (\psi_1 \ \psi_2)^T$. The energy density functional is exact and can be written with Hamiltonian elements (2.7):

$$\mathcal{E}\left[(\psi_1 \ \psi_2)^T\right] = \int d^3\boldsymbol{r}(\psi_1^* \ \psi_2^*) \begin{pmatrix} H_{11} & 0 \\ 0 & H_{22} \end{pmatrix} \begin{pmatrix} \psi_1 \\ \psi_2 \end{pmatrix} \tag{2.8}$$

In this work, we do not consider effects of the coherent coupling, and consequently, the particle numbers of each spin component are conserved. We impose the desired normalization on each wavefunction ψ_i independently $N_i = \int d^3\boldsymbol{r}|\psi_i(\boldsymbol{r})|^2$ by adding $-\mu_i N_i$ to corresponding matrix elements H_{ii}.

2.1.2 Dipolar BECs

Dipolar gases, thanks to their long-range and anisotropic interactions, offer a wide range of interesting phenomena. As we have already presented in section (1.3), the mean-field theory of these systems is insufficient to characterize the experimental results. In particular, strongly interacting dipolar gases were demonstrated to undergo the phase transition from the superfluid to the supersolid state, in the regime of the relative interaction strength ε_{dd}, for which the mean-field theory predicts a collapse. A careful investigation revealed that by incorporating quantum fluctuations, the corrected theory faithfully models the spontaneous transition to the modulated phase. In this section we present the technical aspect of the

extended Gross-Pitaevskii equation (1.55), its origin from the DFT, as well as numerical techniques to calculate the non-local dipole-dipole interaction.

The energy density functional for dipolar BECs consists of three elements:

$$\mathcal{E}_{\mathrm{eGPE}} = \mathcal{E}_{\mathrm{GPE}} + \mathcal{E}_{\mathrm{d\text{-}d}} + \mathcal{E}_{\mathrm{QF}}, \tag{2.9}$$

where $\mathcal{E}_{\mathrm{GPE}}$ is the mean-field Gross-Pitaevskii part, which involves the kinetic term, external potential and the contact interaction potential. The dipole-dipole contribution $\mathcal{E}_{\mathrm{eGPE}}$ reads:

$$\mathcal{E}_{\mathrm{d\text{-}d}} = \frac{1}{2}\int d^3\boldsymbol{r} d^3\boldsymbol{r}'\ V_{dd}(\boldsymbol{r}-\boldsymbol{r}')|\psi(\boldsymbol{r}')|^2|\psi(\boldsymbol{r})|^2, \tag{2.10}$$

where V_{dd} is given by (1.46). The dipolar potential is inherently non-local, making its evaluation in the real space time-consuming. In contrast, the V_{dd} potential has a simple form in the momentum space, where the calculation of the dipole-dipole interaction is straightforward, thanks to the convolution theorem of the Fourier transform. Therefore, we calculate this contribution to the energy in the following way:

$$\mathcal{E}_{\mathrm{d\text{-}d}} = \frac{1}{2}\int d^3\boldsymbol{r}\ \mathcal{F}^{-1}\left\{\tilde{V}_{dd}(\boldsymbol{k})\tilde{n}(\boldsymbol{k})\right\}, \tag{2.11}$$

where the dipole-dipole potential in the momentum space reads

$$\tilde{V}_{dd}(\boldsymbol{k}) = C_{dd}\left(\frac{k_z^2}{|\boldsymbol{k}|^2} - \frac{1}{3}\right) \tag{2.12}$$

and $\tilde{n}(\boldsymbol{k}) = \mathcal{F}\{|\psi(\boldsymbol{r})|^2\}$ is the Fourier transform of the density. The side effect of using the Fourier transform is that it enforces periodic boundary conditions on the real-space grid. In almost all simulations performed in this thesis, we benefited from this feature, because most of systems under study were trapped in a long tubular geometry, which corresponds to the ring configuration. The only drawback of introducing periodic boundary conditions is related to the long-range nature of dipole-dipole interaction. The $V_{dd}(r)$ potential has an infinite range as it vanishes slowly as $1/r^3$. For this reason, one has to introduce a momentum cut-off or design the numerical domain with a large offset to avoid the spurious interaction with the system's copies introduced by the boundary conditions. We chose the latter method.

The last element of the energy density functional dedicated for dipolar condensates accounts for quantum fluctuations and is called the Lee-Huang-Yang correction (LHY). This term is the first beyond-mean-field correction as it characterizes interactions between the condensed state and all excited states. Since we want to limit the numerical model to a single-particle wavefunction, we need to include quantum fluctuations in the form of an effective single-particle potential. To achieve this, we use the Bogoliubov theory to calculate the energy contribution arising from quantum fluctuations and use it as the corresponding energy density functional. For uniform systems, we have shown that this energy is given by (2.13):

$$\frac{E_{QF}}{V} = \frac{2}{5}\gamma(\epsilon_{dd})n^{\frac{5}{2}} \qquad \text{where} \qquad \gamma(\epsilon_{dd}) = \frac{32}{3\sqrt{\pi}}ga^{\frac{3}{2}}\mathcal{Q}_5(\varepsilon_{dd}) \tag{2.13}$$

and $\mathcal{Q}_5(\varepsilon_{dd})$ is defined in (1.54). For trapped system, the LHY correction is in principle difficult to derive analytically. Provided that the inhomogeneity introduced by the presence of the external potential is smooth and varies only on large distances, one can use the local density approximation as the best estimate of the LHY correction. In our simulations

this condition is fulfilled, as we simulate relatively large systems with periodic boundary conditions, which removes the position dependence of the density on one of the coordinates.

Lastly, we remark that the function $\mathcal{Q}_5$ acquires a small imaginary part for $\varepsilon_{dd} > 1$. This indicates that even though we included quantum fluctuations, the state is still energetically unstable. In the range of ε_{dd} considered in this work, the imaginary part of $\mathcal{Q}_5$ is at least two orders of magnitude smaller than its real part, and for that reason we neglect it.

To conclude this section, we write the eGPE energy density functional for the simulation of dipolar condensates:

$$\begin{aligned}\mathcal{E}[\psi^*,\psi] = \int d^3\boldsymbol{r}\ \psi^*(\boldsymbol{r})\Bigg[&-\frac{\hbar^2}{2m}\nabla^2 + V_{ext}(\boldsymbol{r}) + \frac{1}{2}g|\psi(\boldsymbol{r})|^2 + \frac{2}{5}\gamma(\epsilon_{dd})|\psi(\boldsymbol{r})|^3 \\ &+ \int d^3\boldsymbol{r}' V_{dd}(\boldsymbol{r}-\boldsymbol{r}')|\psi(\boldsymbol{r}')|^2\Bigg]\psi(\boldsymbol{r}).\end{aligned} \tag{2.14}$$

Using the functional derivative, one finally obtains the extended Gross-Pitaevskii equation, derived within the DFT framework:

$$\begin{aligned}\frac{\delta\mathcal{E}[\psi^*,\psi]}{\delta\psi^*} = \Bigg[&\frac{\hbar^2}{2m}\nabla^2 + V_{ext}(\boldsymbol{r}) + g|\psi(\boldsymbol{r},t)|^2 + \int d^3\boldsymbol{r}' V_{dd}(\boldsymbol{r}-\boldsymbol{r}')|\psi(\boldsymbol{r}',t)|^2 \\ &+ \gamma(\varepsilon_{dd})|\psi(\boldsymbol{r},t)|^3\Bigg]\ \psi(\boldsymbol{r},t),\end{aligned} \tag{2.15}$$

2.2 Real time evolution

The second pillar of numerical simulation of Bose-Einstein condensates is the algorithm with which one can solve the time-dependent Gross-Pitaevskii equation. This algorithm provides a means of simulating the dynamics of the BEC, with which one can model a real experiment. Our real time evolution is based on the fourth order Runge-Kutta method (RK4) of integrating differential equations [127]. It is known for its stability and ease of use, as the time derivative is evaluated with four intermediate steps, without Fourier transforms. The global error of this method is $\mathcal{O}(dt^4)$, which makes it a reliable algorithm even for long simulation times, provided that the time step is sufficiently small.

In the RK4 method, for a given first-order differential equation $dy/dt = f(t,y)$ and its initial condition $y(t=0) = y_0$, the time evolution of the function $y(t)$ is given by

$$y(t_{n+1}) = y(t_n) + \tfrac{dt}{6}\left(k_1 + 2k_2 + 2k_3 + k_4\right), \tag{2.16}$$

where n indicates the iteration number, and the k_i functions read:

$$\begin{aligned}k_1 &= f(t_n, y(t_n)),\\ k_2 &= f\big(t_n + \tfrac{1}{2}dt,\ y(t_n) + \tfrac{1}{2}k_1\big),\\ k_3 &= f\big(t_n + \tfrac{1}{2}dt,\ y(t_n) + \tfrac{1}{2}k_2\big),\\ k_4 &= f(t_n + dt,\ y(t_n) + k_3).\end{aligned} \tag{2.17}$$

In this method, the derivative $dy/dt\ (t_n)$ is evaluated with four slopes given by the function $f(t,y)$ at the beginning of the time step t_n, in the middle $(t_n + dt/2)$ and at its end $t_{n+1} =$

$t_n + dt$. In the context of the DFT approach, the function y corresponds to the condensate wavefunction ψ, while:

$$f(t, y) \equiv -\frac{i}{\hbar} \frac{\delta \mathcal{E}[\psi^*, \psi]}{\delta \psi^*}. \tag{2.18}$$

The RK4 scheme works well regardless of the energy density functional, provided that the time step dt is small enough. To choose an appropriate value of dt one should estimate the shortest timescale of the dynamics for a given system and ensure it is larger than dt. In order to assess the quality of the integration of the GPE, one can measure the change in the total energy and in the number of particles. The time evolution conserves the norm of the wavefunction and, if the Hamiltonian does not depend on time, also the total energy. However, the RK4 algorithm does not enforce either conservation law by design, thus it is essential to monitor the two quantities throughout the time evolution. In every simulation performed in this thesis, the norm was always conserved and the energy drift with respect to its initial value was at most of the order 10^{-3} %. Consequently, none of the results were influenced by non-physical effects introduced by inaccurate integration of the equations of motion.

Chapter 3

Speeds of Sound in a Dipolar BEC

The first experimental observations of the superfluid dipolar gas in the form of a droplet array have intensified efforts to find signatures of its supersolid behavior. In order to identify a BEC as a supersolid, we require that the gauge symmetry and translational invariance are broken spontaneously. According to the Goldstone theorem, this means that there are two gapless modes in the excitation spectrum of a one-dimensional supersolid [38]. One of them is related to the $U(1)$ symmetry breaking, whereas the other one is associated to the lattice phonon. Thus, we expect that collective excitations of a supersolid will have a dual superfluid and crystal nature. The first experiments on collective modes in dipolar condensates [12], including axial breathing mode [10], reported two frequencies on the supersolid side of the phase transition, providing striking evidence to support the claim of supersolidity in dipolar gases.

Among all collective excitations, sound waves deserve special recognition, as they define the lowest-energy response of a given system to long-wavelength perturbations. Their characterization provides valuable information on the thermodynamic properties of the gas, such as compressibility or superfluid fraction. Moreover, they govern the temperature dependence of all thermodynamic functions at low temperatures. Within the microscopic Gross-Pitaevskii theory, sound waves are phonons that are associated with Nambu-Goldstone particles, which appear after the spontaneous breaking of continuous symmetries. Each of the three phases of dipolar BECs: superfluid (SF), supersolid (SS) and the independent droplet (ID) phase, is characterized by a dedicated phononic spectrum. The SF and ID phases exhibit only one sound mode. The former breaks the U(1) symmetry and features the regular superfluid sound, while the ID phase is not coherent and hosts only the lattice phonon. The supersolid phase is the most intriguing, as it merges the properties of the other two phases and thus hosts two kinds of sound. Because the lattice structure of a supersolid is defined by the peaks of a continuous density profile, crystalline properties are inherently coupled to the density. Consequently, both sounds will have a hybridized superfluid and crystal nature. Theoretical investigation of their character using the Bogoliubov-de Gennes equations revealed that the two sounds are a linear combination of density and lattice oscillations [128]. The first sound involves a synchronized compression of the density and lattice structure, while the second sound is an out-of-phase oscillation of the two (see Fig. (3.1)).

To date, speeds of sound have not been measured experimentally, mainly due to the small sizes of dipolar BECs and their short lifetimes. Here we propose a protocol for measuring

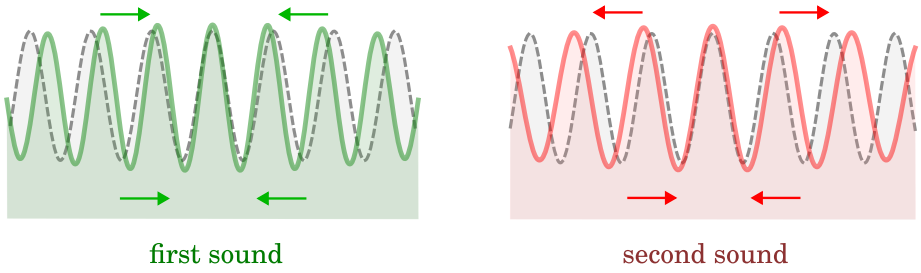

Figure 3.1: Schematic presentation of the character of the two sound modes in supersolids. The first sound is an in-phase oscillation of the density and the lattice sites, while the second mode is the out-of-phase oscillation of the two. The dashed line represents the density profile at equilibrium.

the speeds of sound across the superfluid-supersolid phase transition in a ring-shaped trap. Our aim is to design a method within the scope of present experimental capabilities. The proposed protocol is based on linear response theory, which we use to measure the speeds of sound, as well as selected static properties of the system. Moreover, the generalized version of this protocol provides a simple way to probe the dispersion relation.

In the second part of this chapter, we confront the values of the two speeds of sound calculated using the extended Gross-Pitaevskii equation with the formula derived from the hydrodynamic theory of supersolids. We find a good agreement between the two approaches with small discrepancies of known origin. Furthermore, we show that by measuring the two speeds of sound and the isothermal compressibility, the hydrodynamic theory accurately provides values of the superfluid fraction. Thus, our protocol introduces a novel way to measure this parameter.

3.1 Linear-response framework for sound excitations

The speed of sound in every BEC is a quantity that is sensitive to density variations. In harmonically trapped systems, the density profile is not uniform, thus the speed of sound at the edge of the trap is lower than in its center. In order to measure it with good accuracy, one needs to design the external potential so that its density profile in the direction of sound propagation is uniform. A standard approach is to use box traps, where the sharp boundaries ensure a uniform density in the bulk. For supersolids, however, box traps are unsuitable for probing bulk properties, since the gas tends to accumulate near the trap edges due to long-range repulsion [129, 130]. To avoid the edge effect, a ring trap seems to be an optimal geometry, as its periodic boundary conditions ensure that any supersolid held inside will have a discrete rotational symmetry. The ring topology not only allows the system to represent the bulk supersolid but also ensures that the undamped sound waves can propagate as long as the lifetime of the system. Moreover, the ring geometry permits the existence of permanent currents, which we will investigate in the next chapter.

Once we chose the optimal geometry, let us introduce the procedure to excite and measure the speed of sound. We begin by considering a gas confined in a ring of radius R and radial width $r \ll R$. With this assumption, the azimuthal angle φ is the only relevant coordinate in the context of dynamical evolution. In such a configuration, transverse dynamics can be neglected and only the longitudinal modes will propagate. Our protocol begins with the

preparation of the initial state in the presence of an additional potential of the form

$$V_{\text{protocol}}(\varphi) = V_0 \cos(n\varphi), \tag{3.1}$$

where $n \in \mathbb{Z}$ is the winding number and V_0 is small so that the linear response theory is applicable. This potential excites all lowest-energy quasiparticles, which due to the closed geometry take discretized wavevector values $q = n \times 2\pi/L$, where $L = 2\pi R$ is the circumference of the ring. In order to study the sound waves, we want to excite the longest-wavelenght modes, so we set the winding number n equal unity. The ring size is important because one has to ensure that the lowest excitation wavevector $q = 2\pi/L$ belongs to the linear part of the dispersion relation.

In the second part of our protocol, we abruptly remove the perturbation (3.1) at $t = 0$, to trigger the oscillatory dynamics of observables coupled to the density. The time evolution of the density profile is governed by all lowest-energy modes excited by the perturbation. Thus, by measuring the density profile throughout the time evolution, we gain access to the underlying frequencies ω_i of the excited modes. The dispersion relation of sound waves is linear, so the speed of sound corresponding to a mode i is evaluated as $\omega_i = c_i/q$.

Let us now interpret our protocol in terms of the linear response framework to understand its working principles. There are several important differences with respect to the canonical scenario presented in the introduction (1.4). There, the system is prepared in its ground state, while at $t = 0$ an external perturbation is adiabatically applied to drive it with a frequency ω. In our approach, the gas is initially prepared with a static perturbation, whose abrupt removal excites all lowest-energy modes. Therefore, we must include contributions of all the modes to properly assess the response of the system. We begin by writing the cosine in (3.1) as a sum of two operators, with which we can define the perturbation Hamiltonian as

$$H_{\text{pert}} = \frac{V_0}{2} \sum_{i=1}^{N} \left(e^{-in\varphi_i} + e^{in\varphi_i} \right) \theta(-t), \tag{3.2}$$

where we sum over all the particles and $\theta(t)$ is the Heaviside step function. The minus sign in the argument of θ indicates that the perturbation was applied at $t = -\infty$ and turned off at $t = 0$. Since the time dependence of (3.2) is given by the Heaviside step function, our perturbation is not selective in frequencies. It excites all the lowest-energy modes, whose frequencies are governed by the dispersion law. In general, by choosing a proper winding number n, the perturbation (3.2) excites any type of quasiparticles, including rotons and maxons on the superfluid side of the dipolar BECs. On the other hand, if the wavevector of our perturbation $q = \pm n 2\pi/L$ is small, the two operators $\exp(\pm in\varphi)$ excite phonons, which we distinguish as clockwise and anti-clockwise. At zero temperature, the structure factor $S_\pm(\omega)$ relative to the operator $\exp(\pm in\varphi)$ is a sum of delta peaks centered at frequencies of resonant modes:

$$S_\pm(\omega) = \sum_j |\, \langle j_\pm | e^{\pm in\varphi} | 0 \rangle \,|^2 \; \delta(\omega - \omega_j^\pm), \tag{3.3}$$

where $|0\rangle$ denotes the ground state and $|j_\pm\rangle$ are states with an (anti)clockwise j-phonon. In a superfluid at rest, there is only one kind of phonons, while supersolids support two types of such quasiparticles. Following equations (1.67) and (1.70), the response of the system to the cosine perturbation reads:

$$\langle \cos(\varphi) \rangle(t) = \frac{V_0}{2} \int d\omega' \frac{S_+(\omega') + S_-(\omega')}{\omega'} \cos \omega' t, \tag{3.4}$$

where $\cos\omega' t$ appears due to the decomposition of the θ function into its Fourier components. By inserting the structure factor (3.3) into the equation above, we obtain a simple formula for the time-evolution of the mean cosine:

$$F(t) := \langle \cos(n\varphi) \rangle(t) = \frac{V_0}{2} \sum_{j,\pm} \chi_j^{\pm}(q) \cos\big(\omega_j^{\pm}(q) t\big), \tag{3.5}$$

where

$$\chi_j^{\pm}(q) = \frac{|\langle j_{\pm}| e^{\pm i n\varphi} |0\rangle|^2}{\hbar \omega_j^{\pm}}. \tag{3.6}$$

In the absence of currents, the two matrix elements $\langle \pm | e^{\pm i n\varphi} | 0 \rangle$, as well as their frequencies $\omega_j^{\pm}$ are the same, and equation (3.5) is simply:

$$F(t) = \langle \cos(n\varphi) \rangle(t) = V_0 \sum_j \chi_j(q) \cos(\omega_j(q) t). \tag{3.7}$$

The averaged cosine, which we labeled with $F(t)$ is the observable that we measure throughout the time evolution after releasing the static perturbation. With the analysis of its Fourier components or by fitting an appropriate number of cosine functions, we evaluate the frequencies of all the modes propagating in the system. For small wavevectors q, the speeds of sound are given by $c_j = \omega_j / q$.

The precise knowledge of the amplitudes χ_j gives additional insights into thermodynamic properties of the gas. Susceptibilities χ_j quantify how much a given mode j couples to the external perturbation. If the perturbation wavevector q is small, the sum of all χ_j yields the isothermal compressibility κ. This follows from equation (3.4), which at $t = 0$ is equivalent to the compressibility sum rule (1.79):

$$F(t=0)/V_0 = \sum_j \chi_j(q) = \int_0^{\infty} d\omega \, \frac{S(q,\omega)}{\omega} \underset{q\to 0}{=} \frac{N\kappa}{2}. \tag{3.8}$$

Moreover, with all values of ω_j and χ_j, we can recover the dynamic structure factor (3.3), with which we can calculate every sum rule. In this respect, our protocol can be regarded as a discrete-wavevector spectroscopy.

The protocol we defined here is not new and has already been applied to a BEC to measure the quantized Doppler effect in the superfluid phase [131]. By interpreting it in terms of linear response theory, we extended its utility to gain insights into thermodynamic properties of the system under study. In their setup, the perturbation potential was applied with the digital micro-mirror device (DMD) and its sudden removal was equivalent with switching off the laser beam reflected by the DMD. We believe that the same procedure can be applied to any system, including dipolar BECs and binary Bose mixtures. For this reason, we will use this method to excite and measure the speeds of sound in all the systems considered in this thesis.

3.2 Speed of sound measurement

In this section, we show that, in line with the Goldstone theorem, the eGPE simulations predict the appearance of the second sound mode in the supersolid phase of dipolar Bose-Einstein condensates. To measure the two sounds, we apply our protocol to a system, whose parameters are within the reach of a modern experimental setups.

We considered a gas of $N = 8 \cdot 10^4$ ^{164}Dy atoms held in a toroidal trap $V_{\text{ext}}(r_\perp, z) = m\left[\omega_\perp^2 (r_\perp - R_0)^2 + \omega_z^2 z^2\right]/2$, where $r_\perp = \sqrt{x^2 + y^2}$. Although the radius $R_0 \approx 7.64\,\mu$m was chosen such that the total length of the system equals $L = 48\,\mu$m, its actual value $\langle R \rangle$ is greater and depends on relative strength ϵ_{dd}. Due to long-range dipolar interactions the radius increases because the atoms on one side of the trap repel the ones on the other side. In our case, this effect changes the length of the circumference by $\approx 1.7\%$, slightly depending on uniformity of the gas. We design the external potential in a way that the sound waves propagate only in the azimuthal direction of the ring. Therefore, the transverse extensions of the cloud must be small with respect to the system's length. With $\omega_z = \omega_\perp = 2\pi \cdot 100$Hz the radial width FWHM_{XY} changes from $1.41\,\mu$m in the superfluid to $0.7\,\mu$m approaching the crystal phase (see Fig. (3.2)). Along the direction of the dipoles, the width of the cloud is $\text{FWHM}_Z \approx 4\,\mu$m and slightly depend on ε_{dd}. By tuning the relative strength parameter, we decide the phase of the system. The transition from the superfluid to the supersolid phase occurs at $\epsilon_{dd} = 1.387$. For this value, the roton minimum softens, closing the gap at momentum k_{rot}, which defines the width of the first Brillouin zone. Because the appearance of excitations of this momentum does not increase the energy, the density profile hosts modulations proportional to the inverse of the roton momentum in its ground state, yielding the supersolid phase. The toroidal trap was designed such that $L \cdot 2\pi/k_{rot} = 14$. Examples of density profiles, integrated over the Z axis, in all three phases are reported in Fig. (3.2). The density profiles were calculated using the imaginary time evolution of the

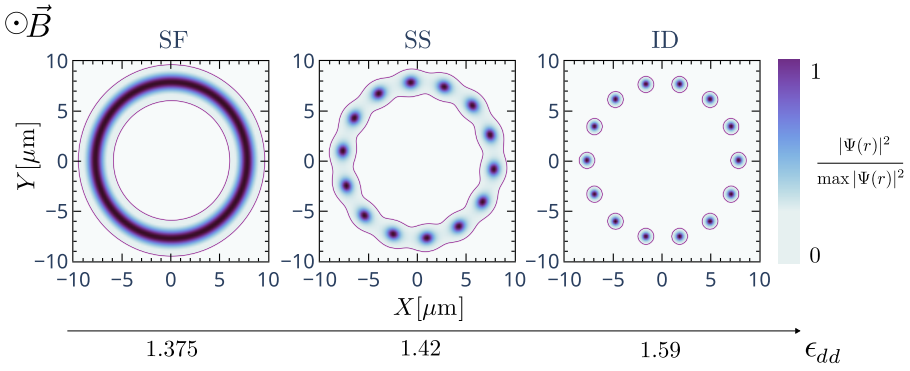

Figure 3.2: Density plots of the dipolar gas in the superfluid, supersolid and crystal phase (left, middle, and right panel respectively), integrated over the z-axis, along which the magnetic field $\vec{B}$ is aligned. Red contours mark 1% of the relative density $|\Psi(\boldsymbol{r})|^2/\max|\Psi(\boldsymbol{r})|^2$.

extended Gross-Pitaevskii equation. The independent droplet state showed in Fig. (3.2) is actually an excited state. The size of the Brillouin zone shrinks with ε_{dd}, elongating the wavelength of the density modulation, which in a fixed external potential forces the system to reduce the number of droplets. In order to avoid discontinuities introduced by this finite-size effect, we decided to fix the number of 14 droplets for every ε_{dd}. To produce such a state in the imaginary time evolution, one has to begin with a modulated initial wavefunction. In order to excite the sound modes, the state preparation was done with the addition of the potential (3.1) with the winding number $n = 1$. Its amplitude $V_0 = 0.01\hbar\omega_{ho}$, where $\omega_{ho} = \sqrt[3]{\omega_z \omega_\perp^2}$ was checked to ensure that the system responds linearly to the external perturbation. Having reached convergence for every ε_{dd}, the states were ready to be evolved in time.

Following our protocol, for every ε_{dd} we performed a time evolution, releasing the external potential V_0 at time $t = 0$. As the system evolved, we measured the averaged cosine (3.7), which stores information about all the modes propagating in the system. An example of the measured signal in the superfluid and supersolid phase is shown in Fig. (3.3). In the

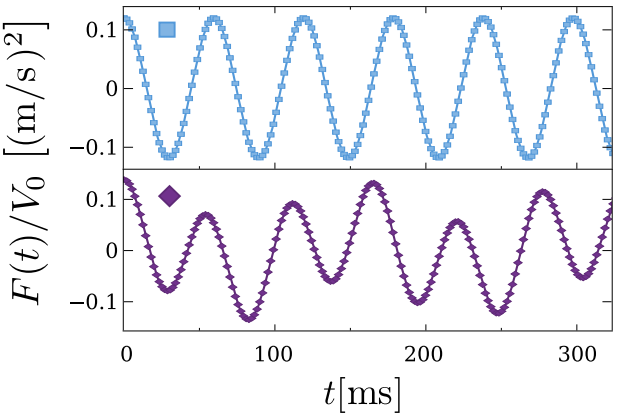

Figure 3.3: Time evolution of the measured signal (3.7) for two values of ϵ_{dd} in the superfluid phase (upper) and in the supersolid phase (lower panel). Depending on the phase, data points are fitted with one on two cosines (solid lines) with excellent quality. Fitted frequencies were used to calculate speeds of sound shown in Fig. (3.4).

superfluid phase, the $F(t)$ is given by a single frequency, whereas in the supersolid phase we observe a beating of two different frequencies. By fitting the function F with an appropriate number of cosines, we extract their frequencies and amplitudes. The latter are related to the speeds of sound, provided that the wavevector $q = 2\pi/L$ of the initial perturbation belonged to the linear part of the dispersion relation. Then, for every frequency the corresponding speed of sound reads $c_i = \omega_i q$. The results of this procedure are shown in Fig. (3.4), where we scanned the phase transition from the superfluid to the supersolid phase.

The amplitudes extracted from the signal shown in Fig. Fig. (3.3) carry valuable information as they are contributions to the compressibility sum rule (1.79). Provided that there are no other modes excited by the protocol, and that the wavevector q is small enough, the sum of the two amplitudes is proportional to the isothermal compressibility κ (see Eq.(3.8) and the discussion below). At zero temperature, this quantity defines the speed of sound of an ordinary superfluid:

$$c_\kappa = \sqrt{\rho\kappa}^{-1}, \tag{3.9}$$

where in harmonically trapped systems $\rho = \rho_0/2$ and ρ_0 is the value of the density in the central, densest part of the trap [32]. This relation also holds for dipolar BECs in the superfluid phase, as shown in Fig. (3.4).

The two sound modes in the supersolid phase demonstrate many interesting features. Remarkably, there is a large gap between values of c_1 and c_2, which does not close even in the vicinity of the phase transition. Secondly, the second sound vanishes for large ε_{dd}, when the system forms an array of almost independent droplets. This feature is expected, as there should be only one sound mode once the system looses its global coherence. We infer, that in this regime, the second sound is predominantly related to the superfluid oscillations and the first sound is given by the crystalline vibrations. This interpretation explains why

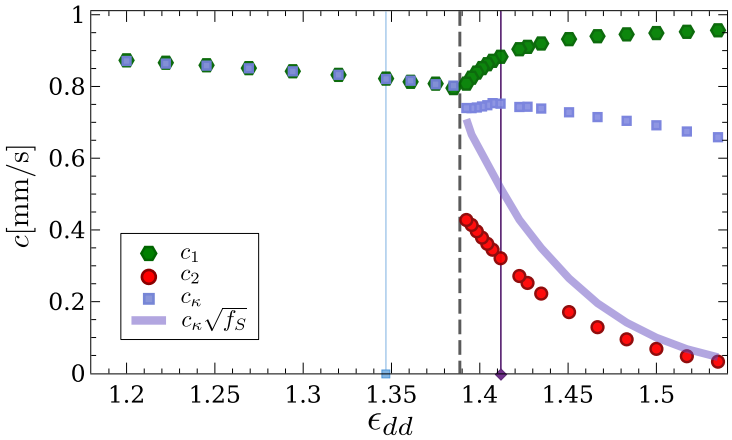

Figure 3.4: Sound velocities c_1 and c_2 determined with the protocol (green hexagons and red circles respectively) across the superfluid-supersolid phase transition. The blue squares correspond to c_κ ($q = 2\pi/L$). For completeness we also report the values $\sqrt{f_s}c_\kappa$ (purple solid line) found for an incompressible lattice (see text). The data points indicated by the two solid vertical lines correspond to the speeds of sound calculated from the measured signal (3.7) shown in figure Fig. (3.3)

values of the first sound depend so weakly on the relative interaction strength close to the transition to the ID phase.

Finally, let us observe that, contrary to the superfluid phase, the isothermal compressibility is not enough to provide an analytical description of either of the sounds. Since a supersolid features solid properties, one may expect that there is another kind of compressibility, related to the lattice structure, which plays the role of the shear modulus. We will investigate this issue in the following section. Near the superfluid phase transition the values of c_κ are close to the first sound, suggesting that in this regime the first sound is mainly of superfluid nature, whereas the second mode would correspond to lattice oscillations. In the next section we will reveal that this intuition is correct and the speed of the second sound converges to the speed of sound given by the elastic constant of the lattice. The elasticity of the dipolar supersolid is trivially observed during the time evolution of the density profile. The droplets visibly compress and decompress locally as the perturbation travels across the ring. If the lattice structure were incompressible, the gas would behave as an ordinary condensate in an optical lattice [132]. In such systems, there is only one sound, whose speed is given by:

$$c_\kappa\sqrt{f_s}, \tag{3.10}$$

where f_s is the superfluid fraction, whose value depends on the depth of the optical lattice. As an additional, quantitative indicator of elasticity, in Fig. Fig. (3.4) we compare the two speeds of sound in the supersolid phase with equation (3.10).

In conclusion of this section, we demonstrated that the eGPE indeed predicts the existence of the two sound modes, in agreement with the Goldstone theorem. Using the protocol designed to be employed under feasible experimental conditions, we characterized the speed of sound across the superfluid phase transition. Our analysis revealed interesting features of the two modes. With a simple phenomenological analysis, we assessed the character of the two sounds and confirmed that they are hybridized in the supersolid phase of dipolar

BECs. Before we proceed to a more thorough investigation of the two sound modes, let us demonstrate further capabilities of our protocol.

3.3 Probing the dispersion relation

Sound waves are elementary excitations of low momenta. In order to study them, we fixed the winding number n in the external perturbation (3.1) to unity so that the wavevector of the excited mode took its lowest value $q = 2\pi/L$ available in a closed geometry. In principle, the winding number can be an arbitrary integer, and the measured signal (3.7) would still feature oscillations. For high n, these frequencies do not correspond to the speed of sound since the created quasiparticles are no longer phonons. Nevertheless, their energies are governed by the Bogoliubov excitation spectrum. Therefore, by measuring oscillations of the signal (3.7) for higher $n = 1, 2, 3, ...$ one can scan the entire dispersion law, at small energies. In particular, in the superfluid phase, such analysis allows for the observation of the appearance of the roton minimum and its softening.

In order to demonstrate this capability, we simulate the same system as described in the previous section. The initial state is prepared on the superfluid side of the phase transition, with additional potential (3.1), for integer winding numbers $n \in [1, 20]$. The same procedure of sudden removal of the perturbation and measurement of $\langle \cos n\varphi \rangle(t)$ leads to the observation of different frequencies for various n. In Fig. (3.5), we present the result of such numerical simulations. There is a clear roton-maxon spectrum at $\varepsilon_{dd} = 1.384$. The roton

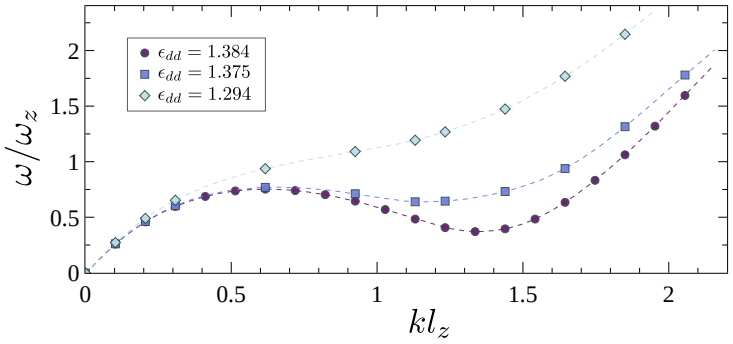

Figure 3.5: Dispersion relation obtained using the proposed protocol, for three values of ϵ_{dd} in the superfluid phase. The roton minimum softens near $k = \sqrt{2}/l_z$, where $l_z = \sqrt{\hbar/m\omega_z}$ is the harmonic oscillator length along the z-axis [61]. Dashed lines are guides to the eye. The phase transition occurs at $\varepsilon_{dd} = 1.387$.

minimum appears at $kl_z \approx \sqrt{2}$, where $l_z = \sqrt{\hbar/m\omega_z}$ is the harmonic oscillator length along the z-axis [61]. This value sets the wavelength of the density modulations in the supersolid phase.

Our method is a new alternative to standard Bragg spectroscopy [103], commonly used in experiments to study the dispersion relation of various cold atomic systems. The advantage of our protocol with respect to Bragg spectroscopy is its simplicity, as we do not require any additional laser beams. The precision of setting the perturbation wavevecotr q is limited only by the uncertainty of determining the length of the system, whereas the precision of

measuring the corresponding frequency ω is given by the resolution of the imaging apparatus and the lifetime of the system.

3.4 Speed of sound in the supersolid hydrodynamics

In the previous section, we have successfully shown that there are two sound branches in the supersolid phase of a dipolar BEC, one of which vanishes as the relative strength approaches the crystal phase. Here, we focus on the analytical way to characterize both speeds of sound, using the hydrodynamic theory of supersolids. We introduce methods to evaluate the thermodynamic properties of dipolar supersolids, which we later use to confront the measured speeds of sound with hydrodynamic predictions.

Hydrodynamic formula

The hydrodynamic formulation of supersolidity has its roots in the seminal work of Andreev and Lifshitz [1], which was further developed by Saslow [116], to see a revival at the beginning of this millennium [113–115, 117, 118]. This theory, as shown in the introduction, incorporates solid properties into the two-fluid model, by introducing new thermodynamic quantities and one equation of motion. The principal idea of the hydrodynamic treatment is to connect the superfluid features with the crystalline structure, which in the zero-temperature limit should act as the normal component of the Landau model. The complete set of hydrodynamic equations is presented in (1.64). Here we limit the hydrodynamic description to one dimension, which is equivalent to the toroidal configuration studied in the previous section.

As with every hydrodynamic theory, one can derive the analytical form of the sound modes by linearizing the equations of motion. We consider small deviations from the equilibrium values of the variables entering equations (1.64). We identify the set of four independent variables $\xi \in \{\rho, v_s, v_n, u_x\}$ and express them as the sum of their equilibrium values ξ^0 and small variations that change slowly in space and time $\delta\xi(x,t) = \delta\xi \exp(i(qx - \omega t))$. Here, we consider a system at rest ($v_n^0 = v_s^0 = 0$), in which the lattice structure is not strained $u_x^0 = 0$. Then, the linearized version of the supersolid hydrodynamic equations reads:

$$\begin{bmatrix} -c & \rho_s & \rho_n & 0 \\ (\rho\kappa)^{-1} - \gamma & -c\rho_s & -c\rho_n & \rho\gamma - \lambda \\ 1/(\rho^2\kappa) & -c & 0 & \gamma \\ 0 & 0 & -1 & -c \end{bmatrix} \begin{bmatrix} \delta\rho \\ \delta v_s \\ \delta v_n \\ u_x \end{bmatrix} = 0, \tag{3.11}$$

where we used equations (1.63) to explicitly write variations of pressure δp and chemical potential $\delta\mu$. The trivial form of the fourth linearized equation is the consequence of the fact that in the absence of currents, the strain u_x defines the velocity of the normal component. In the $q \to 0$ limit, the dispersion law is linear and the slope $c = \omega/q$ defines the speed of sound.

Non-trivial solutions of the hydrodynamic equations require the determinant of the matrix (3.11) to vanish. After a straightforward algebra, this condition takes the following form:

$$\left(c^2 - c_1^2\right)\left(c^2 - c_2^2\right) = 0, \tag{3.12}$$

where

$$c_{1,2}^2 = \frac{1}{2}\left(\beta + c_\kappa^2 - 2\gamma\right) \pm \frac{1}{2}\sqrt{\left(\beta + c_\kappa^2 - 2\gamma\right)^2 - 4\frac{\rho_s}{\rho}\left(\beta c_\kappa^2 - \frac{\rho\gamma^2}{\rho_n}\right)}, \tag{3.13}$$

are the two speeds of sound propagating in the supersolid. As expected, the analytical formulae of the two speeds of sound involve additional thermodynamic quantities. The new parameter $\beta = \lambda/\rho_n$ is the equivalent of the shear modulus of the supersolid, while γ is a phenomenological strain-density coupling. Finally, the last parameter defining the speeds of sound is the superfluid fraction $f_s = \rho_s/\rho$. Since the supersolid state features density modulations, it is expected that the reduced superfluid inertia affects the character of the propagation of the sound.

Let us analyze the limiting values of equations (3.13) to find the hydrodynamic predictions for the speed of sound in all three phases of the dipolar condensates. By setting the two parameters β and γ to zero, we recover the single-sound formula (3.9) valid in the superfluid phase. On the other hand, in the independent droplet phase, the superfluid fraction equals zero, and one of the equations (3.13) vanishes, while the other reduces to $c_{\mathrm{ID}}^2 = \beta + c_\kappa^2 - 2\gamma$. Thus, the hydrodynamic theory of supersolids provides the analytical prediction for the sound modes across the entire phase diagram. It is worth noticing, than in the limit of infinitely stiff lattice ($\beta \to \infty$) the solution with + sign becomes infinite, while the other speed of sound coincides with (3.10) derived for a superfluid in an optical lattice.

Having seen that the extended Gross-Pitaevskii equation predicts the appearance of the second sound mode in the supersolid phase, one may use this microscopic theory to check the validity of equations (3.13). The agreement between the eGPE and the hydrodynamic model of supersolids is not guaranteed, as the former is an effective theory, based on an approximation of the contribution of the quantum fluctuations term. This work was the first attempt to confront predictions of the two theories.

Numerical methods

In order to calculate all the parameters entering equations (3.13), we need to understand their definition in the microscopic picture. We begin with κ, β and γ, because they are defined as second derivatives of the energy ε. To show this, let us expand the total energy with respect to the density and strain variations around their equilibrium values:

$$\varepsilon \approx \varepsilon_0 + \frac{1}{2}\frac{\partial^2\varepsilon}{\partial\rho^2}\delta\rho^2 + \frac{1}{2}\frac{\partial^2\varepsilon}{\partial u_x^2}(u_x)^2 + \frac{\partial^2\varepsilon}{\partial u_x \partial\rho}u_x\delta\rho \tag{3.14}$$

Using the definition of the chemical potential $\mu = \partial\varepsilon/\partial\rho$ and the Gibbs-Duhem relation

$$dp = \frac{1}{\rho\kappa}d\mu - (1 - u_x^0)d\Lambda, \tag{3.15}$$

where the equilibrium strain $u_x^0 = 0$ and $d\Lambda = \lambda u_x + \gamma\delta\rho$ denotes variation of the stress constant[1], one can relate the derivatives in (3.14) to thermodynamic parameters by comparison with constitutive equations (1.63). In this way, we find:

$$\frac{1}{\rho\kappa} = \frac{\partial^2\varepsilon}{\partial\rho^2}, \qquad \rho_n\beta = \frac{\partial^2\varepsilon}{\partial u_x^2} \quad \text{and} \quad \gamma = \frac{\partial^2\varepsilon}{\partial\rho\partial u_x}. \tag{3.16}$$

All three parameters can be numerically evaluated by measuring the difference in total energy $\varepsilon = \int d^3\boldsymbol{r}\ \mathcal{E}_{\mathrm{eGPE}}[\psi(\boldsymbol{r})]/L$ with respect to small changes of one of the two parameters ρ, u_x. Before we describe this procedure in details, we shall discuss the optimal geometry of the gas for the comparison with the hydrodynamic model.

[1] In three-dimensional supersolids Λ becomes a tensor.

Thus far, we simulated the dipolar BEC contained in a torus by evolving in time a three-dimensional gas in a ring-shaped trap. The choice of such a geometry was motivated by the aim of simulating the system in a real experimental setup. In order to compare the speeds of sound predicted by the eGPE and the supersolid hydrodynamics, we simulate the dipolar condensate in a tube with periodic boundary conditions imposed on its ends. We motivate this change by an increased precision of determining the derivatives with respect to the strain u_x. Furthermore, the linear geometry is equivalent to the ring, provided that its length is large enough to neglect the curvature effects. The tube confinement is computationally less demanding than the 3D ring, thus we can afford to double the length of the system with respect to the previous analysis.

Our gas consists of $N = 1.6 \cdot 10^5$ ^{164}Dy atoms confined, in a tube of length $L = 96\mu$m with periodic boundary conditions and with a transverse potential given by $m\omega_\perp^2 r^2/2$, where $\omega_\perp = 2\pi \cdot 100$Hz. Dipoles are aligned by an external magnetic field along the z-direction, whereas the tube extends along the x-axis. In order to calculate the two speeds of sound, we use the same protocol as before (3.1), where the azimuthal angle corresponds to $2\pi/L \cdot x$, where $x \in [-L/2, L/2)$. Therefore, the ground state is prepared with the perturbation:

$$V_{\mathbf{protocol}} = V_0 \cos\left(n \times 2\pi \frac{x}{L}\right). \tag{3.17}$$

By measuring the same observable (3.7), we gain access to the two speeds of sound.

To calculate c_1 and c_2 from the hydrodynamic model (3.13), we need to evaluate second derivatives of the total energy per particle with respect to ρ and u_x. We use the 5-point stencil method, in which the second derivative of a function $f(x)$ at $x = x_0$ is given by 5 values of f, evaluated at $\{x_0 - 2h, x_0 - h, x_0, x_0 + h, x_0 + 2h\}$:

$$\left.\frac{d^2 f(x)}{dx^2}\right|_{x=x_0} \approx \frac{-f(x_0+2h) + 16f(x_0+h) - 30f(x_0) + 16f(x_0-h) - f(x_0-2h)}{12h^2}. \tag{3.18}$$

To calculate the isothermal compressibility κ, we determine the total energy of a given state for different densities. We change ρ by imposing an appropriate normalization condition on the norm of the condensate wavefunction. In order to find a method to calculate the other two derivatives, we need to understand how to evaluate the strain u_x. Although a supersolid has a continuous density profile, its lattice properties are represented by discretized quantities. The lattice sites correspond to the density maxima and with $u(x_i)$ we defined the displacement of the lattice site i with respect to its equilibrium position. Since $u(x_i)$ is a discrete function, the derivative u_x essentially equals its change Δu on the distance between the neighboring sites a_0. From the point of view of a unit cell, the displacement difference Δu is equivalent to a change in the lattice constant with respect to its equilibrium value a_0. Thus, any derivative with respect to u_x can be written as:

$$\left.\frac{\partial}{\partial(u_x)}\right|_{\rho=const.} \equiv a_0 \left.\frac{\partial}{\partial a}\right|_{\rho=const.}, \tag{3.19}$$

where we assume every other parameter to be constant. Therefore, such derivatives can be calculated by varying the total length of the system L, wile keeping the density and number of droplets constant. Using this technique, we calculate the lattice compressibility β and the strain-density coupling constant γ as:

$$\beta = \frac{1}{\rho_n} \cdot a_0^2 \frac{\partial^2 \varepsilon}{\partial a^2} \quad \text{and} \quad \gamma = a_0 \frac{\partial^2 \varepsilon}{\partial a \partial \rho}, \tag{3.20}$$

where the energy density ε is given by the extended Gross-Pitaevskii energy density functional. Finally, the three parameters c_κ^2, β and γ are shown in Fig. (3.6a) as a function of the relative interaction strength ε_{dd}. As expected, the strain-density coupling γ is negligible

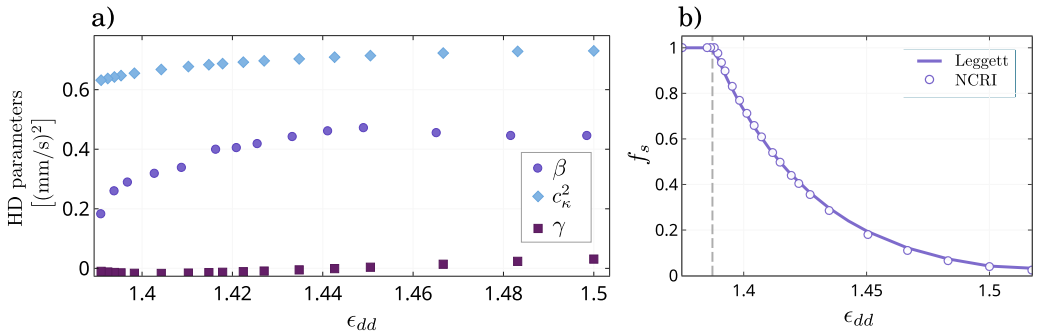

Figure 3.6: a) Hydrodynamic parameters β, γ, c_κ^2 in the supersolid phase of a dipolar BEC, calculated with the total energy derivatives. b) Superfluid fraction calculated with the NCRI (3.21) (symbols) and the Legget's upper bound (1.41) (line).

with respect to β, thus we do not include it in our analysis.

The last parameter that we must calculate to compare the hydrodynamic formula (3.13) with the results of our protocol is the superfluid fraction. According to its definition (1.43), the f_s measures the decreased response of a superfluid system to small rotations. In the tubular configuration, the angular velocity corresponds to the linear velocity v and the superfluid fraction is measured as:

$$f_s = \lim_{v\to 0} 1 - \frac{\langle P_x \rangle}{Nmv}, \tag{3.21}$$

where $\langle P_x \rangle = -i\hbar \int d^3\boldsymbol{r}\ \psi^*(\boldsymbol{r})\partial_x\psi(\boldsymbol{r})$ is the total momentum along the x-axis. Numerically, we create states with finite currents by using the imaginary time evolution with an additional element $-vP_x$ added to the eGPE Hamiltonian. This method effectively changes the reference frame to the one moving with velocity v. In a one-dimensional supersolid, the superfluid fraction calculated with the NCRI almost coincides with Leggett's upper bound (1.41), as can be seen in Fig. (3.6b).

Results

Finally, after all relevant thermodynamic parameters have been determined, we can compare the hydrodynamic formula (3.13) with the two speeds of sound measured in the time-dependent calculations using our protocol. In Fig. (3.7) we present predictions of the two theories for c_1 and c_2. For reference, we also plot c_κ and $c_\beta = \sqrt{\beta}$. The qualitative agreement between the two theories is good enough to claim that the extended Gross-Pitaevskii equation gives a reliable description of the two speeds of sound. Relative discrepancies in the values of c_1 and c_2 are smaller than 10%. We shall now discuss their sources.

There are several factors limiting the agreement between the two methods of calculating c_1 and c_2. The most important one is that we applied the protocol to a system, which was artificially strained by the periodic boundary conditions. For every value of ε_{dd}, we prepared the system in a configuration with 27 periods of the density modulation in a fixed length $L = 96\mu$m. This value was chosen so that it matches the integer multiplication of

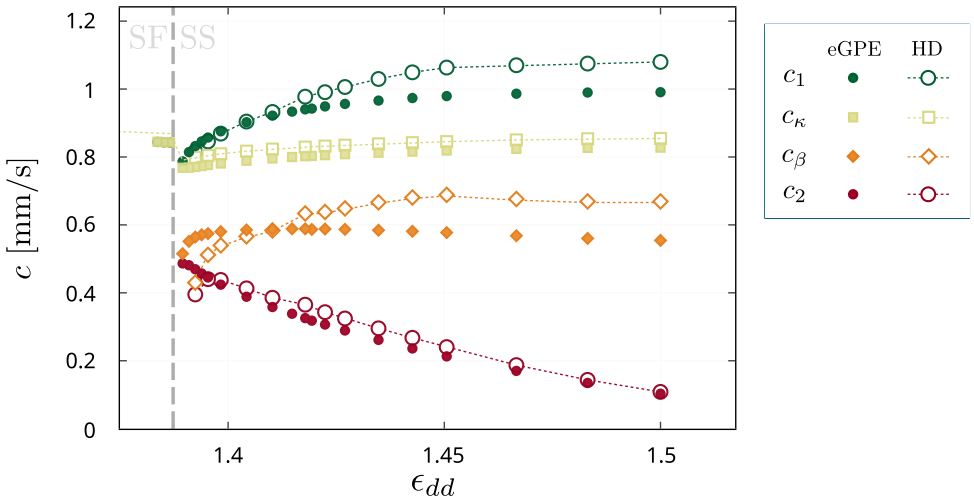

Figure 3.7: Comparison of the two speeds of sound (green and red) in the supersolid phase of dipolar BECs calculated with the dynamic protocol (full symbols) and predicted by the hydrodynamic formula (3.13) (empty symbols and dotted lines). For comparison, we plot two velocities $c_\kappa = (\rho\kappa)^{-1/2}$ and $c_\beta = \beta^{1/2}$ (see text).

$2\pi/k_{rot}$, which means that the crystal is not strained at the critical point. However, we noticed that this distance grows with ε_{dd}, indicating that in a fixed geometry, the system prefers a state with lower number of droplets. Therefore, by fixing both the total length and the number of droplets, we measured the propagation of sound in a strained supersolid. The correct approach (used to calculate the empty symbols in Fig. (3.7)) requires finding the equilibrium length for every ε_{dd} and applying the protocol to a system confined in a tube of this particular length. The significance of this error was recognized only too late to recalculate all the results of the demanding time-dependent simulations. This error can be seen in Fig. (3.7) where the values of $c_\beta = \sqrt{\beta}$ evaluated with the total energy derivative (empty symbols) differ significantly from c_β calculated with equation (3.25), which uses c_κ, c_1 and c_2 from the protocol and assume the validity of the HD formula (3.13).

The second source of the discrepancies is another finite-size effect. As elaborated in (3.1), our protocol generates excitations of finite wavevectors q, which correspond to sound waves only in the $q \to 0$ limit. The constant difference of $\approx 3.5\%$ between the values of c_κ calculated from the compressibility sum rule (3.8) and the energy derivative (3.16) reveals that the perturbation wavevector is not precisely in the linear part of the dispersion law. Consequently, values of c_1 and c_2 are slightly lower with respect to their thermodynamic limit values.

In conclusion, we have found a good agreement between the speeds of sound predicted by the extended Gross-Pitaevskii equation and the hydrodynamic theory of supersolids. These results, originally published in [133], are the first indication that the two theories are coherent in the description of long-wavelength dynamics of supersolid gases. The same results were also found in [123, 134], where the authors simulated infinite systems and extracted the speeds of sound using Bogoliubov-de Gennes equations.

Utility of the HD theory

Now that the validity of the supersolid hydrodynamics has been confirmed, we investigate its utility in terms of determining thermodynamic quantities. We show that our protocol provides the measures to calculate the isothermal compressibility κ, the lattice compressibility β and the superfluid fraction f_s.

In the supersolid phase of a dipolar BEC, the measured observable has two components:

$$F(t) = \chi_1 \cos\omega_1 t + \chi_2 \cos\omega_2 t, \tag{3.22}$$

corresponding to the two sounds. As we have already shown at the beginning of this chapter, the sum of the two amplitudes is proportional to the isothermal compressibility κ, provided that $q \to \infty$:

$$\frac{F(t=0)}{V_0} = \chi_1 + \chi_2 = \chi \underset{q\to 0}{=} \frac{N\kappa}{2}. \tag{3.23}$$

The sum $\chi_1 + \chi_2$ can be evaluated either by measuring the static response $F(t=0)$ or by summing the two amplitudes extracted from the fit to the time signal $F(t)/V_0 = \sum_{j=1,2} A_j \cos(\omega_j t)$. In an experimental setup it is often difficult to precisely measure the amplitude of the applied perturbation V_0 and equation (3.23) might not be enough to precisely determine the compressibility. Fortunately, using the $f-$sum rule and the inversely weighted sum rule, one can prove the following relation:

$$R \equiv \frac{\chi_2}{\chi} = \frac{c_1^2 - c_\kappa^2}{c_1^2 - c_2^2}, \tag{3.24}$$

which sets the contribution of the second sound mode to the compressibility sum rule. Thus, the two speeds of sound and amplitudes $\chi_{1,2}$ obtained from the fit to the signal $F(t)$ may be used to calculate the isothermal compressibility κ without knowing V_0.

Assuming the validity of the supersolid hydrodynamics, our protocol enables measurements of the layer compressibility β and the superfluid fraction f_s. Both parameters can be obtained using the hydrodynamic formula (3.13). In particular:

$$c_\beta^2 \equiv \beta = c_1^2 + c_2^2 - c_\kappa^2 \tag{3.25}$$

and

$$f_s = \left(\frac{c_1 c_2}{c_\kappa c_\beta}\right)^2 \tag{3.26}$$

Remarkably, the superfluid fraction of a supersolid can be determined entirely from the knowledge of c_1, c_2 and c_κ. This finding introduces a new method of evaluating f_s in supersolid platforms. In Fig. (3.8) we compare the results of (3.26) with Leggett's upper bound and the definition of the superfluid fraction (3.21). Minor discrepancies are caused by the finite-size effects discussed above.

In analogy to equation (3.24), we may use the energy-weighted and inverse energy-weighted sum rules to calculate the contributions of the two sounds to the $f-$sum rule (1.78):

$$\frac{m_1^{(1)}}{m_1} = \frac{c_2^2}{c_\kappa^2}\frac{c_1^2 - c_\kappa^2}{c_1^2 - c_2^2} \qquad \text{and} \qquad \frac{m_1^{(2)}}{m_1} = \frac{c_2^2}{c_\kappa^2}\frac{c_1^2 - c_\kappa^2}{c_1^2 - c_2^2}. \tag{3.27}$$

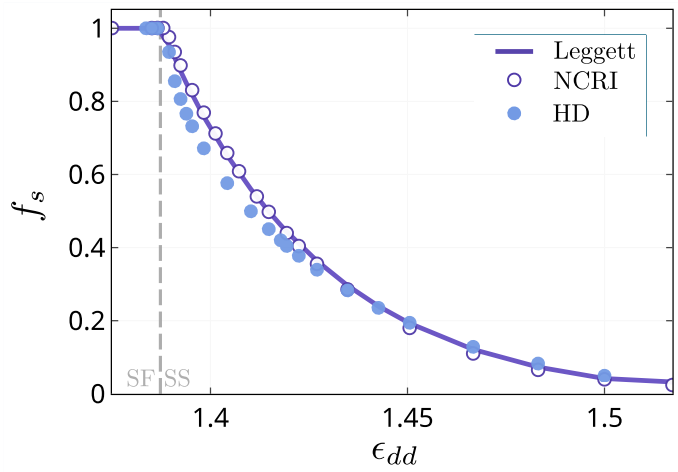

Figure 3.8: Superfluid fraction calculated using the speeds of sound (3.26) (full symbols) compared with NCRI (empty symbols) and Leggett's upper bound (solid line).

The relative contribution to the two sum rules is presented in Fig. (3.9). Interestingly, in the independent droplet phase, where $c_2 = 0$ and $c_1^2 = c_\kappa^2 + c_\beta^2$, the energy-weighted sum rule is exhausted by the only sound mode, whereas the compressibility sum rule is not, as (3.24) is not equal unity. This reveals the occurrence of a diffusive mode at zero frequency. This mode represents the natural continuation of the second sound mode beyond the transition to the crystal phase [135] and corresponds to the diffusive permeation mode of a smectic-A liquid crystal [118, 135]. The evolution of the second mode from propagating to diffusive is analogous to the fate of second sound (the entropy sound) in a uniform fluid above the superfluid critical temperature (see, e.g., [136, 137]).

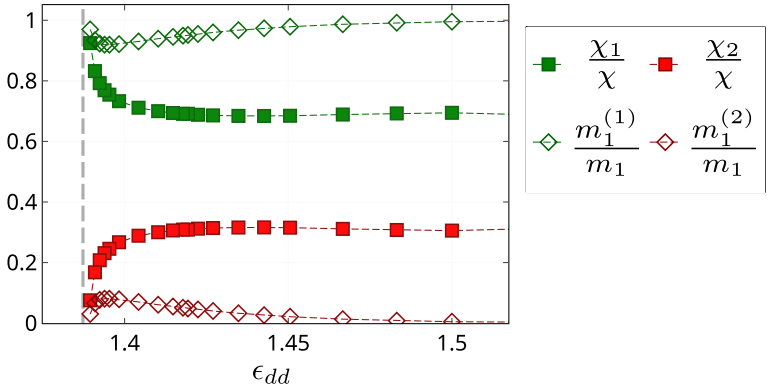

Figure 3.9: Relative contribution of each sound to the compressibility sum rule (3.24) (full symbols) and to the f-sum rule (3.27) (empty symbols) under the two-mode assumption.

Lastly, we point out that in the vicinity of the superfluid phase transition, within the supersolid region, we find that our perturbation excites an additional mode. We associate

this third frequency to the Higgs mode, which becomes gapless at the critical point [128, 134]. Although its presence does not prevent us from using the protocol, the two-mode approximation used in (3.24) and (3.27) becomes invalid. The appearance of additional modes can be observed by using the two speeds of sound and their amplitudes to evaluate the f-sum rule (1.78). In Fig. (3.10) we show that the two sound modes do not exhaust this sum rule, indicating the presence of other modes.

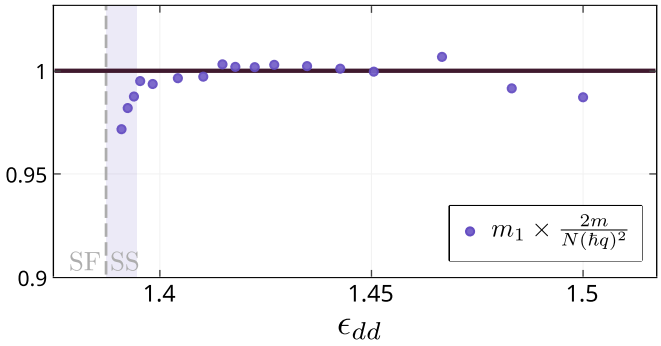

Figure 3.10: f-sum rule calculated with the two speeds of sound and amplitudes $\chi_{1,2}$. For ε_{dd} belonging to the shaded area, the two sounds do not exhaust the energy-weighted sum rule, indicating presence of other modes.

Chapter 4

Doppler Effect in Density-Modulated Superfluids

The Doppler effect appears in every physical system that exhibits wave properties. The canonical example of this phenomenon is the change in sound wave frequency caused by the relative motion of the source and the observer. For waves that propagate in a medium, such as sound waves, the frequency shift also depends on the velocity of the medium. To simplify the discussion, let us assume that both the source and the observer are at rest in the laboratory frame of reference. In ordinary fluids moving at a small velocity v_f, the sound speed c_0 is modified as $c^{\pm} = c^0 \pm v_f$, depending on whether the sound propagates parallel $(+)$ or antiparallel $(-)$ to the velocity v_f. This effect is purely kinematic, as it stems from the Galilean transformation of the equations of motion. The same shift occurs in uniform superfluids at zero temperature. The Galilean transformation of the energy and momentum in a moving superfluid modifies its dispersion relation $\epsilon'(\boldsymbol{p}) = \epsilon(\boldsymbol{p}) + \boldsymbol{p} \cdot \boldsymbol{v}_f$ as seen from the lab frame (see section (1.2.1)). For this reason, although there is only one sound mode, we may interpret the excitation spectrum of a moving superfluid in terms of two phonon branches, distinguished by the direction relative to the superfluid velocity. A schematic representation of the modified dispersion relation is shown in Fig. (4.1)

The kinematic form of the Doppler effect in uniform superfluids was reported in experiment [131], where the gas of ultracold sodium atoms was held in a ring trap, imposing quantization of the superfluid current. Using the same protocol, which we employed in the

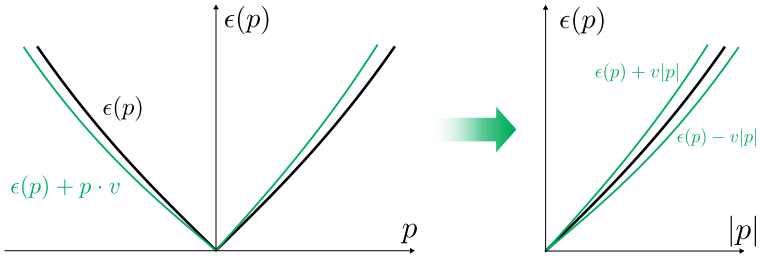

Figure 4.1: A sketch of elementary excitation spectrum in the presence of a current in an uniform BEC.

previous section, the authors created sound waves and determined the Doppler shift by measuring precession of the density profile. Their results confirmed the kinematic character of the effect and the quantized form of the superfluid current.

Interestingly, superfluid platforms can host two types of currents at finite temperatures, as explained by the two-fluid model. Although the system consists of one atomic species, it effectively acts as a mixture of a superfluid and a normal gas. The two-fluid model does not make any assumptions about the relation between normal and superfluid velocities, allowing them to take different values. A canonical example of such a system is the superfluid helium in porous media, in which the normal component is locked and the superfluid part is free to move. In such a case, for a finite superfluid velocity, a reference frame in which both components would be at rest does not exist, and the Doppler effect becomes non-trivial.

The problem of sound entrainment in the two-fluid model was first addressed by Khalatnikov [13] for superfluid helium at finite temperature. He demonstrated that the second sound exhibits an anomalous Doppler shift, whose values depend on all thermodynamic properties of the system. Further theoretical studies have pointed out the occurrence of non-trivial, anomalous Doppler shifts in ^{4}He, including the first [15] and the fourth sound [14, 15, 138]. The effect does not depend on quantum statistics and was later addressed in superfluid ^{3}He [139] as well as in ^{4}He$-^3$He mixtures [16, 140].

The Doppler effect of the fourth sound in Helium was observed in [141, 142] as a method to detect superflow, but the authors did not characterized it. To our knowledge, a clear experimental confirmation of the anomalous Doppler effect in liquid helium is still missing. Fortunately, superfluid helium is not the only platform that can be effectively described with the two-fluid model, as every atomic gas routinely produced in ultracold experiments will also be partly superfluid at finite temperatures below the critical point. With their long lifetime and versatile tunability, these gases seem to be perfect systems to study the anomalous Doppler effect.

Remarkably, superfluids at zero temperature may also exhibit a non-trivial Doppler effect, provided that their density profile is not uniform. In such systems, the superfluid fraction is reduced owing to the Leggett's upper bound (1.41) and the remaining part acts as a normal component. In this chapter, we investigate the Doppler effect in density-modulated superfluids, including superfluids in optical lattices and supersolids. We show that these systems exhibit anomalous Doppler shifts, similarly to liquid helium platforms. Our analysis includes both hydrodynamic and microscopic GPE treatment, with the comparison between the two revealing a good agreement.

4.1 Doppler effect in superfluids in optical lattices

Optical lattices are external potentials usually created with two counter-propagating lasers of momentum k and the same frequency [143, 144]. Their interference leads to a rapidly oscillating standing wave, whose time-averaged intensity is proportional to $\cos^2(kx)$. By changing the intensity of the light and the relative angle between the two laser beams, one can modify the amplitude and the periodicity of the external potential. This flexibility makes an optical lattice a perfect system for studying many interesting phenomena, including localization effects [145], superfluid-Mott insulator phase transition [146], and quantum simulations [147]. In our case, the primary function of the optical lattice is to lower the superfluid fraction by modulating the density profile. According to Leggett's upper bound (1.41), every superfluid, whose density profile is not uniform, will exhibit a reduction of its superfluid inertia even at zero temperature. Although the whole system is coherent, part

of the fluid will effectively act as an ordinary gas. This makes density-modulated BECs a perfect system for studying the anomalous Doppler effect reported in superfluid helium. In both ^{3}He and ^{4}He, the sound entrainment became non-kinematic once the superfluid velocity differed from the normal velocity. Such conditions can be obtained in our atomic gas platform by fixing the position of the optical lattice and moving the superfluid part. Since the periodic external potential gives rise to the normal part, fixing it results in setting the normal velocity to zero.

In this section, we investigate the sound propagation and Doppler effect in superfluid atomic gas in a stationary optical lattice at zero temperature. The sound propagating in such a configuration is equivalent to the fourth sound in liquid helium. We derive an analytic prediction for the speed of sound and the Doppler effect using the hydrodynamic equations (1.2.2) and confront them with predictions of the Gross-Pitaevskii equation.

Hydrodynamic model

Consider a one-dimensional superfluid in an optical lattice at $T = 0$. If the external periodic potential is stationary, the normal component is locked and its velocity $v_n = 0$. Although in general the two-fluid model consists of four equations, in the zero temperature limit, there are only two hydrodynamic equations necessary to characterize our system. In the presence of the optical lattice, the Hamiltonian does not commute with the momentum operator $[\hat{H}, \hat{P}] \neq 0$ and the momentum conservation law (1.37) is not valid. Furthermore, at $T = 0$, the entropy conservation law (1.39) is irrelevant, and the remaining equations (1.36) and (1.38) are:

$$\partial_t \rho + \partial_x(\rho_s v_s) = 0 \tag{4.1a}$$

$$\partial_t v_s + \partial_x \left(\mu_s + \frac{1}{2} v_s^2\right) = 0, \tag{4.1b}$$

where μ_s is the chemical potential in the superfluid rest frame. The standard procedure to calculate the speed of sound relies on linearization of HD equations by representing all variables as a sum of their equilibrium values and small variations dependent on space and time. Primarily, one identifies ρ and v_s as the only two independent variables that enter the equations (4.1). Denoting their equilibrium values with ρ^0 and v_s^0 respectively, one can write $\rho(x,t) = \rho^0 + \delta\rho(x,t)$ and $v_s(x,t) = v_s^0 + \delta v_s(x,t)$. Both variations are then assumed to be slowly varying in space and time as $\delta\xi(x,t) = \delta\xi \exp(-i(\omega t - qx))$. In the $q \to 0$ limit, the ratio ω/q gives the speed of sound. The superfluid density ρ_s and chemical potential μ_s depend on ρ and v_s, so their variations can be expressed with partial derivatives with respect to these variables. Here we will only consider velocities v_s small with respect to the speed of sound, effectively neglecting all terms of order higher than linear in v_s. Since the dependence of ρ_s on v_s is quadratic, the superfluid density can be written as

$$\rho_s(x,t) = \rho_s^0 + \rho_s' \delta\rho(x,t), \quad \text{where} \quad \rho_s' \equiv \frac{\partial \rho_s}{\partial \rho}. \tag{4.2}$$

To assess the variation of the chemical potential, one has to identify its dependence on ρ and v_s. Using Galilean transformation of the free energy, one can show that $\mu_s = \mu_0 - \rho_n'(v_n - v_s)^2/2$ [122], where μ_0 is the chemical potential in the absence of currents and therefore depends only on the density ρ. In fact, the variation $\delta\mu_0$ is fixed by isothermal compressibility κ, whose inverse in unmodulated superfluids at zero temperature gives the speed of sound (3.9). Finally, the complete variation of the chemical potential reads $\delta\mu_s =$

$1/((\rho^0)^2\kappa)\delta\rho - \rho_n' v_s^0 \delta v_s$ and the linearized HD equations are conveniently written in the matrix form:

$$\begin{pmatrix} -\omega \pm q v_s^0 \rho_s' & q\rho_s^0 \\ \dfrac{q}{(\rho^0)^2\kappa} & -\omega \pm q v_s^0 \rho_s' \end{pmatrix} \begin{pmatrix} \delta\rho \\ \delta v_s \end{pmatrix} = 0, \tag{4.3}$$

where the $\pm$ sign depends on the angle between the perturbation wavevector q and the superfluid velocity v_s^0. The only non-trivial solutions are given by the vanishing determinant of the matrix above. Then, using the long-wavelength relation $c = \omega/q$, the speed of sound reads:

$$c^{\pm} = c^{(0)} \pm \rho_s' v_s^0 = \sqrt{f_s} c_\kappa \pm \left(f_s + \rho^0 \frac{\partial f_s}{\partial \rho} \right) v_s^0 \ , \tag{4.4}$$

where $+$ $(-)$ denotes the sound mode co-propagating (counter-propagating) with v_s. The first term is the speed of sound in an optical lattice in the absence of currents (3.10). Its dependence on the superfluid fraction has been recently confirmed experimentally [132, 148]. The second term is the Doppler shift, which has been also derived in [138] in the case of superleak helium configurations, and in [149, 150] in the case of atomic Bose-Einstein condensates in optical lattices, after linearization of the time-dependent Gross-Pitaevskii equation (GPE).

Intuitively, one might expect that the Doppler shift of the fourth sound is given by the supercurrent $j/\rho^0 = f_s v_s^0$, which is the only part of the system that moves. This picture is in contradiction with the hydrodynamic formula (4.4), which involves both the superfluid fraction and its derivative with respect to the total density. Analogous discrepancy between the hydrodynamic formula and the kinematic prediction for the fourth sound was found in liquid helium [14, 15, 138]. This finding suggests that, contrary to a common interpretation of the fourth sound, the normal part is also involved in the propagation of this sound.

Lastly, the result (4.4) can be generalized to superfluid systems in moving optical lattices with a simple Galilean transformation $\{c, v_s\} \to \{c - v_n, v_s - v_n\}$:

$$c^{\pm} = c^0 \pm v' = c^0 \pm \left(\rho_s' v_s^0 + \rho_n' v_n^0 \right) \tag{4.5}$$

Numerical methods and comparison with hydrodynamics

In contrast to liquid helium, ultracold atomic gases can be accurately studied with a microscopic theory. To verify the validity of the hydrodynamic result (4.4), we numerically solve the Gross-Pitaevskii equation. We consider a gas of $N = 2 \cdot 10^5$ ^{87}Rb atoms confined in a tube of length $L = 96\mu$m along the x-axis, subject to periodic boundary conditions, and radially confined by a harmonic potential of the form $1/2\ m\omega_\perp^2 r^2$, with $r^2 = y^2 + z^2$, $\omega_\perp = 2\pi \cdot 150$Hz, with $\sqrt{\hbar/m\omega_\perp} \ll L$. The gas is subjected to an optical lattice implemented as an additional external potential of the form $V_{ext} = sE_R \cos(qx)$, where $E_R = \hbar^2 q^2/2m$ is the recoil energy, and the dimensionless parameter s gives the strength of the external potential. At zero temperature, the gas forms a Bose-Einstein condensate, characterized by a healing length $\xi = \hbar/(\sqrt{2m\mu_0})$, which represents the length scale on which the condensate can react to an external potential. We choose the period of the lattice $d = 2\pi/q = 4\mu$m to be much larger than the healing length: $d \approx 16.7\xi$. In the opposite regime, $d \ll \xi$, the superfluid fraction becomes density independent and the kinematic Doppler shift is recovered [151]. An example of the transversely integrated GPE ground state density $\rho_{GP}(x)$ is reported in Fig. (4.2).

In order to study the Doppler effect of the fourth sound, we employ the linear response protocol (3.1) to a system with a permanent current. The state preparation in such a

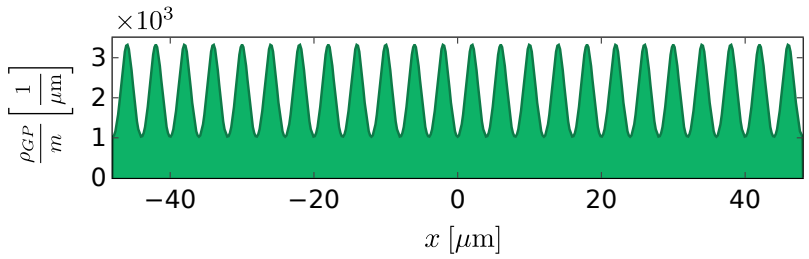

Figure 4.2: Example of a transversely integrated fluid density in an optical lattice of strength $s = 3$.

system requires a minor modification with respect to the procedure described in the previous chapter, as we use the imaginary time evolution in the moving frame of reference to create a finite superfluid velocity field. Thus, we minimize the energy of a system, whose Hamiltonian contains an additional term $-v_s^0 P_x$, where P_x is the x component of the momentum operator. This numerical technique enables the GPE minimization algorithm to find the phase pattern that minimizes the energy. The same pattern can be then used in the laboratory frame of reference to create a stationary current. In our system, the superfluid velocity equals $v_s^0 = 2\pi\hbar/(mL) = 47.8\mu$m/s and satisfies the proper boundary condition.

Furthermore, to excite sound modes, we minimize the energy with the perturbation (3.1), for the winding number $n = 1$ and its amplitude $V_0 = 0.01\hbar\omega_\perp$. In the second part of the protocol, we suddenly remove the external perturbation by setting its amplitude $V_0 = 0$ and then evolve the system in real time, in the laboratory frame of reference. There is one undesirable effect involved in this procedure. The initial state prepared in the moving frame assumes that the optical lattice is stationary. Then, in the lab frame, this external potential would move with velocity v_s^0, while we keep it stationary in this frame either. Therefore, with the change of the reference frame, we also abruptly stop the optical lattice, which causes the total energy to drop. We did not observe any unphysical consequences of this effect, nonetheless, we mention it for completeness. When applied to a gas in motion, the protocol excites two modes, which correspond to phonons propagating parallel and antiparallel to the current. According to linear response theory the observed signal $\langle \cos qx \rangle(t)$ features a beating of two frequencies, whose difference gives twice the Doppler shift:

$$F(t)/V_0 = \langle \cos qx \rangle(t)/V_0 = \chi^- \cos\big((\omega^0 - \Delta\omega)t\big) + \chi^+ \cos\big((\omega^0 + \Delta\omega)t\big). \tag{4.6}$$

For an ordinary BEC, the wavevector $q = 2\pi/L$ for $L = 96\mu$m is short enough to excite modes from the linear spectrum of the dispersion law. Consequently, the speed of sound at rest c^0 is evaluated as ω^0/q and the Doppler shift as $\Delta c = \Delta\omega/q$. Following the analysis of the previous chapter, we calculate the isothermal compressibility using the inverse-energy weighted sum rule (1.79). According to equation (3.10) (and the HD model of supersolids for an infinitely stiff lattice), the speed of sound at rest should be given by $\sqrt{f_s} c_\kappa$. We use the values of c^0 extracted with our protocol and c_κ calculated with sum rules, to evaluate the superfluid fraction. Results of this analysis are presented in Fig. (4.3). The excellent agreement is in line with the results of recent experiment [132], which used a similar method to measure the superfluid fraction.

In order to compare the measured values of the Doppler effect with the HD prediction (4.4), we need to calculate the derivative $\rho_s' = \partial\rho_s/\partial\rho$. We employ the same 5-point stencil method used to calculate energy derivatives (3.16). By varying the total number of particles

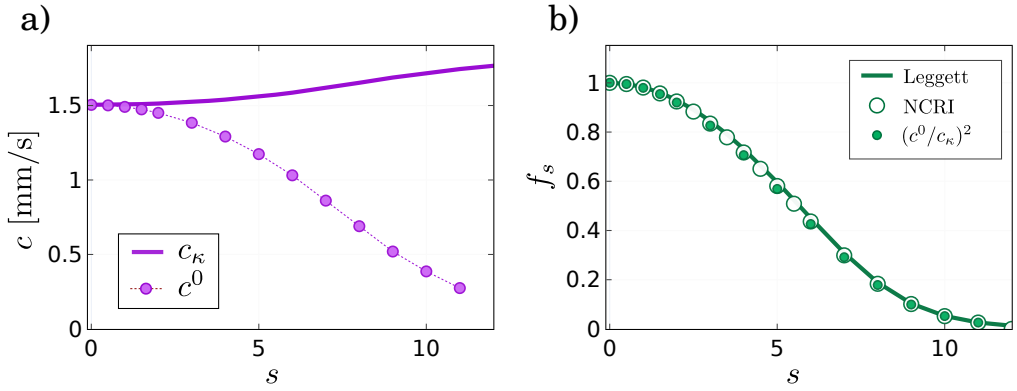

Figure 4.3: a) Speed of sound in superfluids in an optical lattice at rest c^0 and the inverse compressibility c_κ as a function of the depth parameter s. The square of the ratio of these two quantities gives the superfluid fraction as seen in b). Their values agree with the f_s calculated with NCRI (3.21) and with Leggett's upper bound (1.41).

around $N = 2\times10^5$, we prepare states, whose superfluid fractions - calculated with Leggett's upper bound - are subsequently used to determine $\rho_s' = f_s + \partial f_s/\partial\rho$. Finally, the comparison between HD model and Gross-Pitaevskii theory for the Doppler effect of the fourth sound is shown in Fig. (4.4) For the chosen parameters, we can see that there exists a broad region in

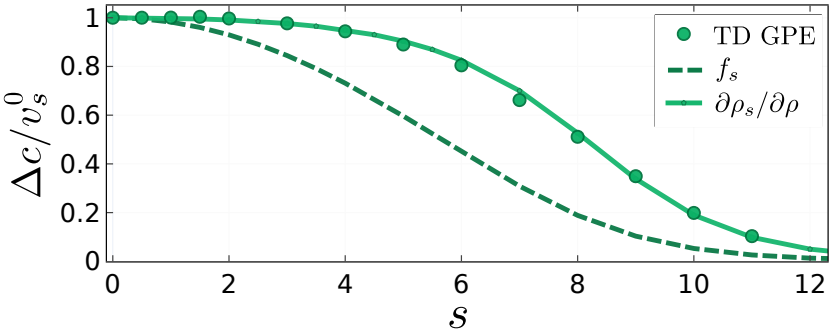

Figure 4.4: Doppler shift relative to v_s^0 of fourth sound in a stationary optical lattice as a function of the strength parameter s. Numerical results of time-dependent GPE (points) are compared with the hydrodynamic prediction from Eq. (4.4) (solid line) and with the kinematic estimate $\Delta c/v_s^0 = f_s$ (dashed line).

the lattice depth s where the kinematic shift substantially underestimates the Doppler effect. Our numerical simulations confirm hydrodynamic predictions, also found in [138, 149, 150]. Bose-Einstein condensates in optical lattices thus exhibit a non-kinematic Doppler effect. Owing to their long lifetimes and high tunability, the BECs are promising platforms for an experimental verification of this curious effect. In principle, an experiment analogous to that reported in [131] with an additional optical lattice created with the digital micro-mirror device, would be capable of measuring the reduced Doppler shift via the precession of the

density profile.

4.2 Doppler effect in supersolids

Supersolids define another class of ultracold atomic gases described within the two-fluid model. Their emergent density modulation reduces the superfluid fraction and thereby gives rise to a normal component, consistent with Leggett's upper bound — the very same mechanism responsible for the normal part in Bose–Einstein condensates in optical lattices. In fact, a BEC in an optical lattice can be seen as a limiting case of an infinitely stiff supersolid, whose rigidity is enforced by the external potential. Therefore, we expect that the Doppler effect in supersolids will also take a non-trivial form, provided that the two components flow at different velocities. Moreover, we have already confirmed the existence of two distinct sound modes, which are both excited with our linear response protocol. Whether the two sounds experience an equal Doppler shift is unknown, however, following the results in liquid helium [13–15], we might expect they do not. In this section we investigate the Doppler effect in moving supersolids. We begin with linearization of the hydrodynamic equations of supersolids (1.64) assuming finite velocities v_n^0 and v_s^0 to derive the formula for the Doppler shifts of the two sound modes. In the numerical part, we first discuss the independence of superfluid and normal velocities and their relation to the phase of the condensate wavefunction. Then, we confirm the validity of hydrodynamic predictions by employing the linear response protocol to measure the Doppler shifts in a numerical simulation of a dipolar BEC based on the extended GPE.

4.2.1 Hydrodynamic formula

Similarly to the case of BECs in optical lattices, in the presence of a finite current, each sound mode splits into two. This is again the consequence of lifting the degeneracy between the phonons that copropagate (+) and counterpropagate (-) with respect to the current j. Then, we expect four solutions of the linearized equations of supersolid hdrodynamics. The derivation of Doppler shifts is rather long and involves many parameters, thus for the sake of clarity of this section, we present it in Appendix (A). Here we briefly sketch the whole procedure, to focus on the resulting Doppler shifts.

Following the method described in the previous chapter, we linearize the HD equations around stationary values of the four independent variables: $\{\rho^0, v_s^0, v_n^0, u_x^0 = 0\}$. Since we study the sound modes in moving supersolids, this time the two velocities v_n^0 and v_s^0 are finite, and their inclusion leads to additional solutions of the linearized HD equations. As a result, we find four modes $\omega_{1,2}^{\pm} = |q|c_{1,2}^{\pm}$, where:

$$c_{1,2}^{\pm} = c_{1,2}^0 \pm (v' + w^0 \Delta_{1,2}) \tag{4.7}$$

and the two speeds of sound at rest $c_{1,2}^0$ are given by (3.13), while the Doppler shift consists of two parts. The first one, $v' = \rho_n' v_n^0 + \rho_s' v_s^0$, has the same form as the Doppler shift of the sound propagating in ordinary BECs in an optical lattice (cf. eq. (4.5)). When the superfluid and normal components move together ($w^0 = 0$), both sounds are simply shifted by the kinematic Doppler effect, fixed by the fluid velocity $v' = v_s^0 = v_n^0$. When $w^0 \neq 0$, we

instead find the additional contribution $w^0\Delta_{1,2}$, where

$$\Delta_{1,2} = -\frac{1}{2}\frac{\left(\frac{\rho_s^u}{\rho_n} - 4\rho_s'\right)\left(c_{1,2}^0\right)^2 + \frac{1}{\rho\kappa}\left(2(f_s+\rho_s') - \frac{\rho_s^u}{\rho_n}\right) + \gamma\left(\rho_s^u - 2\rho_s - 2\rho\rho_s' + 4\rho_s\rho_s'\right)/\rho_n}{2\left(c_{1,2}^0\right)^2 - \frac{1}{\rho\kappa} - \beta + 2\gamma} \tag{4.8}$$

is a dimensionless parameter[1] that depends on all thermodynamic quantities of the supersolid, and some of its derivatives, including the new term $\rho_s^u := \partial\rho_s/\partial u_x$. In general, Eq. (4.8) predicts that the Doppler effect affects the two sounds differently. This result corresponds to the zero-temperature analogue of the predictions obtained for the first and second sound velocities in superfluid ^{4}He [13, 15]. The formula (4.8) is general and valid for any supersolid. Here we will focus on dipolar supersolids, for which we have shown that the strain-density coupling γ can be neglected (see also [123]). The Doppler shift of the two sounds is therefore given by a simplified formula:

$$\Delta c_{1,2} = v' - \frac{w}{2}\frac{\frac{\rho_s^u}{\rho_n}\left[\left(c_{1,2}^0\right)^2 - c_\kappa^2\right] + 2\left(f_s+\rho_s'\right)c_\kappa^2 - 4\rho_s'\left(c_{1,2}^0\right)^2}{2\left(c_{1,2}^0\right)^2 - c_\kappa^2 - c_\beta^2}, \tag{4.9}$$

where $c_\kappa^2 \equiv 1/(\rho\kappa)$ and $c_\beta^2 \equiv \beta$. In the limit of an incompressible lattice, i.e., as $\beta \to \infty$, the Doppler shift approaches the $v' = \rho_s' v_s^0 + \rho_n' v_n^0$, which coincides with the result obtained above for the fourth sound (4.5). Moreover, approaching the crystal phase, i.e., $\rho_n \to \rho$ ($\rho_n^u \to 0,\ \rho_n' \to 1$), one finds $\Delta_{1,2} \to 0$, confirming the intuitive result that in the crystal phase, the sound speed simply feels a kinematic Doppler shift, given by the normal velocity v_n^0. Without knowing the character of the new derivative ρ_s^u, it is difficult to check the behavior of the HD formula close to the superfluid phase transition. The first term in the nominator of (4.9) is divided by the normal density, which suggests that if the derivative ρ_n^u is finite, then the Doppler shift of the second sound diverges when $\rho_n \to 0$. Thus, in the next section we perform numerical simulations to check this intriguing effect. Prior to comparison with the eGPE simulations, we characterize persistent currents in our geometry, and discuss the relation between macroscopic velocities v_n and v_s and the phase of the order parameter in eGPE theory.

4.2.2 Supersolids in motion

The two-fluid model of Landau does not impose any constraint on the normal and superfluid velocities, allowing them to vary independently. A clear example of this independence is seen in the liquid helium in a porous medium, which locks the position of the normal part but does not affect the superflow. Since dipolar BECs are also described by a two-fluid model, the two velocities must be independent in the supersolid phase. Their independence does not imply that in a stable configuration they would take arbitrary values because the persistence of a current is subject to energetic stability. To explore these metastable states we first need to understand how the two macroscopic velocities $v_{s,n}$ are incorporated into the extended Gross-Pitaevskii theory. Hydrodynamic theory is inherently macroscopic, which means that the only connection with the eGPE can be done through proper averages over the lengths much larger than any microscopic length scale. An example of such coarse-graininig is the Leggett's upper bound (1.41), which in some cases gives the exact value of the superfluid fraction.

[1] The anomalous term Δ_i is related to the anomalous Doppler shift from [152] via $\delta_i = \Delta_i + \rho_n'$

We consider a supersolid confined in a quasi-one-dimensional tube of length L with periodic boundary conditions, in a reference frame moving with velocity V. The Hamiltonian in such a frame can be written as $\mathcal{H} = \mathcal{H}_0 - VP_x$, where $\mathcal{H}_0$ contains the kinetic energy, external potential, and interaction terms, while P_x stands for the x component of the momentum. We assume that the transverse degrees of freedom do not play any role in the following discussion, their typical excitation energy being much larger than that associated with the excitation of the longitudinal modes. The superfluid and normal parts will be identified as different contributions to the current $\langle j \rangle = L^{-1} \int dx \rho(x) v(x)$, where $\rho(x)$ and $v(x)$, are the local density and the local velocity fields, respectively. At zero temperature, in Gross-Pitaevskii theory, they are directly related to the wavefunction $\psi(x)$ of the condensate as $\psi(x) = \sqrt{\rho(x)/m}\exp\{i\phi(x)\}$, where $\phi(x) \in \mathbb{R}$ is the phase of the order parameter. Its gradient gives the potential flow $v(x) = \hbar/m\ \partial_x\phi$, where m denotes the atomic mass. Using the continuity equation in the moving reference frame, $\partial_t\rho + \partial_x[\rho(x)(v(x) - V)] = 0$, one finds that the velocity field for a stationary solution must satisfy:

$$\partial_x[\rho(x)(v(x) - V)] = 0 \ \text{ i.e. } \ v(x) = V + C/\rho(x). \tag{4.10}$$

The constant C is determined by imposing the proper boundary condition for the phase ϕ, i.e., $\int v(x)dx = s \cdot 2\pi\hbar/m$, where $s \in \mathbb{Z}$ is the winding number. Therefore, the velocity field reads:

$$v(x) = V\left(1 - \frac{\rho_s^{\mathcal{L}}}{\rho(x)}\right) + s\frac{\rho_s^{\mathcal{L}}}{\rho(x)}\frac{2\pi\hbar}{mL}, \tag{4.11}$$

where $\rho_s^{\mathcal{L}}$ is the Leggett's upper bound to the superfluid density (1.41)

$$\rho_s^{\mathcal{L}} = L\left(\int_0^L \frac{dx}{\rho(x)}\right)^{-1}. \tag{4.12}$$

In our quasi one-dimensional configuration, this microscopic upper bound corresponds to the actual value of the superfluid density, i.e. $\rho_s^{\mathcal{L}} = \rho_s$ [50]. In the following we will make explicit use of this identification. From Eq.(4.12) it then follows that only in a homogeneous system will the superfluid density ρ_s coincide with the average density $\langle\rho\rangle = L^{-1}\int dx\rho(x)$. Starting from Eq. (4.11) we calculate the current $\langle j\rangle = L^{-1}\int dx\rho(x)v(x)$ flowing in the system as:

$$\langle j\rangle = \left(\langle\rho\rangle - \rho_s^{\mathcal{L}}\right)V + \rho_s^{\mathcal{L}}\frac{2\pi\hbar}{mL}s. \tag{4.13}$$

By comparison with the two-fluid hydrodynamic expression $j = \rho_n v_n + \rho_s v_s$, we identify the following relations:

$$\rho_s = \rho_s^{\mathcal{L}}, \quad \rho_n = \langle\rho\rangle - \rho_s^{\mathcal{L}}, \qquad v_n = V \ \text{ and } \ v_s = s\frac{2\pi\hbar}{mL} \tag{4.14}$$

Therefore, as intuitively expected, the velocity of the reference frame defines the normal velocity, while the superfluid velocity is fixed by the usual quantized value $s2\pi\hbar/(mL)$. Ultimately, to bridge the two-fluid parameters with the microscopic functions, we want to express the two velocities with only the averages of microscopic quantities. Using equation (4.11) we find:

$$v_s = \langle v\rangle \tag{4.15}$$

$$v_n = \frac{\langle 1/\rho\rangle\langle\rho v\rangle - \langle v\rangle}{\langle 1/\rho\rangle\langle\rho\rangle - 1}, \tag{4.16}$$

where an average $\langle f \rangle = 1/L \int f(x)dx$. The superfluid velocity is then given by the average potential flow defined with the gradient of the order parameter. Its independence from density modulations is expected, as the superfluid velocity is given only by the boundary conditions for the phase of the order parameter. On the other hand, we have already stated that the appearance of the normal phase is subject to an inhomogeneous density profile. Unsurprisingly, we find that equation (4.16) relates the normal velocity with local variations of $v(x)$ caused by these density modulations. Therefore, the phase of the order parameter encodes both the superfluid and the normal velocity. The former is set by choosing appropriate boundary conditions, while the normal velocity is defined by the deviations from the constant gradient of the phase.

Rotating frame ground state

Having linked macroscopic velocities with the phase of the order parameter, we are ready to investigate supersolids in motion. We consider $N = 1.6 \cdot 10^5$ ^{164}Dy atoms confined, in a tube of length $L = 96\mu$m with periodic boundary conditions and with a transverse potential given by $m\omega_\perp^2 r^2/2$, where $\omega_\perp = 2\pi \cdot 100$Hz. Dipoles are aligned by an external magnetic field along the z-direction. The phase diagram of dipolar gases is characterized by the ratio ϵ_{dd} between the dipolar and contact 2-body interaction strengths. Depending on its value, the system can be in a homogeneous superfluid, supersolid, or independent droplet phase. Fixing the value of ϵ_{dd}, we prepare the initial state of the system by evolving the extended GPE in imaginary time in the moving frame with velocity V. We change the reference frame by adding the term $-VP_x$ to the extended GPE Hamiltonian, where P_x is the momentum operator along x. We have already shown that velocity of the moving frame sets the normal velocity of the gas. On the other hand, the superfluid velocity is governed by the energy minimization condition in the moving frame. By comparing the energy of states with different supercurrents, we determine the ground state corresponding to every normal velocity. In Fig. (4.5), we show the two velocities v_s and v_n in the rotating frame ground state, together with its corresponding total current j. By confining the supersolid

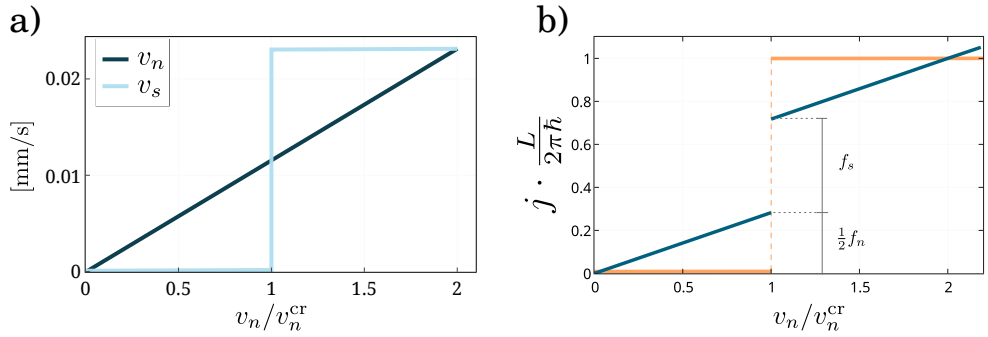

Figure 4.5: a) Superfluid and normal velocities and b) current j in a supersolid configuration corresponding to the ground state in the reference frame moving with velocity v_n. The orange line characterizes the current in the superfluid phase of the dipolar BEC.

in a closed geometry, we imposed the quantization of the supercurrent $v_s = s \cdot 2\pi\hbar/(mL)$, where $s \in \mathbb{Z}$. The creation of each quantum of the supercurrent costs a discretized amount of energy and in rotating-frame ground state occurs when $v_n = (2s-1)v_n^{\rm cr}$ [153, 154], where in our system $v_n^{\rm cr} \equiv \pi\hbar/(mL) = 12.7\mu$m/s. The discontinuous character of the superfluid

velocity influences the total current j. For small v_n, it linearly increases with the velocity of the reference frame and exhibits a jump given by the superfluid fraction f_s at $v_n = v_n^{\mathrm{cr}}$, as shown in Fig. (4.5). In our geometry, the critical normal velocity does not depend on the relative interaction strength ε_{dd}.

As can be seen in Fig. (4.5), in a stable configuration, a relative velocity $w = v_n - v_s$ can be tuned from $-v_n^{\mathrm{cr}}$ to v_n^{cr} for a given value of v_s. In principle, equation (4.13) shows that there are two degrees of freedom in defining the total current, as the velocity of the reference frame and superfluid winding number s are independent variables. In theory, one could prepare a state of arbitrary v_n and (quantized) v_s, including a counter flow of the two components. However, the stability of such a state is subject to energy minimization, and thus may quickly decay to a more stable configuration.

Let us now confirm the relation between the normal and superfluid velocities and the gradient of the phase of the order parameter. For every choice of the macroscopic velocities, we find the corresponding phase pattern by evolving the eGPE in imaginary time in moving reference frame. The energy minimization provides also the shape of the density profile, which we use to calculate $v(x)$ using equation (4.11). We can compare this $v(x)$ with numerically calculated gradient of the phase. An example of such comparison is shown in Fig. (4.6). The upper panel presents the density profile of a dipolar supersolid in a tube, whose normal part moves along the x-axis with velocity $v_n = v_n^{\mathrm{cr}}$ while the superfluid component remains at rest. The phase $\phi(x, 0, 0)$ in this configuration varies spatially from 0 to $\phi_{\max} \approx 0.01\pi$. The amplitude of these variations $\phi_{\max}$ depends linearly on the normal velocity, while their shape is governed by density modulations. The phase gradient shows an interesting behavior, as in low-density regions it is negative, suggesting a local counter-flow with respect to the motion of the density peaks. However, as we have already seen in this section, local values of the velocity field $v(x)$ does not represent the effective motion of the supersolid. To show the effect of the appearance of the supercurrent, we also plot the phase gradient for the same normal velocity $v_n = v_n^{\mathrm{cr}}$.

There is one more relation regarding the normal velocity of supersolids, which we can easily confirm. The last equation of supersolid hydrodynamics relates the v_n with the lattice displacement u via Lin's constraint (see (3.11)). In the lowest order, it is approximated as $v_n \approx \partial_t u$. Therefore, motion of the lattice structure fixes the normal velocity. Since position of lattice sites are determined by the local maxima of the density profile, we can measure the normal velocity by tracking the position of the peaks in time. To demonstrate this, we evolve the state presented in Fig. (4.5) in real time in the laboratory frame of reference. The results of this simulation are shown in Fig. (4.7), where the motion of each droplet is clearly given by the normal velocity.

4.2.3 Anomalous Doppler effect

Thus far we have thoroughly analyzed the ground state of moving supersolids, characterizing their motion in terms of normal and superfluid velocities. Ultimately, this knowledge is important in terms of the Doppler effect that we shall numerically investigate in this section. We will use the same linear response framework, to excite and measure all Doppler-split modes, which will provide the microscopic predictions for the anomalous Doppler effect of the two sounds.

For completeness, we recall the parameters of the simulated system and numerical methods to study the sounds. Our gas consists of $N = 1.6 \cdot 10^5$ ^{164}Dy atoms confined, in a

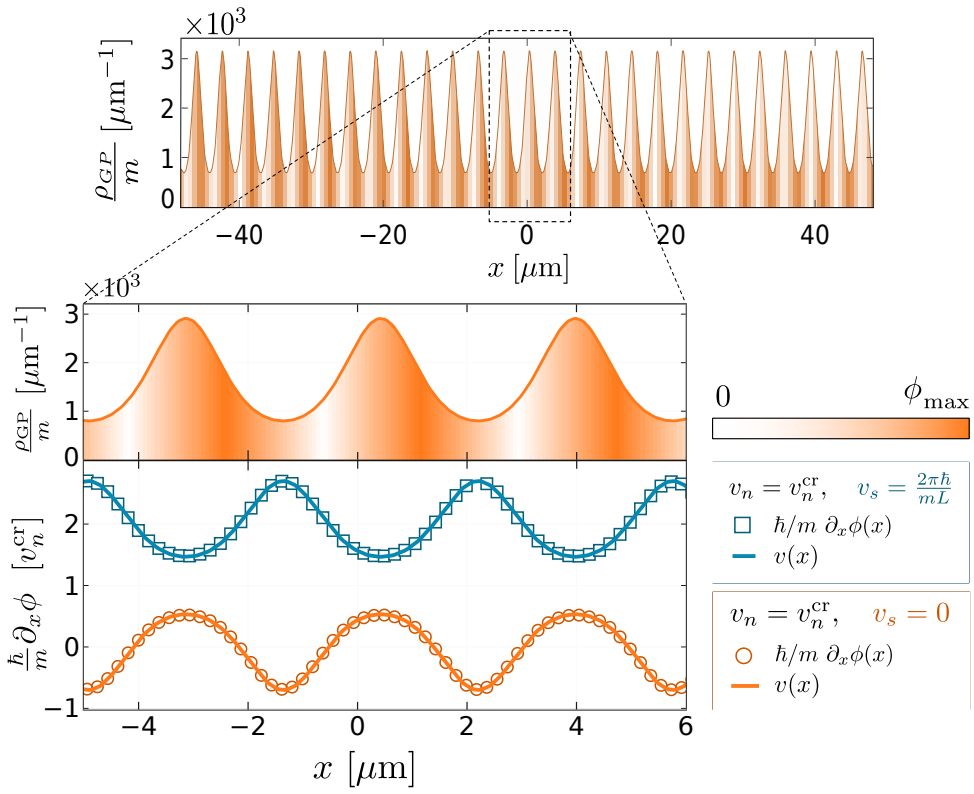

Figure 4.6: (upper panel) A selected part of transversely integrated density and the phase pattern at $\rho(x, 0, 0)$ at $v_n = v_n^{\rm cr}$ in the absence of the superfluid current. Values of $\phi_{\rm max}$ linearly depend on v_n and are of the order 0.01π for systems considered in this paper. (lower panel) Gradients of the phase of the order parameter $\phi(x)$ (symbols) for $v_s = 0$ (orange) and $v_s = 2\pi/mL$ (blue). The phase profile in both cases was obtained by minimizing the eGPE energy functional in the reference frame moving with velocity $v_n^{\rm cr}$. Lines represent Eq. (4.11) calculated with the density profile obtained from the eGPE simulation.

tube of length $L = 96\mu$m with periodic boundary conditions and with a transverse potential given by $m\omega_\perp^2 r^2/2$, where $\omega_\perp = 2\pi \cdot 100$Hz. Dipoles are aligned by an external magnetic field along the z-direction. Fixing the value of ϵ_{dd}, we prepare the initial state of the system by evolving the extended GPE in imaginary time in the moving frame with velocity V. We change the reference frame by adding the term $-VP_x$ to the extended GPE Hamiltonian, where P_x is the momentum operator along x. As we have already shown, this approach unequivocally determines both the superfluid and the normal velocities in the rotating frame ground state. In particular the velocity of the normal component coincides with the velocity of the moving frame ($v_n^0 = V$), while the appearance of the supercurrent is dictated by the energy minimization condition in the same moving frame. The quantized superfluid velocity exhibits the first jump to a finite value $v_s^0 = 2\pi\hbar/(mL)$ at the critical value $V^{cr} = v_n^{\rm cr} = \hbar\pi/(mL) = 12.7\mu$m/s. The change of the reference frame is necessary to accurately determine the phase profile of a moving supersolid. Once converged, such a

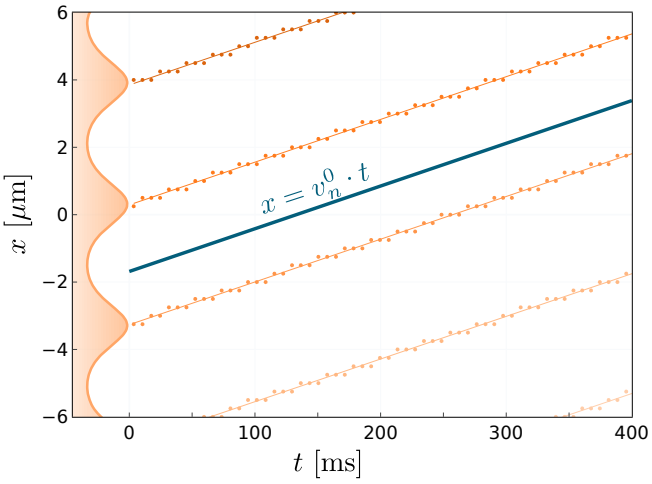

Figure 4.7: Positions of the local density maxima (orange dots) in a time evolution of a supersolid moving with velocities $v_n = v_n^{\mathrm{cr}}$ and $v_s = 0$. Numerical data are fitted with a linear functions, whose slopes are consistent with v_n^{cr} (blue line). This numerical simulation directly shows, that the normal velocity is given by the motion of density peaks, as predicted by the hydrodynamic theory.

wavefunction can be used as the initial state to be evolved in the lab frame.

In order to excite the sound modes, we add the small perturbation $V_0 \cos qx$ to the eGPE Hamiltonian in the moving frame, and find the corresponding lowest-energy state by minimizing the eGPE energy density functional. This state is then used in the real-time evolution in the laboratory frame of reference, where its phase pattern provides normal and superfluid currents. By abruptly removing the external perturbation at $t = 0$, we trigger density oscillations, which carry information about all the modes propagating in the system. The supersolid phase at rest exhibits two phononic modes, each of which splits into two in the presence of a current. By measuring the average cosine $\langle \cos qx \rangle$ we evaluate all four frequencies, which for $q \to 0$ are linearly related to speeds of sound $\omega = c|q| = c \cdot 2\pi/L$. An example of Doppler splitting of the two sound modes $c_{1,2}$ in the supersolid phase is presented in Fig. (4.8). All sound modes experience an abrupt change of their speeds at $v_n/v_n^{\mathrm{cr}} = 1$, when the phase of the order parameter starts hosting a quantum of circulation. Let us also notice that, remarkably, the Doppler shift for the sound speed c_2 can be negative, i.e. the velocity c_2^+ of the phonon copropagating with the current is smaller than c_2^0 (shaded region in Fig. (4.8)). We will comment on that in the end of this chapter. All four modes presented in Fig. (4.8) are of the form $c_{1,2}^{\pm} = c_{1,2}^0 \pm (v' + w\Delta_{1,2})$, where $w = v_n - v_s$ and $v' = \rho_n' v_n + \rho_s' v_s$ are known parameters. For each relative strength ε_{dd}, we extract the anomalous Doppler term Δ_i from the difference $\frac{1}{2}\left(c_i^+ - c_i^-\right)$ calculated in the time-dependent eGPE simulation.

In order to make a quantitative comparison between the eGPE and the predictions of the linearized hydrodynamic equations, we need to calculate the parameters entering the HD result (4.9). The parameters entering the speeds of sound in the absence of permanent currents (f_s, κ, β and γ) have been discussed in the previous chapter. The superfluid fraction in our geometry corresponds to Leggett's upper bound (1.41), while the other three parameters are second derivatives of the energy with respect to the total density ρ and

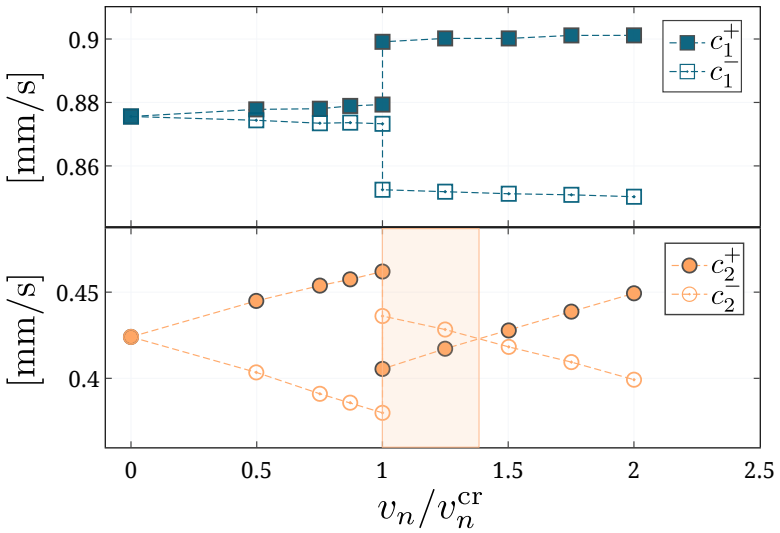

Figure 4.8: The splitting of the first and second sound (respectively: upper and lower panels) into four phonon modes for the system presented in Fig. (4.6). Within the shaded area, the Doppler shift of the second sound becomes negative.

lattice strain u_x . In particular, we have shown that the strain-density coupling γ is very small for the supersolid phase of a dipolar gas and will be neglected in our analysis. The new parameters ρ_n' and ρ_s' are determined numerically by marginally changing the total atom number N, while the derivative ρ_s^u, quantifying the change in the superfluid density with respect to $\partial_x u$, is calculated by varying the inter-droplet distance (see (3.19) for the numerical method of calculating derivatives with respect to the lattice strain). In Fig. (4.9) we compare the two derivatives of the superfluid density with the superfluid fraction.

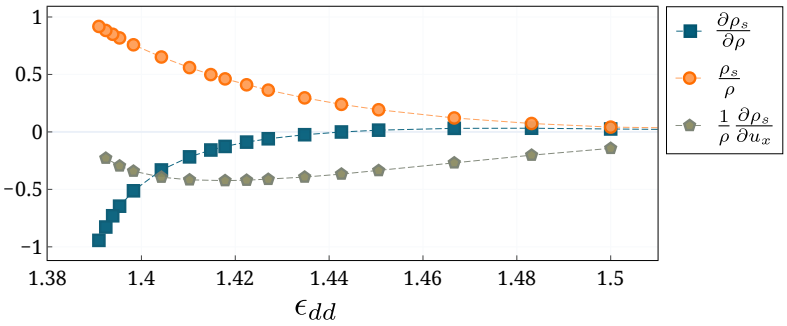

Figure 4.9: Derivative of the superfluid density ρ_s with respect to the total density ρ (blue) and strain u_x (gray), compared with the superfluid fraction calculated with Leggett's upper bound (4.12) (orange).

Finally, we can compare the anomalous terms $\Delta_{1,2}$ in the Doppler shifts of the two sounds calculated with the time-dependent eGPE protocol and predicted by the hydrodynamic theory. In Fig. (4.10), we present a good agreement between the two theories for both sound

modes, which confirms the highly nontrivial form of the Doppler effect in supersolids. The two sounds experience Doppler shifts of opposite signs, as can be also inferred from Fig. (4.8). The effect is especially pronounced close to the superfluid-supersolid phase transition.

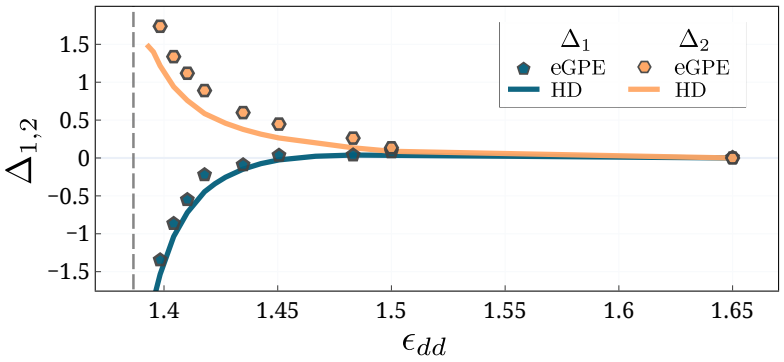

Figure 4.10: Anomalous Doppler shift of the first (blue) and second (orange) sound in the supersolid phase. Results of time-dependent simulations (markers) are compared with the hydrodynamic model (solid lines). The gray vertical line marks the superfluid-supersolid transition point.

4.2.4 Negative Doppler effect

Pioneering studies on the anomalous Doppler effect in ^{4}He have revealed, that within a certain temperature range, the Doppler shift may become negative [13–16]. Intuitively, we refer to the Doppler effect as negative when the sound mode co-propagating along the current c_i^+ has a smaller speed than the value c_i^0 at rest. At the same time, the speed of sound of the counter-propagating mode c_i^- would be greater than c_i^0 (see Fig. (4.8)). For supersolids, we define the negativity condition as:

$$v' + w\Delta_i < 0 \quad \longrightarrow \quad \frac{v_n}{v_s} < 1 - \frac{1}{\Delta_i + \rho_n'}, \tag{4.17}$$

which occurs only in the presence of a finite supercurrent. Since the minimum of v_n/v_s equals 0.5 (see Fig. (4.5)) and $\Delta_1 + \rho_n'$ is always less than 1, the first sound mode cannot exhibit the negative Doppler shift. On the other hand, there exists a parameter range for which the second sound manifests the negative Doppler effect, as shown in Fig. (4.11).

Conclusions

This chapter is a comprehensive study of density-modulated superfluids in motion, in terms of the sound propagation. We began with characterization of the current in both supersolids and in superfluids in optical lattices. While the latter case has been already well studied, supersolids in motion have not been entirely characterized before. In particular, the relation between the two hydrodynamic velocities v_n and v_s and the phase of the order parameter in the Gross-Pitaevskii theory was unclear. We demonstrate, that the superfluid velocity is given by the potential flow $\hbar/m\langle\nabla\phi\rangle$ averaged over long distances, while the normal velocity is encoded in the variations of the phase ϕ caused by the density modulations. These relations, bridging the velocities in the two theories, are crucial to understand the independence

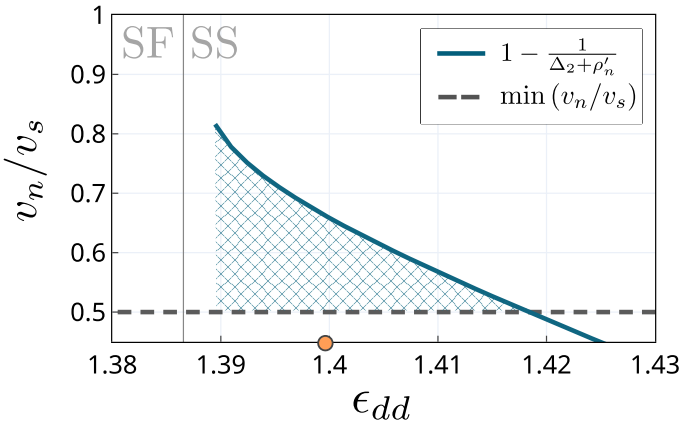

Figure 4.11: Parameter range for which the Doppler shift of c_2 is negative (crossed area). The point on the horizontal axis represent the interaction parameter used in Fig. (4.8). The parameter space closer to the superfluid phase is numerically inaccessible due to the emergence of non-linear effects.

between v_n and v_s in ultracold atomic supersolids. Furthermore, we characterized persistent currents in the rotating-frame ground states of dipolar BECs trapped in a linear tube with periodic boundary conditions. Due to the closed geometry, the supercurrent is quantized and the total current features discontinuities whenever the superflow winding number s is changed. We found a clear correspondence in the ground state values of v_n and v_s, as the supercurrent increases at $v_n = (2s-1)v_n^{\mathrm{cr}}$, which was also found in [153, 154]. It is worth noticing that both v_n^0 and v_s^0 could be in principle fixed in an independent way, by properly modifying the phase pattern ϕ with imprinting techniques. The value of the superfluid velocity is determined by the phase winding at the boundaries of the configuration, while the velocity of the normal component is determined by the space variations of the phase at a microscopic scale, fixed, in the case of a supersolid, by the inter-droplet distance. However, such a state of arbitrary normal and superfluid velocities would not in general correspond to an equilibrium configuration in the moving frame. Consequently, its persistence would strongly depend on energetic stability of the current.

The second and most important part of this chapter reports the theoretical predictions for the Doppler effect in density-modulated superfluids at zero temperature. If the inhomogeneity of the density profile is enforced externally, the system features one sound only, to which we refer as the fourth sound, provided that the external potential is stationary. We showed excellent agreement between the hydrodynamic prediction and time-dependent GPE simulations, where we employed our linear response protocol to measure the Doppler shift. Notably, our results confirmed the anomalous form of the Doppler effect, as the fourth sound was shifted by $\rho_s' v_s$, where ρ_s' in principle also differs from the superfluid fraction. Unlike superfluids in optical lattices, supersolids feature two sound modes, which are differently affected by the presence of the current. By linearizing the hydrodynamic equations of supersolids, we derived a highly non-trivial form of the Doppler shifts. Using the same protocol as before, we measured the two shifts in the time-dependent eGPE simulations. The two theories provide the same anomalous predictions for the Doppler shift within a wide range of the relative strength parameter ε_{dd}. Interestingly, for certain values of the parameters, the second sound features a negative sign of the Doppler shift. In such a case,

the co-propagating mode is characterized by a speed of sound, whose value is lower than that of the counter-propagating one.

To conclude this chapter, let us hint an intuitive interpretation of the anomalous Doppler effect. In both cases, the anomalous term affected the sound propagation only if the normal part moved at a velocity different from that of the superfluid. In supersolid platforms, the two sound modes are hybridized superfluid and lattice oscillations, indicating that if $v_n - v_s \neq 0$, the medium that carries the sound moves at two different velocities. Since there is no rest frame of reference for such a current, the Doppler effect cannot be explained by a simple Galilean transformation.

Chapter 5

Doppler effect in Superfluid Mixtures

In the previous chapter, we studied density-modulated superfluids in the presence of finite currents. We demonstrated that the Doppler effect becomes non-trivial whenever the sound carrier moves at two different velocities. Density-modulated superfluids in closed geometries are suitable platforms to study this peculiar effect, as the current quantization naturally allows relative flows $v_n \neq v_s$. Both types of systems studied in the previous chapter consisted of a superfluid, which appears at ultralow temperatures, and the normal part, whose presence is given by density modulations. However, in the context of the anomalous Doppler effect, the second component does not need to be in the normal phase and can also be superfluid, thereby broadening the set of platforms exhibiting this unusual phenomenon. In this chapter, we investigate the Doppler effect in a binary mixture of weakly interacting Bose-Einsten condensates. We demonstrate that these platforms also exhibit a non-kinematic Doppler effect, as a consequence of the interspecies interaction which couples the motion of the two fluids. Superfluid properties of both components bring along an important advantage over density-modulated superfluids. Since the superfluid velocity is set by the boundary conditions of the phase of the order parameter, a counterflow of two superfluids is expected to be more robust against noise of various sources, inevitably present in every experiment. As the relative velocity is the crucial requirement for the occurrence of a non-kinematic Doppler effect, we believe that Bose mixtures are particularly promising in terms of experimental verification of the results presented in this thesis. For this reason, we develop modified protocol schemes to precisely measure the anomalous Doppler effect in ultracold atomic mixtures.

The study of the Doppler effect in a mixture of two superfluids can be realized with an arbitrary choice of the two components. In particular, qualitative results do not depend on the spin statistics and are valid for bosonic and fermionic gases, as well as Bose-Fermi mixtures. In this work, we consider an atomic two-component Bose-Einstein condensate and assume that the components are two different hyperfine levels $|i\rangle$, $i = 1, 2$, of the same atomic species with mass m. In the weakly interacting case, the particles interact only via contact interaction potentials, which are characterized by parameters g_{11}, g_{22} and g_{12} assessing the strength of intraspecies and interspecies coupling, respectively. They are related to the s-wave scattering lengths a_{ij} via the expression $g_{ij} = 4\pi\hbar^2 a_{ij}/m$. In order for the mixture to

be stable, the intraspecies interaction g_{ii} must be positive and, without loss of generality, we also assume $g_{12} > 0$ in the rest of our work. In the following we use a description of the mixture in terms of density and polarization or spin density. Given the single-component densities n_i, we define the total density $n = n_1 + n_2$ and the spin density $s_z = n_1 - n_2$. For a generic homogeneous Bose mixture, the equation of state can be written as

$$\epsilon = \frac{1}{2} g_d n^2 + \frac{1}{2} g_s s_z^2 + \frac{1}{2} g_{ds} n s_z, \tag{5.1}$$

where we have defined the following combinations of the coupling constants: $g_d = (g+g_{12})/2$ and $g_s = (g - g_{12})/2$ with $g = (g_{11} + g_{22})/2$ as well as $g_{ds} = (g_{11} - g_{22})/2$. The stability of the system requires the energy to be a convex function of n and s_z, which gives rise to the further condition

$$\Delta = 4 g_d g_s - g_{ds}^2 \geq 0. \tag{5.2}$$

If the inequality (5.2) is violated, the gas is unstable towards phase separation[1]. In the present work we require the system to be miscible, hereafter assuming the stability condition is always met.

The long-wavelength, low energy dynamics of the system is captured by the superfluid hydrodynamic (HD) equations, which take into account the total particle number conservation, the polarization conservation as well as the equation related to the order parameter for the broken $U(1) \times U(1)$ symmetry. As dynamical variables for the latter we use the total $\Phi_T = \phi_1 + \phi_2$ and the relative $\phi = \phi_1 - \phi_2$ phase. Finally, by introducing the chemical potential $\mu = \partial\epsilon/\partial n = g_d n + g_{ds} s_z/2$ and the polarizing field $h = \partial\epsilon/\partial s_z = g_s s_z + g_{ds} n/2$ the HD equations read:

$$\partial_t n + \partial_x j = 0 \tag{5.3a}$$

$$\partial_t s_z + \partial_x j_z = 0 \tag{5.3b}$$

$$m \partial_t v_T + \partial_x \left(\frac{m v_T^2}{2} + \frac{m w^2}{2} + \mu \right) = 0 \tag{5.3c}$$

$$m \partial_t w + \partial_x \left(m w v_T + h \right) = 0 \tag{5.3d}$$

where $v_T = \hbar \partial \Phi_T/(2m)$ and $w = \hbar \partial \phi/(2m)$ are the total and the relative flow velocity, respectively. The density and polarization currents in the HD equations are given by:

$$j = n v_T + s_z w \tag{5.4a}$$

$$j_z = s_z v_T + n w \tag{5.4b}$$

and correspond respectively to the sum and to the difference of the two single-component currents $j_i = n_i v_i$. In the absence of permanent currents the hydrodynamic theory of superfluids predicts the propagation of two sounds where the two fluids oscillate in phase (density-like sound) and out of phase (spin-like sound). The corresponding sound velocities are given by (see, e.g., [19, 40])

$$c_{d/s}^0 = \left[\frac{g n + g_{ds} s_z \pm \sqrt{(g n + g_{ds} s_z)^2 - \Delta (n^2 - s_z^2)}}{2m} \right]^{1/2} \tag{5.5}$$

and have been found in good agreement with experiments [41–43]. The discretized spin mode oscillations have been also investigated in [155]. The nature of the two sounds is

[1] The stability in terms of the intra- and interspecies interactions reads: $g_1 g_2 - g_{12}^2 \geq 0$. For $g_{12} < 0$ the instability would lead to the collapse of the mixture.

rather complex as they are strongly hybridized. In the limit of a non-interacting mixture, when $g_{12} = 0$, the equation (5.5) reduces to $\sqrt{g_{ii} n_i / m}$ and the two modes coincide with two single-component density oscillations. On the other hand, when the gas exhibits $\mathbb{Z}_2$ symmetry ($g_{ds} = s_z = 0$), the two sound modes coincide with pure total density and spin density oscillations. For the sake of notation, we use the d (s) subscript to refer to the sound mode (5.5) with the + (−) sign and call it *density-like* (*spin-like*) mode[2].

In the presence of persistent currents, each of the two sound modes splits into pairs of phonons whose speeds depend on their direction relative to the total current. The sound modes are derived using the linearization procedure, where we consider small deviations from the equilibrium values of the variables entering the equations (5.3). We identify the set of four independent variables $\xi \in \{n, s_z, v_T, w\}$ and express them as the sum of their equilibrium values ξ^0 and small variations, slowly changing in space and time $\delta\xi(x,t) = \delta\xi \exp(i(qx - \omega t))$. In the $q \to 0$ limit, the dispersion law is linear, and its slope $c = \omega/q$ defines the speed of sound. The linearized HD equations (5.3) are neatly represented in the matrix form:

$$\begin{bmatrix} -c + v_T^0 & w^0 & n^0 & s_z^0 \\ w^0 & -c + v_T^0 & s_z^0 & n^0 \\ g_d & g_{ds}/2 & m(-c + v_T^0) & m w^0 \\ g_{ds}/2 & g_s & m w^0 & m(-c + v_T^0) \end{bmatrix} \begin{bmatrix} \delta n \\ \delta s_z \\ \delta v_T \\ \delta w \end{bmatrix} = 0, \tag{5.6}$$

from which one finds four solutions, corresponding to the two Doppler shifted pairs of modes. All sound modes are roots of the fourth order polynominal given by the determinant of the matrix above. Finding their exact values is complicated, thus we use Taylor expansion to estimate the Doppler shifts caused by small currents[3]. Assuming $v_T^0,\ w^0 \ll c_{d/s}^0$, we find the following results for the Doppler-shifted sound velocities:

$$c_{d/s}^{\pm} = c_{d/s}^0 \pm \left(v_T^0 + \delta_{d/s} w^0 \right), \tag{5.7}$$

where the +(-) sign corresponds to the sound co-propagating (counter-propagating) with the current, and

$$\delta_d = -\delta_s = \frac{g_{ds} + g m_z}{\sqrt{(g + g_{ds} m_z)^2 - \Delta(1 - m_z^2)}}, \tag{5.8}$$

with $m_z = s_z^0 / n^0$ the spin polarization. The hydrodynamic theory reveals the highly non-trivial nature of the Doppler effect in a superfluid Bose mixture, which depends on all the microscopic parameters of the gas. As anticipated, the Doppler shift becomes trivial once the interspecies coupling constant g_{12} vanishes. In such a limit, Eq. (5.8) reduces to $\delta_{d/s} = \pm 1$ and Eq. (5.7) simply coincides with the kinematic Doppler shift for each component, i.e., $v_T^0 + \delta_{d/s} w^0 = v_{1/2}^0$. The same result is trivially found in the single-component limit where $m_z = \pm 1$.

Aside from inter-species interaction, non-trivial effects in the Doppler effect require the presence of a relative motion between the two components of the mixture ($w^0 \neq 0$). In a classical fluid, collisional effects prevent the formation of any stable mixture with two different velocity fields. Instead, in a superfluid, a state with relative velocity w^0 can be obtained by imposing different conditions on the phases of the two order parameters, satisfying the proper boundary conditions.

Without loss of generality, in the following we assume that only the first superfluid component has a finite velocity v_1, while the second one remains at rest. With this choice,

[2] If g_{12} were negative ± in the Eq. (5.5) has to be replaced by ∓.

[3] For details of this procedure, applied to supersolid hydrodynamics, see Appendix (A)

the Doppler shifts of the two sounds read

$$\Delta c_{d/s} = \frac{v_1}{2}\left(1 + \delta_{d/s}\right). \tag{5.9}$$

Moreover, since $\delta_{d/s}$ differs only in sign between the two modes, we focus only on the density-like one. Contrary to previously studied systems, here the Doppler shift does not depend on any derivatives of thermodynamic quantities, which must be determined numerically. For a given set of gas parameters, we can analytically provide the corresponding Doppler shift without any numerical simulations. In Fig. (5.1a) we show the Doppler shift of the density-like sound as a function of g_{12}/g for $g_{ds} = 0$ and different polarizations m_z. We compare the analytical formula (5.8) with the results of time-dependent GPE simulations (see next section for details). Both theories must be in excellent agreement, since the HD equations can be derived from the Gross-Pitaevskii equation (see 1.1.2).

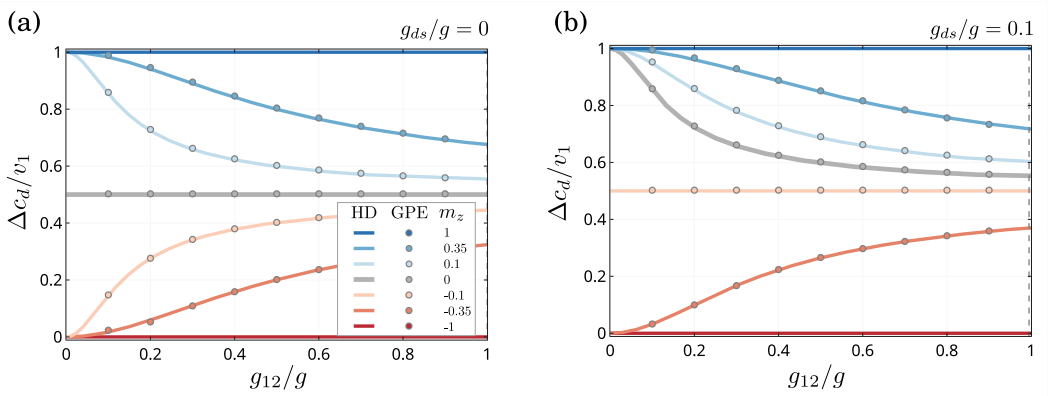

Figure 5.1: The Doppler shift of the density-like sound relative to the velocity of the first component as a function of interspecies interaction coupling g_{12} for $v_2 = 0$ and *(a)* $g_{ds} = 0$ and *(b)* $g_{ds}/g = 0.1$. Each solid line corresponds to a HD prediction for different values of polarization m_z. The symbols represent results of the GPE simulation, whose details are contained in the next section. The g_{12} and m_z dependence of the Doppler shift of the spin-like sound mode (Δc_s) is the same as of the density-like mode, but mirrored with respect to the $y = 0.5$ line. The vertical dashed line marks the stability condition (5.2).

The Doppler shift of the density-like sound is, as expected, always smaller than v_1 and reaches the value $\delta_{d/s} = \pm m_z$ by approaching the SU(2) symmetry point as $g_{12} \to g$.

It is intriguing to notice, that for every set of interaction constants, there exists a special value, $m_z = -g_{ds}/g$, for which the nominator of Eq. (5.2) vanishes. Consequently, the Doppler shift of both sounds is given by $v_T^0 = v_1/2$ and is independent of the value of the g_{12} coupling. An example of this unusual dependence is shown in Fig. (5.1b), where $g_{ds}/g = 0.1$. For the $\mathbb{Z}_2$ symmetric gas, such an effect is observed if $g_{ds} = 0$ (see Fig. (5.1a)). This result is true as long as the relative velocity is small enough, i.e.,

$$mw^2 \ll g_{12} n^0 \sqrt{1 - m_z^2}, \tag{5.10}$$

which shows that for either $g_{12} \to 0$ or $m_z \to 1$ the peculiar results of having an equal Doppler shift for both sounds cannot hold. In fact, in the limit of small coupling constant g_{12}, the two sounds continuously change the character from density- and spin-like oscillations

to single-component modes at $c_d^0 - c_s^0 \approx v_T^0$. For $m_z = -g_{ds}/g$, the difference between the two speeds of sound at rest is comparable to the velocity v_T^0 when $g_{12}/g \approx \sqrt{2m/(gn^0)}v_T^0$. For the parameters used in Fig. (5.1) this evaluates to $g_{12}/g \approx 0.005$, satisfying the condition (5.10).

As mentioned before, the Doppler shift of the spin-like sound differs from the one of the density-like only in sign of the δ term (5.2). This means that the entrainment of the spin-like sound has the same dependence on g_{12} as the ones depicted in Fig. (5.1a) and Fig. (5.1b), but reflected with respect to the $y = 0.5$ axis.

GPE simulation

We verify hydrodynamic predictions of the Doppler effect with numerical simulations of two coupled Gross-Pitaevskii equations. Both theories must yield the same results, as equations (5.3) can be derived from the GPE (see 1.1.2). In this section, we use our linear-response protocol to calculate the two speeds of sound and their Doppler shifts for different gas parameters. The methods presented in this section will be the foundation for enhanced protocols designed to excite and measure the Doppler effect of each sound independently.

Numerical simulations of Bose mixtures require one Gross-Pitaevskii equation for every component. The equations of motion are conveniently represented in a matrix form:

$$i\hbar\frac{\partial}{\partial t}\begin{pmatrix}\psi_1\\ \psi_2\end{pmatrix} = \begin{pmatrix}h_1 & 0\\ 0 & h_2\end{pmatrix}\begin{pmatrix}\psi_1\\ \psi_2\end{pmatrix}, \tag{5.11}$$

where ψ_i is the order parameter of the i-th component, $h_i = -\frac{\hbar^2}{2m}\nabla^2 + g_{ii}n_i + g_{12}n_{3-i}$ is the corresponding single-component Hamiltonian, with $n_i(x,t) = |\psi_i(x,t)|^2$ the densities of the two parts. We investigate solutions of Eq. (5.11) in one dimension, where periodic boundary conditions allow for the existence of permanent currents. We simulate a gas of ^{23}Na particles in a tube of length $L = 96\mu m$ with a fixed total density $n = 3125\ \mu m^{-1}$. For every choice of gas parameters, the ground state is found by evolving Eq. (5.11) in the imaginary time. To study the Doppler effect we require finite velocity fields for both components. In a uniform superfluid, the phase profile of the order parameter is linearly changing from 0 to $s \times 2\pi$, where the integer s specifies the winding number of the quantized current. We imprint such linear patterns in the phase profile of each ψ_i to create a state with the desired currents j and j_z.

We study the sound excitations by adding a static, low-amplitude potential in the form of $V_0 \cos qx$ to both single-particle Hamiltonians h_i. The perturbation wavevector $q = 2\pi/L$ excites sound waves, provided that $q \to 0$ belongs to the linear part of the dispersion law. We prepare the initial state in the presence of this potential. Then, at the beginning of the real-time evolution, we suddenly remove it to trigger the density profile dynamics. According to the linear response theory, the observable:

$$\sum_i \langle\cos(qx)\rangle_i = \sum_i \int dx\ n_i(x,t)\cos(qx)\ , \tag{5.12}$$

gives access to the frequencies of the phonon modes excited by the periodic density perturbation. For a mixture at rest, this protocol yields the excitation of two modes, one associated with the density-like oscillation of the mixture and one with the spin-like one. In the presence of a finite current, each mode splits into two, due to the Doppler effect. Since, for small wavevectors q the phonon dispersion relation is linear, the frequency of the excited modes gives the corresponding speed of sound $c_i = \omega_i/q$. Finally, for each sound, the Doppler

shifts are calculated as $\Delta c_i = (\omega_i^+ - \omega_i^-)/2q$, where ω_i^+ and ω_i^- represent, respectively, the frequency of the co- and counter-propagating phonons. The numerical results of this protocol are shown in Fig. (5.1a) and Fig. (5.1b). As anticipated, the agreement with the hydrodynamic model is very good.

5.1 Selective sound excitation protocol

In the previous section we used a protocol, which excites all sound modes of the two-component BEC mixture. In the presence of a finite current, this means a total of four sound modes were present in the observed signal (5.12), as each sound mode is split into two due to the Doppler effect. Consequently, the time evolution has to be sufficiently long to precisely discriminate all frequencies. However, the large time scale renders the protocol unfeasible for any experimental setup. Therefore, in this section, we will explore two ways to remove one of the sound modes from the observed signal, to design a protocol for experimental verification of the anomalous Doppler effect. The first modification of the linear-response protocol changes the potential with which sound waves are excited in a way that only one of the modes is present in the time evolution of the total density. The alternative method keeps the perturbation unchanged but alters the observable, requiring separate measurements of the two component densities to selectively probe each sound mode.

The protocol used in the previous section assumes that the two components are subject to the cosine-shaped external potential with equal strengths. Therefore, this additional potential is the total density perturbation. Consequently, it couples only slightly to the spin-like mode, and is completely decoupled for $s_z = 0$. On the other hand, if we employed the same procedure with the small potential $V_i \cos qx$ applied to each component with opposite amplitudes $V_1 = -V_2$, such a perturbation would mainly couple to the spin degree of freedom. Thus, it seems possible to find a combination of perturbation amplitudes $V_{1,2}$, such that for every set of gas parameters, our generalized protocol would excite only one sound mode. This feature is novel with respect to previously considered systems, as every external potential coupled to both the superfluid and the normal part. Since in the microscopic approach each component is described by a dedicated wavefunction, it is in principle possible to address them in a separate manner.

Let us consider an extended protocol with the perturbation potential given by

$$V \begin{pmatrix} \psi_1 \\ \psi_2 \end{pmatrix} = \begin{pmatrix} V_1 \cos qx & 0 \\ 0 & V_2 \cos qx \end{pmatrix} \begin{pmatrix} \psi_1 \\ \psi_2 \end{pmatrix}, \tag{5.13}$$

where we apply the same cosine potential with different, small amplitudes V_i to each component. In the hydrodynamic picture, the additional potential introduces a small perturbation of the energy, and hence the chemical potential of each component. We assume it is slowly varying in space and time and write it in the form $\lambda_i \exp(-i(\omega t - qx))$, where λ_i linearly depends on V_i. We further assume that the density and velocity perturbations have the same time and space dependence: $n_i(x,t) = n_i^0 + \delta n_i \, e^{-i(\omega t - qx)}$ and $v_i(x,t) = v_i^0 + \delta v_i \, e^{-i(\omega t - qx)}$, where $v_i^0 = 0$ since, for simplicity, we consider the gas to be at rest. The four HD equations

written in the single-component notation read:

$$\partial_t n_1 + \partial_x(n_1 v_1) = 0 \tag{5.14a}$$

$$\partial_t n_2 + \partial_x(n_2 v_2) = 0 \tag{5.14b}$$

$$\partial_t v_1 + \partial_x\left(\frac{1}{2}v_1^2 + \mu_1 + \lambda_1 e^{-i(\omega t - qx)}\right) = 0 \tag{5.14c}$$

$$\partial_t v_2 + \partial_x\left(\frac{1}{2}v_2^2 + \mu_2 + \lambda_2 e^{-i(\omega t - qx)}\right) = 0, \tag{5.14d}$$

where $\mu_i = g_i n_i + g_{12} n_{3-i}$. After linearlization, the first two equations (5.14a) and (5.14b) directly relate the velocity variations δv_i to δn_i, hence Eqs. (5.14) reduce to two equations. We are interested in the total density variation $\delta n = \delta n_1 + \delta n_2$ caused by the presence of the external potential (5.13). After straightforward calculations, we find:

$$\delta n(\omega, q) = \frac{\sum_{i=1,2} \lambda_i n_i^0 \left[\omega^2 + q^2 n_{3-i}^0 (g_{12} - g_{ii})\right] q^2}{\left[\omega^2 - (q c_d^0)^2\right]\left[\omega^2 - (q c_s^0)^2\right]}, \tag{5.15}$$

where the two speeds of sound c_s^0 and c_d^0 are given by (5.5). As anticipated, the density response has in general two pairs of poles - one pair for every sound mode. To decouple one of them, the nominator of (5.15) must take the form $(n_1^0\lambda_1 + n_2^0\lambda_2)\left[\omega^2 - (q c_i^0)^2\right]$ to cancel out the two corresponding poles. This condition introduces a relation between the two amplitudes λ_i, which reads:

$$\frac{\lambda_1}{\lambda_2} = -\frac{g_{11} - g_{12} - \left(c_i^0\right)^2 / n_1^0}{g_{22} - g_{12} - \left(c_i^0\right)^2 / n_2^0}, \tag{5.16}$$

where the index $i = d, s$ indicates the mode selected to be suppressed. The condition above defines a ratio of the two external perturbation strengths applied to the two components of the BEC mixture, provided that their densities n_i or their intraspecies coupling constant g_{ii} are different. In the symmetric case, i.e. $g_{11} = g_{22} \neq g_{12}$ and $n_1^0 = n_2^0$, it can easily be shown that equations (5.14) require $\lambda_1 = \lambda_2$ ($\lambda_1 = -\lambda_2$) for the spin-like (density-like) mode to vanish from the observed signal. In Fig. (5.2) we compare observable (5.12) measured during the time evolution of a particular interacting Bose mixture, where we used the linear-response protocol with different amplitudes V_i. The Fourier transform of the measured signal shows a significant suppression of the selected mode by the appropriate selection of perturbation amplitudes V_i.

In order to extend the formula (5.16) to systems with currents, one should linearize the HD equations (5.14) with finite values of v_1^0 and v_2^0. This would lead to a complicated equation of the total density variation (5.15), which would have four different poles. In practice, for small currents the formula (5.16) still provides a significant suppression of one pair of the sound modes, as the Doppler shift is small with respect to static values of the speeds of sound c_i^0.

The procedure above requires the two components to be subject to different external potentials, so that the information about one of the modes is removed from the time evolution of the total density. In practice, implementation of such a protocol may be challenging, as the use of two spatially varying potentials to a miscible mixture may be difficult to implement.

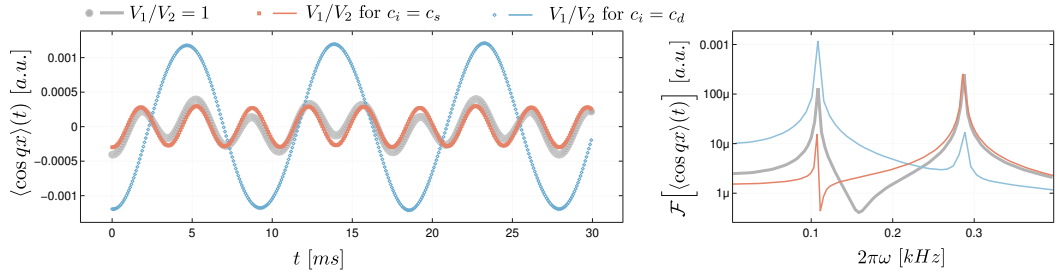

Figure 5.2: The time evolution of the observable $\langle \cos qx \rangle(t)$ (left) and its Fourier transform (right) in a Bose mixture at rest, for different ratios of the perturbation amplitudes V_i. The measured signal in the standard version of the protocol (gray) features a beating of two modes, whose frequencies correspond to the speeds of density- and spin-like sounds. On the other hand, if the ratio of the two amplitudes V_1/V_2 is chosen according to Eq. (5.16), the measured observable contains only the spin-like mode (blue) or the density-like mode (red). The remnants of the other mode, in both cases, persist due to imprecise values of c_i inserted to Eq. (5.16)

For this reason, we consider another variant of the linear-response protocol, where both components are addressed with equal strengths, but the observable is modified so that either spin-like or density-like mode is captured individually. We use the HD equations (5.14) where now $\lambda_1 = \lambda_2 = \lambda$ and linearize them to obtain the following variations of the total density and polarization:

$$\delta n = \lambda n^0 \frac{\omega^2 - q^2(1-m_z^2)n^0 g_s}{[\omega^2 - (qc_d^0)^2]\,[\omega^2 - (qc_s^0)^2]} q^2 \tag{5.17a}$$

$$\delta s_z = \lambda n^0 \frac{\omega^2 - \frac{1}{2}q^2(1-m_z^2)n^0 g_{ds}}{[\omega^2 - (qc_d^0)^2]\,[\omega^2 - (qc_s^0)^2]} q^2, \tag{5.17b}$$

We consider a generalized observable (5.12), which is a linear combination of $\langle \cos qx \rangle_\pm \equiv \int dx(|\psi_1(x,t)|^2 \pm |\psi_2(x,t)|^2)\cos(qx)$:

$$G(t) = \alpha \langle \cos qx \rangle_+ + \beta \langle \cos qx \rangle_- \tag{5.18}$$

Similarly to the previous protocol extension, the observable G includes one sound mode only, provided that the nominator of $\alpha\delta n + \beta\delta s_z$ is proportional to $\omega^2 - (qc_i^0)^2$, where $i \in \{s, d\}$. Using the speeds of sound (5.5) and equations (5.17) this condition leads to the parameter ratio:

$$\frac{\alpha}{\beta} = -\frac{m_z g + (2m_z^2 - 1)g_{ds} \pm m_z D}{g + m_z g_{ds} + 2(m_z^2 - 1)g_s \pm D}, \tag{5.19}$$

where $D = \sqrt{(g + m_z g_{ds})^2 - \Delta(1 - m_z^2)}$ and the "+" ("-") sign removes the density-like (spin-like) mode from the time evolution of the generalized observable. In Figure (5.3) we present an example of the Fourier transform of (5.18) for a certain choice of gas parameters and different ratios (5.19). Clearly, with the choice of parameters α and β according to (5.19), one can independently measure each of the modes.

Precession experiment

Thus far we have developed two variants of the modified linear-response protocol to selectively measure one of the two sound modes. Provided that one sound is greatly suppressed,

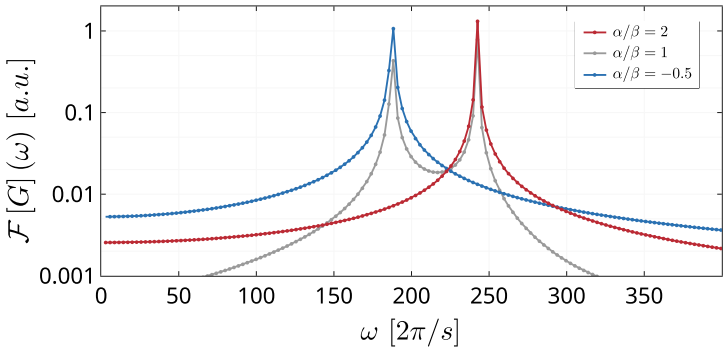

Figure 5.3: Selective mode measurement with the modified observable (5.18). The three curves represent Fourier transforms of (5.18) for a given interacting Bose mixture at rest, where the parameter ratio $\alpha/\beta = 1$ (gray) corresponds to the standard version of the protocol, $\alpha/\beta = -0.5$ (blue) measures the spin-like mode only, whereas $\alpha/\beta = 2$ (red) features only the density-like mode.

both methods provide the means to determine the speeds of the remaining two Doppler-split modes. In the context of the Doppler effect, this information is redundant, as we only need to know their difference. Direct access to this quantity is obtained by studying the precession of the density profile during the time evolution. This approach has already been applied in a single-component BEC [131]. Using the protocol with the appropriate choice (5.16) of the amplitudes λ_i, we show that the Doppler shift of each sound can be efficiently studied by measuring the precession of the density profile.

According to linear response theory, the time evolution of the density variation $\delta n(x,t)$ induced by a small perturbation is given by all the modes propagating in the system. Provided that the perturbation strengths satisfy the condition (5.16), in the presence of a small current, there are only two Doppler-split modes affecting the total density:

$$\delta n(x,t) = A_i^+ \cos\left(qx - \omega_i^+ t\right) + A_i^- \cos\left(qx + \omega_i^- t\right), \tag{5.20}$$

where $\omega^\pm = \omega_i^0 \pm \Omega_i$, and Ω_i is the Doppler shift of the i-th mode. For small currents, the difference between the two amplitudes $A_i^\pm$ can be neglected, as $A_i^+ - A_i^- \propto \Omega_i/[(\omega_i^0)^2 - \Omega_i^2]$. Under this assumption, the density profile evolves as

$$\delta n(x,t) \approx A_i \cos(qx - \Omega_i t)\cos\left(\omega_i^0 t\right), \tag{5.21}$$

where $A_i = A_i^+ + A_i^-$ and the Doppler shift is explicitly separated from the rest value of the the i-th mode frequency ω_i^0. At stroboscopic times, when $\omega_i^0 t$ equals an integer multiplication of 2π, the position of the density maximum changes with respect to its initial value by $\Omega_i t$. Thus, the slope of this dependence provides the value of the Doppler shift.

To demonstrate the utility of this method, we simulate the two-component Bose mixture in the same one-dimensional configuration as in the previous section. To amplify the signal, we imprint a current with the winding number $s = 3$ in the phase pattern of the first component, while the second remains at rest. To independently study the Doppler shifts of the two sounds, we fix the protocol amplitudes according to equation (5.16). At time $t = 0$ we suddenly remove the spin dependent potential to observe the time evolution of the total density profile $n(x,t)$. In Fig. (5.4) we present the results of the numerical simulation

of the precession experiment for both sound modes. The maximum of the total density clearly follows the hydrodynamic prediction indicated by the corresponding solid line. This

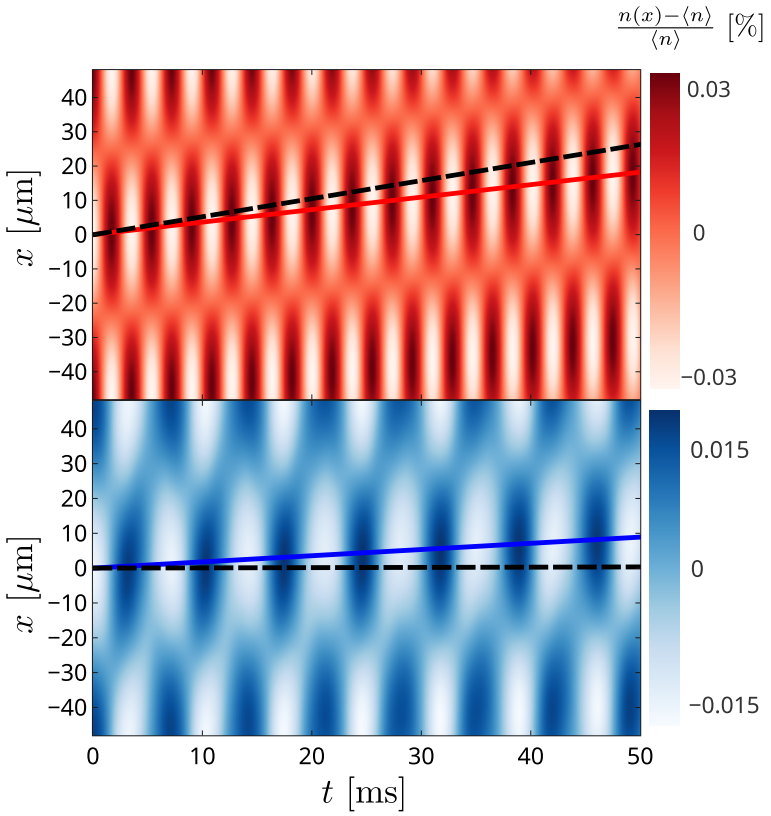

Figure 5.4: Precession of the total density profile $n(x) - \langle n \rangle$ with selectively excited density-like mode (upper panel) and spin-like mode (lower panel). In each panel, the solid line indicates the trajectory of the density maximum at stroboscopic times, as given by the hydrodynamic formula (5.9). The results correspond to the following gas parameters: $m_z = 0.1$, $g_{ds}/g = 0.1$, $g_{12}/g = 0.55$ and $v_T^0 = w^0 = 3 \times 2\pi\hbar/(mL)$, for which $\delta_d = 0.67$ and $\delta_s = 0.33$. The dashed line presents the Doppler shift for the same gas parameters but with interspecies interaction $g_{12} = 0$, where the density-like (spin-like) mode corresponds to the oscillation of the density of the first (second) component.

simulation shows that the anomalous Doppler effect can be measured in Bose mixtures, using the same experimental method employed in a single-component BEC [131].

5.2 Andreev-Bashkin effect

In the previous sections, we have considered the mean-field case, where the superfluid current in each component is determined only by its superfluid velocity. In general, however, cross terms are present due to the so-called Andreev-Bashkin dissipationless drag [156]. As a result, a finite velocity field of one component gives a contribution to the current in the

other superfluid component:

$$j_i = (n_i - n_D)v_i + n_D v_{3-i} \tag{5.22}$$

where n_D is the so-called superfluid drag and can be seen as the (quantum) dressing of one component by the other. The current entrainment introduces an additional term in the total energy density $\epsilon_D = -\frac{1}{2}n_D(v_1 - v_2)^2 = -2n_D w^2$, which alters the hydrodynamic equations:

$$\partial_t n + \partial_x j = 0 \tag{5.23a}$$
$$\partial_t s_z + \partial_x (j_z - 4n_D w) = 0 \tag{5.23b}$$
$$\partial_t v_T + \partial_x \left(\frac{v_T^2}{2} + \frac{w^2}{2} - 2\partial_n n_D w^2 + \frac{\mu}{m} \right) = 0 \tag{5.23c}$$
$$\partial_t w + \partial_x \left(w v_T - 2\partial_{s_z} n_D w^2 + \frac{h}{m} \right) = 0. \tag{5.23d}$$

Linearization of these equations leads to the two speeds of sound at rest:

$$c^0_{d/s} = \left[\frac{n^0}{2m} \left(g + m_z g_{ds} - 4 f_D g_s \pm \sqrt{(g + m_z g_{ds} - 4 f_D g_s)^2 - \Delta \left[1 - 4 f_D - m_z^2 \right]} \right) \right]^{1/2}, \tag{5.24}$$

where we introduce the drag fraction $f_D = n_D^0/n^0$. Linearization of the hydrodynamic equations (5.23) yields the same form of the Doppler shift of the two sound modes: $\Delta c_{d/s} = v_T^0 + \delta_{d/s} w^0$, where the $\delta_{d/s}$ term is modified by the Andreev-Bashkin drag and reads:

$$\delta_d = -\delta_s = \frac{g m_z + g_{ds}(1 - 2f_D) - \frac{4}{n^0}\partial_{s_z} n_D^0 \left[\left(c^0_{d/s} \right)^2 - \mu^0 \right] - \frac{4}{n^0}\partial_n n_D^0 h^0}{\sqrt{(g + m_z g_{ds} - 4 f_D g_s)^2 - \Delta \left[1 - 4 f_D - m_z^2 \right]}}, \tag{5.25}$$

where $\mu^0 = g_d n^0 + g_{ds} s_z^0/2$ and $h^0 = g_s s_z^0 + g_{ds} n^0/2$. For weakly interacting Bose mixtures, the drag density n_D is very small, because of its linear dependence on the two gas parameters $\eta_i = \sqrt{n_i a_{ii}^3}$ [157]. Thus, inclusion of this effect will not visibly change the Doppler shift. Nonetheless, it is interesting to notice a qualitative change in the regime of large imbalance $s_z \approx -n$. There, the drag density is approximately equal:

$$n_D \approx 0.4(n + s_z) \left(\frac{g_{12}}{g - g_{ds}} \right)^2 \eta_2 \tag{5.26}$$

and the two derivatives read:

$$\partial_{s_z} n_D = 0.2 \left(\frac{g_{12}}{g - g_{ds}} \right)^2 \left(2 - \frac{1 + m_z}{1 - m_z} \right) \eta_2 \tag{5.27a}$$
$$\partial_n n_D = 0.2 \left(\frac{g_{12}}{g - g_{ds}} \right)^2 \left(2 + \frac{1 + m_z}{1 - m_z} \right) \eta_2 \tag{5.27b}$$

This result shows that, in contrast to the mean-field case, for $m_z = -g_{ds}/g$, the nominator of (5.25) does not vanish. Consequently, for this value of magnetization, the presence of the dissipationless drag lifts the independence of the Doppler shift from the g_{12} coupling constant. While the effect is negligible in dilute Bose mixtures, in other systems, the Doppler effect may serve as a good observable for detecting the Andreev-Bashkin effect.

Conclusions

In this chapter, we investigated the Doppler effect in binary Bose mixtures, where we revealed a non-trivial sound entrainment caused by the intraspecies interaction and the relative velocity between the two components. Using the hydrodynamic theory of two coupled superfluids, we derived a formula describing the Doppler shift of the spin-like and the density-like sounds. The complex dependence of the Doppler shift on the thermodynamic properties of the system are consistent with what we have found in density-modulated superfluids in the previous chapter, and the theoretical works on liquid helium platforms [13–16]. Among all these systems, the Bose mixture gas seems to be the most promising one in the context of an experimental observation of the non-trivial Doppler effect, thanks to the versatile access to both wavefunctions and their long lifetime. Consequently, employing the linear response theory, we proposed experimental protocols to individually study the Doppler shift of each sound mode. Our proposals generalize the method that was successfully applied in a single-component BEC [131] to observe the same effect.

Finally, we considered the Andreev-Bashkin effect in the context of the Doppler effect. We demonstrated that, in weakly coupled Bose mixtures, this effect slightly alters the Doppler shift of each sound. In principle, in systems where the Andreev-Bashkin effect is more pronounced, our protocol provides the means to measure the dissipation-less drag.

Lastly, we stress that the results of this work are general to all superfluid mixtures, being applicable to fermionic gases, as well as mixtures of different quantum statistics.

Conclusions

This thesis is a comprehensive study of sound propagation in superfluid Bose gases with two broken continuous symmetries, which predominantly focuses on recently observed supersolid phase of dipolar BECs. In the first part, we confirmed the existence of two distinct sound modes within the framework of the extended Gross-Pitaevskii equation and characterized them as a function of the relative interaction strength ε_{dd}. We proposed an experimental protocol to measure the two speeds of sound in all three phases of dipolar BECs, utilizing the linear response theory. Our protocol can be used not only to study sound waves but also all the high-momenta excitations, providing a new way to characterize the entire low-energy excitation spectrum. Having measured values of the two sounds in the supersolid phase of dipolar BECs, we provided the first quantitative comparison between the predictions of the eGPE and the hydrodynamic theory of supersolids. Our analysis showed a good agreement between the two theories, thereby opening new ways for determining key properties of the system. In particular, we demonstrated that the supersolid hydrodynamics provides a novel way to measure the superfluid fraction.

In the second part, we investigated the Doppler effect in density-modulated superfluids, in which we predict the sound entrainment to have a highly non-trivial form that depends on all thermodynamic parameters of the gas. We began with the analysis of ordinary BECs in optical lattices, in which we confirmed the anomalous form of the Doppler effect with the numerical simulation of the Gross-Pitaevskii equation. Then, we considered the same phenomenon in moving supersolids, whose two sound modes experience different Doppler shifts. To set the stage, we first discussed the relation between macroscopic quantities - such as superfluid and normal velocities - and the gradient of the phase of the order parameter. Then, we characterized the ground state of a supersolid in a moving frame of reference to assess values of currents in metastable states. Finally, by linearizing the supersolid hydrodynamic equations, we derived the formulas for the Doppler shifts of the two sounds in supersolids. We validated them with numerical simulations of the eGPE, showing a good agreement. Therefore, our analysis demonstrated the existence of the anomalous Doppler effect in density-modulated superfluids, even at zero temperature.

The last chapter considered the same phenomenon in mixtures of two Bose-Einstein condensates, where there exist two sound modes of hybrid density and spin nature. Using the same linear-response protocol, we showed the anomalous form of the Doppler effect in a Bose mixture, where one of the components remained at rest. The results of numerical simulations are in perfect agreement with analytical formulas, which we derived from the hydrodynamic theory of superfluid mixtures.

Historically, the anomalous Doppler effect was first predicted to occur in liquid helium but has never been verified experimentally. Thanks to their stability and tunability, superfluid mixtures seem to serve as perfect platforms to observe this unusual effect. Therefore, we proposed two similar experimental schemes for the individual measurement of the two

sound modes. Our proposals are extensions of a method that has been successfully applied to study the Doppler effect in ordinary BECs [131]. Lastly, we considered the influence of the Andreev-Bashkin effect on the Doppler shifts. Although its presence changes the analytical formulas, the difference in weakly interacting Bose gases is too small to be observed. In principle, in systems where the superfluid drag is more pronounced, the Doppler effect may provide useful means of measuring the Andreev-Bashkin effect.

Following the results of this thesis and previous studies on liquid helium, we can draw general conclusions about the anomalous Doppler effect. All systems in which the Doppler shift is not simply given by the current j/ρ consist of two fluids that in a stable configuration can move at different velocities. Liquid helium platforms were investigated at finite temperatures, where thermal fluctuations are responsible for the appearance of the normal part. In this thesis, we showed that density-modulated superfluids at $T = 0$ are also described by a dedicated two-fluid hydrodynamic model, in which the normal part appears because of the Leggett's upper bound on the superfluid fraction. The difference in the velocity fields in these systems can be enforced externally (with an optical lattice fixing the velocity of the normal part) or internally (supersolids in closed geometries have a well-defined relation between v_n and v_s in the rotating frame ground state). Moreover, we demonstrated that the anomalous Doppler effects occur also in superfluid mixtures, therefore without requiring the presence of a normal component. The relative current in these systems is given by different boundary conditions for the phase of the two order parameters.

All of the aforementioned platforms host sound modes of hybrid character, which means that both fluids are involved in the propagation of the sound. The anomalous Doppler effect occurs only when the two components move with different velocities. In such a case, the Doppler shift cannot be explained by a simple Galilean transformation because there is no reference frame in which the entire sound carrier is at rest. Superfluids are great platforms to study this effect, as quantization of the supercurrent in closed geometries aids the stability of the relative velocity. Through comprehensive analytical and numerical analysis, this thesis establishes the theoretical basis for the first experimental observation of the anomalous Doppler effect.

Appendix A

Derivation of the Doppler shift in supersolid hydrodynamics

In this appendix, we present the detailed derivation of Doppler shifts of the two sounds in supersolids. We begin with writing all relevant HD equations of a one-dimensional supersolid (see (1.64) and discussion therein for definitions of all the parameters):

$$\partial_t \rho + \partial_x j = 0 \tag{A.1a}$$
$$\partial_t j + \partial_x \left(p + \rho_n v_n^2 + \rho_s v_s^2\right) = 0 \tag{A.1b}$$
$$\partial_t v_s + \partial_x (v_n v_s + \mu) = 0 \tag{A.1c}$$
$$\partial_t u_x + \partial_x (v_n u_x - v_n) = 0, \tag{A.1d}$$

where $j = \rho_s v_s + \rho_n v_n$ and the two constitutive equations:

$$\delta\mu = \frac{1}{\rho^2\kappa}\delta\rho + \gamma u_x + \frac{\rho_s'}{2}\delta w^2 - \frac{1}{2}\delta v_n^2 \tag{A.2a}$$
$$\delta p = \left(\frac{1}{\rho\kappa} - \gamma\right)\delta\rho + (\gamma\rho - \lambda)\, u_x + \frac{\rho_n - \rho\rho_n'}{2}\delta w^2. \tag{A.2b}$$

The standard procedure for calculating the speeds of sound is based on linearization of HD equations by representing all variables as a sum of their equilibrium values ξ^0 and small variations $\delta\xi(x,t)$. Here we identify a set of four independent variables $\{\rho, w, v_n, u_x\}$, whose variations are assumed to be slowly varying in space and time as $\delta\xi(x,t) = \delta\xi \exp(-i(\omega t - qx))$. Variations of every other hydrodynamic parameter in (A.1) can be expressed with variations of the four variables above. In particular, the variation of the superfluid density reads:

$$\delta\rho_s = \rho_s'\delta\rho + \rho_s^u u_x, \tag{A.3}$$

where $\rho_s^u \equiv \partial\rho_s/\partial u_x$. Its dependence on velocities w and v_n is quadratic, and can be neglected in the first order. Here we will only consider velocities small with respect to the speed of sound, effectively neglecting all terms of order higher than linear. In the limit where $q \to 0$, the dispersion of ω is linear and the speed of sound is given by ω/q. Finally, the

linearized hydrodynamic equations are neatly represented in the matrix form:

$$\begin{pmatrix} -c+v' & -\rho_s & \rho & -w\rho_s^u \\ -v'(c-v')+ \\ +\frac{1}{\rho\kappa}-\gamma & \rho_s(c-v'-v_n)+ \\ +w(\rho_s+\rho_n\rho_s') & \rho(-c+2v_n-2wf_s) & \rho\gamma-\lambda \\ +w(c-2v_n+w)\rho_s^u \\ \frac{1}{\rho^2\kappa} & c-v' & -c+v_n-w & \gamma \\ 0 & 0 & 1 & c-v_n \end{pmatrix} \begin{pmatrix} \delta\rho \\ \delta w \\ \delta v_n \\ u_x \end{pmatrix} = 0 \tag{A.4}$$

where $v' \equiv v_n\rho_n' + v_s\rho_s'$. The last row gives a simple relation between the strain u_x and the normal velocity v_n, which we use to reduce the 4×4 matrix to 3×3:

$$\begin{pmatrix} -c+v' & -\rho_s & -\rho(c-v')+w(\rho\rho_s'-\rho_s^u) \\ -v'(c-v')+ \\ +\frac{1}{\rho\kappa}-\gamma & \rho_s(c-v'-v_n)+ \\ +w(\rho_s+\rho_n\rho_s') & \rho\gamma-\lambda+\rho(c-v')^2+ \\ +\rho(c-v')\left[-v_n+w(2f_s-2\rho_s'+\rho_s^u/\rho)\right] \\ \frac{1}{\rho^2\kappa} & c-v' & (c-v')^2+(1-2\rho_s')(c-v')w+\gamma \end{pmatrix} \begin{pmatrix} \delta\rho \\ \delta w \\ u_x \end{pmatrix} = 0 \tag{A.5}$$

In order to further reduce the number of variables in linearized HD equations we change the reference frame to the one that moves with v'. This Galilean transformation introduces the following changes: $(c-v') \to c$ and $(v_n - v') \to \rho_s' w$, while w remains unaltered. The hydrodynamic equations in the new reference frame read:

$$\begin{pmatrix} -c & -\rho_s & -\rho c + w(\rho\rho_s'-\rho_s^u) \\ \frac{1}{\rho\kappa}-\gamma & \rho_s c+ \\ & +w(\rho_s+\rho\rho_s'-2\rho_s\rho_s') & \rho c^2+\rho\gamma-\lambda \\ & & +c\left[2\rho_s-3\rho\rho_s'+\rho_s^u\right]w \\ \frac{1}{\rho^2\kappa} & c & c^2+(1-2\rho_s')wc+\gamma \end{pmatrix} \begin{pmatrix} \delta\rho \\ \delta w \\ u_x \end{pmatrix} = 0. \tag{A.6}$$

Non-trivial solutions require the determinant of this matrix ($\det M$) to vanish. Therefore, to calculate the speeds of sound, one has to find all roots of the fourth-order polynominal:

$$\begin{aligned} \det M =& \rho_n\left(c^2-(c_1^0)^2\right)\left(c^2-(c_2^0)^2\right) + w\left[\rho_s^u - 4\rho_s'\rho_n\right]c^3 + \\ &+ w\left[\frac{1}{\rho\kappa}\left(2\rho_n(f_s+\rho_s') - \frac{\rho_s^u}{\rho_n}\right) + \gamma\left(\rho_s^u - 2\rho_s - 2\rho\rho_s' + 4\rho_s\rho_s'\right)\right]c, \end{aligned} \tag{A.7}$$

where c_i^0 denote the two speeds of sound at rest (3.13). Finding the exact formulae for all four roots of (A.7) is possible, but very complicated. Since we assume all velocities are small with respect to speeds of sound, we use Taylor expansion around $w=0, c=c_{1,2}^0$ to approximate the change of rest values c_i^0 introduced by finite currents as:

$$\det M \approx \det M\Big|_{\substack{c=c_i^0\\w=0}} + \frac{\partial \det M}{\partial w}\bigg|_{\substack{c=c_i^0\\w=w^0}} w + \frac{\partial \det M}{\partial c_i}\bigg|_{\substack{c=c_i^0\\w=0}} \Delta c_i. \tag{A.8}$$

Since both determinants are zero, the Doppler shifts read:

$$w\Delta_i \equiv - w\frac{\frac{\partial \det M}{\partial w}}{\frac{\partial \det M}{\partial c_i}} = \\ - \frac{w}{2}\frac{\left(\frac{\rho_s^u}{\rho_n} - 4\rho_s'\right)\left(c_{1,2}^0\right)^2 + \frac{1}{\rho\kappa}\left(2(f_s+\rho_s') - \frac{\rho_s^u}{\rho_n}\right) + \gamma\left(\rho_s^u - 2\rho_s - 2\rho\rho_s' + 4\rho_s\rho_s'\right)/\rho_n}{2\left(c_{1,2}^0\right)^2 - \frac{1}{\rho\kappa} - \frac{\lambda}{\rho_n} + 2\gamma} \tag{A.9}$$

and all four solutions can be approximated as:

$$c_{1,2}^{\pm} = c_{1,2}^0 \pm (v' + w\Delta_{1,2}). \tag{A.10}$$

This formula for the Doppler shifts in supersolids is exactly the same as in our original paper [152], where the anomalous term here Δ_i is related to δ_i from [152] by: $\Delta_i + \rho_n' = \delta_i$.

List of Publications

[1] B. Tüzemen, T. Zawiślak, G. Wlazłowski, and P. Magierski, "Disordered structures in ultracold spin-imbalanced Fermi gas", New Journal of Physics **25**, 033013 (2023).

[2] M. Šindik, T. Zawiślak, A. Recati, and S. Stringari, "Sound, Superfluidity, and Layer Compressibility in a Ring Dipolar Supersolid", Phys. Rev. Lett. **132**, 146001 (2024).

[3] T. Zawiślak, M. Šindik, S. Stringari, and A. Recati, "Anomalous Doppler Effect in Superfluid and Supersolid Atomic Gases", Phys. Rev. Lett. **134**, 226001 (2025).

[4] T. Zawiślak, S. Stringari, and A. Recati, *Anomalous Doppler effect in two-component Bose-Einstein condensates*, 2025, arXiv:2508.04398 [cond-mat.quant-gas].

Bibliography

[1] A. F. Andreev and I. M. Lifshitz, “Quantum Theory of Defects in Crystals”, Sov. Phys. JETP **29**, 1107 (1969).

[2] G. V. Chester, “Speculations on Bose-Einstein Condensation and Quantum Crystals”, Phys. Rev. A **2**, 256 (1970).

[3] A. J. Leggett, “Can a Solid Be "Superfluid"?”, Phys. Rev. Lett. **25**, 1543 (1970).

[4] J.-R. Li et al., “A stripe phase with supersolid properties in spin–orbit-coupled Bose–Einstein condensates”, Nature **543**, 91 (2017).

[5] J. Léonard et al., “Supersolid formation in a quantum gas breaking a continuous translational symmetry”, Nature **543**, 87 (2017).

[6] L. Tanzi et al., “Observation of a Dipolar Quantum Gas with Metastable Supersolid Properties”, Phys. Rev. Lett. **122**, 130405 (2019).

[7] L. Chomaz et al., “Long-Lived and Transient Supersolid Behaviors in Dipolar Quantum Gases”, Phys. Rev. X **9**, 021012 (2019).

[8] F. Böttcher et al., “Transient Supersolid Properties in an Array of Dipolar Quantum Droplets”, Phys. Rev. X **9**, 011051 (2019).

[9] P. Ilzhöfer et al., “Phase coherence in out-of-equilibrium supersolid states of ultracold dipolar atoms”, Nature Physics **17**, 356 (2021).

[10] L. Tanzi et al., “Supersolid symmetry breaking from compressional oscillations in a dipolar quantum gas”, Nature **574**, 382 (2019).

[11] M. Guo et al., “The low-energy Goldstone mode in a trapped dipolar supersolid”, Nature **574**, 386 (2019).

[12] G. Natale et al., “Excitation Spectrum of a Trapped Dipolar Supersolid and Its Experimental Evidence”, Phys. Rev. Lett. **123**, 050402 (2019).

[13] I. Khalatnikov, “The Propagation of Sound in Moving Helium II and the Effect of a Thermal Current upon the Propagation of Second Sound”, Zh. Eksp. Teor. Fiz 30, 617 (1956) [Sov. Phys. JETP 3, 649 (1956)].

[14] Y. Nepomnyashchy and M. Revzen, “Curious Doppler shift of fourth sound in the low temperature limit”, Physics Letters A **161**, 164 (1991).

[15] Y. A. Nepomnyashchy, “Unusual Doppler effect in He II”, Phys. Rev. B **47**, 905 (1993).

[16] N. Gov, A. Mann, Y. Nepomnyashchy, and M. Revzen, “Unusual Doppler shift of fourth sound in a ^{3}He - ^{4}He mixture”, Physics Letters A **182**, 149 (1993).

[17] H. R. Glyde, R. T. Azuah, and W. G. Stirling, "Condensate, momentum distribution, and final-state effects in liquid ^{4}He", Phys. Rev. B **62**, 14337 (2000).

[18] L. D. Landau and E. M. Lifshitz, *Quantum Mechanics: Non-Relativistic Theory*, 3rd, Vol. 3, Course of Theoretical Physics (Butterworth-Heinemann, 2010).

[19] L. Pitaevskii and S. Stringari, *Bose-Einstein condensation and superfluidity* (Oxford University Press, 2016).

[20] I. M. Khalatnikov, *An introduction to the theory of superfluidity*, Advanced book classics (Addison-Wesley, Redwood City, Calif. [etc, 1988).

[21] H. Stoof, D. Dickerscheid, and K. Gubbels, *Ultracold Quantum Fields*, Theoretical and Mathematical Physics (Springer Netherlands, 2008).

[22] M. Faccioli and L. Salasnich, "Spontaneous Symmetry Breaking and Higgs Mode: Comparing Gross-Pitaevskii and Nonlinear Klein-Gordon Equations", Symmetry **10**, 10.3390/sym10040080 (2018).

[23] A. R. P. Lima and A. Pelster, "Beyond mean-field low-lying excitations of dipolar Bose gases", Phys. Rev. A **86**, 063609 (2012).

[24] J. J. A. Houwman et al., "Measurement of the Excitation Spectrum of a Dipolar Gas in the Macrodroplet Regime", Phys. Rev. Lett. **132**, 103401 (2024).

[25] J. Stenger et al., "Bragg Spectroscopy of a Bose-Einstein Condensate", Phys. Rev. Lett. **82**, 4569 (1999).

[26] S. Saccani, S. Moroni, and M. Boninsegni, "Excitation Spectrum of a Supersolid", Phys. Rev. Lett. **108**, 175301 (2012).

[27] G. Bismut et al., "Anisotropic Excitation Spectrum of a Dipolar Quantum Bose Gas", Phys. Rev. Lett. **109**, 155302 (2012).

[28] J. Steinhauer, R. Ozeri, N. Katz, and N. Davidson, "Excitation Spectrum of a Bose-Einstein Condensate", Phys. Rev. Lett. **88**, 120407 (2002).

[29] J. L. Ville et al., "Sound Propagation in a Uniform Superfluid Two-Dimensional Bose Gas", Phys. Rev. Lett. **121**, 145301 (2018).

[30] S. J. Garratt et al., "From single-particle excitations to sound waves in a box-trapped atomic Bose-Einstein condensate", Phys. Rev. A **99**, 021601 (2019).

[31] M. R. Andrews et al., "Propagation of Sound in a Bose-Einstein Condensate", Phys. Rev. Lett. **79**, 553 (1997).

[32] E. Zaremba, "Sound propagation in a cylindrical Bose-condensed gas", Phys. Rev. A **57**, 518 (1998).

[33] M. D. Lachmann et al., "Ultracold atom interferometry in space", Nature Communications **12**, Published: 2021/02/26, 1317 (2021).

[34] M. R. Andrews et al., "Observation of Interference Between Two Bose Condensates", Science **275**, 637 (1997), eprint: https://www.science.org/doi/pdf/10.1126/science.275.5300.637.

[35] T. Berrada et al., "Matter-wave recombiners for trapped Bose-Einstein condensates", Phys. Rev. A **93**, 063620 (2016).

[36] C. Gross et al., "Nonlinear atom interferometer surpasses classical precision limit", Nature **464**, Published: 2010/04/01, 1165 (2010).

[37] M. F. Riedel et al., "Atom-chip-based generation of entanglement for quantum metrology", Nature **464**, Published: 2010/04/01, 1170 (2010).

[38] H. Watanabe and T. š. Brauner, "Spontaneous breaking of continuous translational invariance", Phys. Rev. D **85**, 085010 (2012).

[39] A. Recati and S. Stringari, "Coherently Coupled Mixtures of Ultracold Atomic Gases", Annual Review of Condensed Matter Physics **13**, 407 (2022).

[40] J. Armaitis, H. T. C. Stoof, and R. A. Duine, "Hydrodynamic modes of partially condensed Bose mixtures", Phys. Rev. A **91**, 043641 (2015).

[41] R. Cominotti et al., "Observation of Massless and Massive Collective Excitations with Faraday Patterns in a Two-Component Superfluid", Phys. Rev. Lett. **128**, 210401 (2022).

[42] J. H. Kim, D. Hong, and Y. Shin, "Observation of two sound modes in a binary superfluid gas", Phys. Rev. A **101**, 061601 (2020).

[43] C. Piekarski, N. Cherroret, T. Aladjidi, and Q. Glorieux, "Spin and Density Modes in a Binary Fluid of Light", Phys. Rev. Lett. **134**, 223403 (2025).

[44] L. Tisza, "Transport Phenomena in Helium II", Nature **141**, 913 (1938).

[45] L. Landau, "Theory of the Superfluidity of Helium II", Phys. Rev. **60**, 356 (1941).

[46] D. Forster, *Hydrodynamic fluctuations, broken symmetry, and correlation functions* (W. A. Benjamin, Inc., Reading, MA, Dec. 1974).

[47] S. J. Putterman, *Superfluid hydrodynamics*, North-Holland series in low temperature physics ; 3 (North-Holland, Amsterdam ; 1974).

[48] P. C. Hohenberg, "Existence of Long-Range Order in One and Two Dimensions", Phys. Rev. **158**, 383 (1967).

[49] N. D. Mermin and H. Wagner, "Absence of Ferromagnetism or Antiferromagnetism in One- or Two-Dimensional Isotropic Heisenberg Models", Phys. Rev. Lett. **17**, 1133 (1966).

[50] J. C. Smith, D. Baillie, and P. B. Blakie, "Supersolidity and crystallization of a dipolar Bose gas in an infinite tube", Phys. Rev. A **107**, 033301 (2023).

[51] A. J. Leggett, "On the Superfluid Fraction of an Arbitrary Many-Body System at $T = 0$", J. Stat. Phys. **93**, 927 (1998).

[52] O. Penrose and L. Onsager, "Bose-Einstein Condensation and Liquid Helium", Phys. Rev. **104**, 576 (1956).

[53] Bonfait, G., Godfrin, H., and Castaing, B., "Solid 4He : search for superfluidity", J. Phys. France **50**, 1997 (1989).

[54] D. S. Greywall, "Search for superfluidity in solid ^{4}He", Phys. Rev. B **16**, 1291 (1977).

[55] D. J. Bishop, M. A. Paalanen, and J. D. Reppy, "Search for superfluidity in hcp ^{4}He", Phys. Rev. B **24**, 2844 (1981).

[56] E. Kim and M. H. W. Chan, "Probable observation of a supersolid helium phase", Nature **427**, 225 (2004).

[57] E. Kim and M. H. W. Chan, "Observation of superflow in solid helium", Science **305**, 1941 (2004).

[58] E. Kim and M. H. W. Chan, "Supersolid helium at high pressure", Phys. Rev. Lett. **97**, 115302 (2006).

[59] A. C. Clark, J. T. West, and M. H. W. Chan, "Nonclassical rotational inertia in helium crystals", Phys. Rev. Lett. **99**, 135302 (2007).

[60] D. Y. Kim and M. H. W. Chan, "Absence of supersolidity in solid helium in porous vycor glass", Phys. Rev. Lett. **109**, 155301 (2012).

[61] L. Santos, G. V. Shlyapnikov, and M. Lewenstein, "Roton-Maxon Spectrum and Stability of Trapped Dipolar Bose-Einstein Condensates", Phys. Rev. Lett. **90**, 250403 (2003).

[62] A. Griesmaier et al., "Bose-Einstein Condensation of Chromium", Phys. Rev. Lett. **94**, 160401 (2005).

[63] M. Lu, N. Q. Burdick, S. H. Youn, and B. L. Lev, "Strongly Dipolar Bose-Einstein Condensate of Dysprosium", Phys. Rev. Lett. **107**, 190401 (2011).

[64] K. Aikawa et al., "Bose-Einstein Condensation of Erbium", Phys. Rev. Lett. **108**, 210401 (2012).

[65] K.-K. Ni et al., "A High Phase-Space-Density Gas of Polar Molecules", Science **322**, 231 (2008), eprint: https://www.science.org/doi/pdf/10.1126/science.1163861.

[66] J. Lin et al., "Microwave Shielding of Bosonic NaRb Molecules", Phys. Rev. X **13**, 031032 (2023).

[67] N. Bigagli et al., "Collisionally stable gas of bosonic dipolar ground-state molecules", Nature Physics **19**, 1579 (2023).

[68] N. Bigagli et al., "Observation of Bose–Einstein condensation of dipolar molecules", Nature **631**, Published: 2024-07-01, 289 (2024).

[69] J. Hertkorn et al., "Pattern formation in quantum ferrofluids: From supersolids to superglasses", Phys. Rev. Res. **3**, 033125 (2021).

[70] M. Schmidt, L. Lassablière, G. Quéméner, and T. Langen, "Self-bound dipolar droplets and supersolids in molecular Bose-Einstein condensates", Phys. Rev. Res. **4**, 013235 (2022).

[71] J. Stuhler et al., "Magnetostriction in a degenerate quantum gas", Journal of Magnetism and Magnetic Materials **316**, Proceedings of the Joint European Magnetic Symposia, 429 (2007).

[72] J. L. Bohn, R. M. Wilson, and S. Ronen, "How does a dipolar Bose-Einstein condensate collapse?", Laser Physics **19**, 547 (2009).

[73] T. Koch et al., "Stabilization of a purely dipolar quantum gas against collapse", Nature Physics **4**, 218 (2008).

[74] T. Lahaye et al., "*d*-Wave Collapse and Explosion of a Dipolar Bose-Einstein Condensate", Phys. Rev. Lett. **101**, 080401 (2008).

[75] J. Metz et al., "Coherent collapses of dipolar Bose–Einstein condensates for different trap geometries", New Journal of Physics **11**, 055032 (2009).

[76] T. Lahaye et al., "Strong dipolar effects in a quantum ferrofluid", Nature **448**, 672 (2007).

[77] G. Bismut et al., "Anisotropic Excitation Spectrum of a Dipolar Quantum Bose Gas", Phys. Rev. Lett. **109**, 155302 (2012).

[78] C. Ticknor, R. M. Wilson, and J. L. Bohn, "Anisotropic Superfluidity in a Dipolar Bose Gas", Phys. Rev. Lett. **106**, 065301 (2011).

[79] M. Wenzel et al., "Anisotropic Superfluid Behavior of a Dipolar Bose-Einstein Condensate", Phys. Rev. Lett. **121**, 030401 (2018).

[80] P. Muruganandam and S. Adhikari, "Anisotropic sound and shock waves in dipolar Bose–Einstein condensate", Physics Letters A **376**, 480 (2012).

[81] H. Kadau et al., "Observing the Rosensweig instability of a quantum ferrofluid", Nature **530**, 194 (2016).

[82] M. D. Cowley and R. E. Rosensweig, "The interfacial stability of a ferromagnetic fluid", Journal of Fluid Mechanics **30**, 671 (1967).

[83] R. N. Bisset and P. B. Blakie, "Crystallization of a dilute atomic dipolar condensate", Phys. Rev. A **92**, 061603 (2015).

[84] K.-T. Xi and H. Saito, "Droplet formation in a Bose-Einstein condensate with strong dipole-dipole interaction", Phys. Rev. A **93**, 011604 (2016).

[85] I. Ferrier-Barbut et al., "Observation of Quantum Droplets in a Strongly Dipolar Bose Gas", Phys. Rev. Lett. **116**, 215301 (2016).

[86] H. Saito, "Path-Integral Monte Carlo Study on a Droplet of a Dipolar Bose?Einstein Condensate Stabilized by Quantum Fluctuation", Journal of the Physical Society of Japan **85**, 053001 (2016), eprint: `https://doi.org/10.7566/JPSJ.85.053001`.

[87] A. R. P. Lima and A. Pelster, "Quantum fluctuations in dipolar Bose gases", Phys. Rev. A **84**, 041604 (2011).

[88] F. Wächtler and L. Santos, "Quantum filaments in dipolar Bose-Einstein condensates", Phys. Rev. A **93**, 061603 (2016).

[89] T. D. Lee, K. Huang, and C. N. Yang, "Eigenvalues and Eigenfunctions of a Bose System of Hard Spheres and Its Low-Temperature Properties", Phys. Rev. **106**, 1135 (1957).

[90] T. D. Lee and C. N. Yang, "Many-Body Problem in Quantum Mechanics and Quantum Statistical Mechanics", Phys. Rev. **105**, 1119 (1957).

[91] A. L. Fetter and J. D. Walecka, *Quantum Theory of Many-Particle Systems* (Dover Publications, 2003).

[92] I. S. Gradshteyn and I. M. Ryzhik, *Table of Integrals, Series, and Products*, 7th ed. (Academic Press, New York, 2007).

[93] R. N. Bisset, R. M. Wilson, D. Baillie, and P. B. Blakie, "Ground-state phase diagram of a dipolar condensate with quantum fluctuations", Phys. Rev. A **94**, 033619 (2016).

[94] P. Hohenberg and W. Kohn, "Inhomogeneous Electron Gas", Phys. Rev. **136**, B864 (1964).

[95] W. Kohn and L. J. Sham, "Self-Consistent Equations Including Exchange and Correlation Effects", Phys. Rev. **140**, A1133 (1965).

[96] R. Dreizler and E. Gross, *Density Functional Theory: An Approach to the Quantum Many-Body Problem* (Springer Berlin Heidelberg, 2012).

[97] L. Chomaz et al., "Dipolar physics: a review of experiments with magnetic quantum gases", Reports on Progress in Physics **86**, 026401 (2022).

[98] J. J. A. Houwman et al., "Measurement of the Excitation Spectrum of a Dipolar Gas in the Macrodroplet Regime", Phys. Rev. Lett. **132**, 103401 (2024).

[99] S. Pal, D. Baillie, and P. B. Blakie, "Excitations and number fluctuations in an elongated dipolar Bose-Einstein condensate", Phys. Rev. A **102**, 043306 (2020).

[100] S. Pal, D. Baillie, and P. B. Blakie, "Infinite dipolar droplet: A simple theory for the macrodroplet regime", Phys. Rev. A **105**, 023308 (2022).

[101] A. Boudjemâa and G. V. Shlyapnikov, "Two-dimensional dipolar Bose gas with the roton-maxon excitation spectrum", Phys. Rev. A **87**, 025601 (2013).

[102] D. H. J. O'Dell, S. Giovanazzi, and G. Kurizki, "Rotons in Gaseous Bose-Einstein Condensates Irradiated by a Laser", Phys. Rev. Lett. **90**, 110402 (2003).

[103] D. Petter et al., "Probing the Roton Excitation Spectrum of a Stable Dipolar Bose Gas", Phys. Rev. Lett. **122**, 183401 (2019).

[104] L. Chomaz et al., "Observation of roton mode population in a dipolar quantum gas", Nature Physics **14**, 442 (2018).

[105] E. Casotti et al., "Observation of vortices in a dipolar supersolid", Nature **635**, 327 (2024).

[106] N. Liebster et al., "Supersolid-like sound modes in a driven quantum gas", Nature Physics **21**, 1064 (2025).

[107] L. Tanzi et al., "Evidence of superfluidity in a dipolar supersolid from nonclassical rotational inertia", Science **371**, 1162 (2021), eprint: https://www.science.org/doi/pdf/10.1126/science.aba4309.

[108] G. Biagioni et al., *Sub-unity superfluid fraction of a supersolid from self-induced Josephson effect*, 2023, arXiv:2311.04757 [cond-mat.quant-gas].

[109] A. Putra et al., "Spatial Coherence of Spin-Orbit-Coupled Bose Gases", Phys. Rev. Lett. **124**, 053605 (2020).

[110] K. T. Geier et al., "Dynamics of Stripe Patterns in Supersolid Spin-Orbit-Coupled Bose Gases", Phys. Rev. Lett. **130**, 156001 (2023).

[111] D. Trypogeorgos et al., "Emerging supersolidity in photonic-crystal polariton condensates", Nature **639**, 337 (2025).

[112] D. Nigro et al., "Supersolidity of Polariton Condensates in Photonic Crystal Waveguides", Physical Review Letters **134**, 10.1103/physrevlett.134.056002 (2025).

[113] Y. Pomeau and S. Rica, "Dynamics of a model of supersolid", Phys. Rev. Lett. **72**, 2426 (1994).

[114] C.-D. Yoo and A. T. Dorsey, "Hydrodynamic theory of supersolids: Variational principle, effective Lagrangian, and density-density correlation function", Phys. Rev. B **81**, 134518 (2010).

[115] D. T. Son, "Effective Lagrangian and Topological Interactions in Supersolids", Phys. Rev. Lett. **94**, 175301 (2005).

[116] W. M. Saslow, "Microscopic and hydrodynamic theory of superfluidity in periodic solids", Phys. Rev. B **15**, 173 (1977).

[117] C. Josserand, Y. Pomeau, and S. Rica, "Coexistence of Ordinary Elasticity and Superfluidity in a Model of a Defect-Free Supersolid", Phys. Rev. Lett. **98**, 195301 (2007).

[118] J. Hofmann and W. Zwerger, "Hydrodynamics of a superfluid smectic", Journal of Statistical Mechanics: Theory and Experiment **2021**, 033104 (2021).

[119] L. Landau, "Theory of the Superfluidity of Helium II", Phys. Rev. **60**, 356 (1941).

[120] P. D. Fleming and C. Cohen, "Hydrodynamics of solids", Phys. Rev. B **13**, 500 (1976).

[121] W. M. Saslow, *Dynamics of supersolid state: Normal fluid, superfluid, and supersolid velocities*, Aug. 2025.

[122] M. Liu, "Superfluid dynamics, equilibrium conditions, and centripetal forces", Journal of Statistical Mechanics: Theory and Experiment **2023**, 033104 (2023).

[123] L. M. Platt, D. Baillie, and P. B. Blakie, "Sound waves and fluctuations in one-dimensional supersolids", Phys. Rev. A **110**, 023320 (2024).

[124] J. Nocedal and S. J. Wright, *Numerical Optimization*, 2nd ed., Springer Series in Operations Research and Financial Engineering (Springer, New York, 2006).

[125] NVIDIA Corporation, *cuFFT: CUDA Fast Fourier Transform Library*, Version included in CUDA Toolkit, NVIDIA (2023).

[126] M. Frigo and S. G. Johnson, "The Design and Implementation of FFTW3", Proceedings of the IEEE **93**, 216 (2005).

[127] S. E. Koonin and D. C. Meredith, *Computational Physics* (Westview Press, 1990).

[128] J. Hertkorn et al., *Decoupled sound and amplitude modes in trapped dipolar supersolids*, 2024, arXiv:2404.12384 [cond-mat.quant-gas].

[129] S. M. Roccuzzo, S. Stringari, and A. Recati, "Supersolid edge and bulk phases of a dipolar quantum gas in a box", Phys. Rev. Res. **4**, 013086 (2022).

[130] H.-Y. Lu et al., "Spatial density oscillations in trapped dipolar condensates", Phys. Rev. A **82**, 023622 (2010).

[131] A. Kumar et al., "Minimally destructive, Doppler measurement of a quantized flow in a ring-shaped Bose–Einstein condensate", New Journal of Physics **18**, 025001 (2016).

[132] G. Chauveau et al., "Superfluid Fraction in an Interacting Spatially Modulated Bose-Einstein Condensate", Phys. Rev. Lett. **130**, 226003 (2023).

[133] M. Šindik, T. Zawiślak, A. Recati, and S. Stringari, "Sound, Superfluidity, and Layer Compressibility in a Ring Dipolar Supersolid", Phys. Rev. Lett. **132**, 146001 (2024).

[134] P. B. Blakie, L. Chomaz, D. Baillie, and F. Ferlaino, "Compressibility and speeds of sound across the superfluid-to-supersolid phase transition of an elongated dipolar gas", Phys. Rev. Res. **5**, 033161 (2023).

[135] P. C. Martin, O. Parodi, and P. S. Pershan, "Unified Hydrodynamic Theory for Crystals, Liquid Crystals, and Normal Fluids", Phys. Rev. A **6**, 2401 (1972).

[136] W.F.Vinen, *Physics of Quantum Fluids, ed. by R. Kubo and F. Takano* (Syokabo Pub- lishing Company, Tokyo, 1970).

[137] H. Hu et al., "Second sound and the density response function in uniform superfluid atomic gases", New Journal of Physics **12**, 043040 (2010).

[138] D. J. Bergman, B. I. Halperin, and P. C. Hohenberg, "Hydrodynamic theory applied to fourth sound in a moving superfluid", Phys. Rev. B **11**, 4253 (1975).

[139] A. M. Kenis, Y. A. Nepomnyashchy, A. Mann, and M. Revzen, "Unusual Doppler Effect in the B Phase of Superfluid ^{3}He", Phys. Rev. Lett. **82**, 584 (1999).

[140] F. Pobell and M. Revsen, "Doppler-shift of fourth sound in flowing ^{3}He-^{4}He mixtures", Physics Letters A **55**, 91 (1975).

[141] I. Rudnick, H. Kojima, W. Veith, and R. S. Kagiwada, "Observation of Superfluid-Helium Persistent Current by Doppler-Shifted Splitting of Fourth-Sound Resonance", Phys. Rev. Lett. **23**, 1220 (1969).

[142] H. Kojima et al., "Vortex-Free Landau State in Rotating Superfluid Helium", Phys. Rev. Lett. **27**, 714 (1971).

[143] O. Morsch and M. Oberthaler, "Dynamics of Bose-Einstein condensates in optical lattices", Rev. Mod. Phys. **78**, 179 (2006).

[144] M. Krämer, C. Menotti, L. Pitaevskii, and S. Stringari, "Bose-Einstein condensates in 1D optical lattices", The European Physical Journal D - Atomic, Molecular, Optical and Plasma Physics **27**, 247 (2003).

[145] G. Roati et al., "Anderson localization of a non-interacting Bose–Einstein condensate", Nature **453**, 895 (2008).

[146] M. Greiner et al., "Quantum phase transition from a superfluid to a Mott insulator in a gas of ultracold atoms", Nature **415**, 39 (2002).

[147] J.-y. Choi, "Quantum simulations with ultracold atoms in optical lattices: past, present and future", Journal of the Korean Physical Society **82**, 875 (2023).

[148] J. Tao, M. Zhao, and I. B. Spielman, "Observation of Anisotropic Superfluid Density in an Artificial Crystal", Phys. Rev. Lett. **131**, 163401 (2023).

[149] A. Smerzi and A. Trombettoni, "Nonlinear tight-binding approximation for Bose-Einstein condensates in a lattice", Phys. Rev. A **68**, 023613 (2003).

[150] E. Taylor and E. Zaremba, "Bogoliubov sound speed in periodically modulated Bose-Einstein condensates", Phys. Rev. A **68**, 053611 (2003).

[151] A. Smerzi, A. Trombettoni, P. G. Kevrekidis, and A. R. Bishop, "Dynamical Superfluid-Insulator Transition in a Chain of Weakly Coupled Bose-Einstein Condensates", Phys. Rev. Lett. **89**, 170402 (2002).

[152] T. Zawiślak, M. Šindik, S. Stringari, and A. Recati, "Anomalous Doppler Effect in Superfluid and Supersolid Atomic Gases", Phys. Rev. Lett. **134**, 226001 (2025).

[153] M. N. Tengstrand et al., "Persistent currents in toroidal dipolar supersolids", Phys. Rev. A **103**, 013313 (2021).

[154] M. Nilsson Tengstrand, P. Stürmer, J. Ribbing, and S. M. Reimann, "Toroidal dipolar supersolid with a rotating weak link", Phys. Rev. A **107**, 063316 (2023).

[155] T. Bienaimé et al., "Spin-dipole oscillation and polarizability of a binary Bose-Einstein condensate near the miscible-immiscible phase transition", Phys. Rev. A **94**, 063652 (2016).

[156] A. F. Andreev and E. P. Bashkin, "Three-velocity hydrodynamics of superfluid solutions", Zh. Eksp. Teor. Fiz., v. 69, no. 1, pp. 319-326 (1975).

[157] S. I. Shevchenko and D. V. Fil, "The Andreev-Bashkin effect in a two-component Bose gas", Journal of Experimental and Theoretical Physics **105**, 135 (2007).

List of Figures